Copyright Warning & Restrictions

The copyright law of the United States (Title 17, United States Code) governs the making of photocopies or other reproductions of copyrighted material.

Under certain conditions specified in the law, libraries and archives are authorized to furnish a photocopy or other reproduction. One of these specified conditions is that the photocopy or reproduction is not to be "used for any purpose other than private study, scholarship, or research." If a, user makes a request for, or later uses, a photocopy or reproduction for purposes in excess of "fair use" that user may be liable for copyright infringement,

This institution reserves the right to refuse to accept a copying order if, in its judgment, fulfillment of the order would involve violation of copyright law.

Please Note: The author retains the copyright while the New Jersey Institute of Technology reserves the right to distribute this thesis or dissertation

Printing note: If you do not wish to print this page, then select "Pages from: first page # to: last page #" on the print dialog screen

ABSTRACT

INNOVATIVE LOCAL TEXTURE DESCRIPTORS WITH APPLICATION TO EYE DETECTION

by
Jiayu Gu

Local Binary Patterns (LBP), which is one of the well-known texture descriptors, has broad applications in pattern recognition and computer vision. The attractive properties of LBP are its tolerance to illumination variations and its computational simplicity. However, LBP only compares a pixel with those in its own neighborhood and encodes little information about the relationship of the local texture with the features. This dissertation introduces a new Feature Local Binary Patterns (FLBP) texture descriptor that can compare a pixel with those in its own neighborhood as well as in other neighborhoods and encodes the information of both local texture and features. The features encoded in FLBP are broadly defined, such as edges, Gabor wavelet features, and color features. Specifically, a binary image is first derived by extracting feature pixels from a given image, and then a distance vector field is obtained by computing the distance vector between each pixel and its nearest feature pixel defined in the binary image. Based on the distance vector field and the FLBP parameters, the FLBP representation of the given image is derived. The feasibility of the proposed FLBP is demonstrated on eye detection using the BioID and the FERET databases. Experimental results show that the FLBP method significantly improves upon the LBP method in terms of both the eye detection rate and the eye center localization accuracy.

As LBP is sensitive to noise especially in near-uniform image regions, Local Ternary Patterns (LTP) was proposed to address this problem by extending LBP to three-

valued codes. However, further research reveals that both LTP and LBP achieve similar results for face and facial expression recognition, while LTP has a higher computational cost than LBP. To improve upon LTP, this dissertation introduces another new local texture descriptor: Local Quaternary Patterns (LQP) and its extension, Feature Local Quaternary Patterns (FLQP). LQP encodes four relationships of local texture, and therefore, it includes more information of local texture than the LBP and the LTP. FLQP, which encodes both local and feature information, is expected to perform even better than LQP for texture description and pattern analysis. The LQP and FLQP are applied to eye detection on the BioID database. Experimental results show that both FLQP and LQP achieve better eye detection performance than FLTP, LTP, FLBP and LBP. The FLQP method achieves the highest eye detection rate.

INNOVATIVE LOCAL TEXTURE DESCRIPTORS WITH APPLICATION TO EYE DETECTION

by
Jiayu Gu

A Dissertation
Submitted to the Faculty of
New Jersey Institute of Technology
in Partial Fulfillment of the Requirements for the Degree of
Doctor of Philosophy in Computer Science

Department of Computer Science

January 2014

APPROVAL PAGE

INNOVATIVE LOCAL TEXTURE DESCRIPTORS WITH APPLICATION TO EYE DETECTION

Jiayu Gu

Dr. Chengjun Liu, Dissertation Advisor Associate Professor of Computer Science, NJIT	Date
Dr. James McHugh, Committee Member Professor of Computer Science, NJIT	Date
Dr. Durgamadhab Misra, Committee Member Professor of Electrical and Computer Engineering, NJIT	Date
Dr. Andrew Sohn, Committee Member Associate Professor of Computer Science, NJIT	Date
Dr. Zhi Wei, Committee Member Associate Professor of Computer Science, NJIT	Date

BIOGRAPHICAL SKETCH

Author: Jiayu Gu

Degree: Doctor of Philosophy

Date: January 2014

Undergraduate and Graduate Education:

- Doctor of Philosophy in Computer Science.
  New Jersey Institute of Technology, Newark, NJ, 2014
- Master of Science in Computer Science.
  New Jersey Institute of Technology, Newark, NJ, 1997
- Bachelor of Science in Biomedical Engineering,
  Shanghai University of Science and Technology, Shanghai, P. R. China, 1987

Major: Computer Science

Publications:

Gu, J. & Liu, C. (2013). New Feature Local Texture Descriptors. Submited to *IEEE Transactions on Image Processing*.

Gu, J. & Liu, C. (2013). Feature Local Binary Patterns with Application to Eye Detection. *Neurocomputing*, 13, pp. 138-152.

Gu, J. & Liu, C. (2012). Feature Local Binary Patterns. in *Cross Disciplinary Biometric Systems*, C. Liu & V. Mago, Eds., New York, NY: Springer, pp. 1-13.

Gu, J. & Liu, C. (2012). Local Texture Descriptors for Biometric Detection: New Local Quaternary Pattern Descriptors and Case Study on Eye Detection. in *Biometrics and Kansei Engineering*, K. Saeed & T.Nagashima, Eds., New York, NY: Springer. pp. 129-152

Gu, J. & Liu, C. (2012). Local Quaternary Patterns and Feature Local Quaternary Patterns. in *Proceedings of 16th International Conference on Image Processing, Computer Vision, and Pattern Recognition.*

Gu, J. & Liu, C. (2012). A New Feature Local Binary Patterns (FLBP) Method. in *Proceedings of 16th International Conference on Image Processing, Computer Vision, and Pattern Recognition.*

To my wife, Ying Li

and

my parents, Xiaoying Yang and Yu-dong Gu

ACKNOWLEDGMENT

I would like to express the deepest gratitude to my advisor, Professor Chengjun Liu. His wisdom, knowledge and commitment to the highest standards inspired and motivated me. I am very fortunate to be his student. Without his support, patience and guidance this dissertation would not have been possible.

My committee members, Professor James McHugh, Professor Durgamadhab Misra, Professor Andrew Sohn and Professor Zhi Wei have generously given their precious time and valuable expertise to improve my work. I am full of appreciation to them for their contribution and support to this dissertation.

TABLE OF CONTENTS

TABLE OF CONTENTS
(Continued)

Chapter **Page**

TABLE OF CONTENTS
(Continued)

LIST OF TABLES

LIST OF TABLES
(Continued)

Table **Page**

LIST OF TABLES
(Continued)

LIST OF TABLES
(Continued)

LIST OF FIGURES

LIST OF FIGURES
(Continued)

LIST OF FIGURES
(Continued)

CHAPTER 1

INTRODUCTION

1.1 Feature Local Binary Patterns

The Local Binary Patterns (LBP) method, which defines a gray-scale invariant texture description by comparing a center pixel with its neighbors, is a popular method for texture analysis (Ojala et al., 1994), (Ojala et al., 1996), (Ojala et al., 2002). At an earlier stage for texture analysis, the concept of texture unit and texture spectrum was introduced (L. Wang and He, 1990). A texture unit of a pixel is represented by eight elements, which correspond to the eight neighbors in a 3 × 3 neighborhood with three possible values: 0, 1, 2. The three values represent three possible relationships between the center pixel and its neighbors: “less than”, “equal to”, or “greater than”. As a result, there are 6561 (3^8) possible texture units in total. A texture spectrum of a region is defined by the histogram of the texture units over the region. However, the large number of possible texture units poses a computational challenge. To reduce the computational burden, a method that applies two relationships: “less than” or “greater than or equal to” that are represented by two possible values: 0 or 1 is proposed (Gong et al., 1992), (Ojala et al., 1994). The two relationships method thus reduces the total number of texture units from 6561 to 256 (2^8), which can be represented by eight binary numbers. The two relationship version of texture units is named as local binary patterns or LBP (Ojala et al., 1994).

The LBP method has been applied in many pattern recognition tasks. However, LBP has two problems. First, LBP only compares a pixel with the pixels in its own neighborhood. More information could be revealed if a pixel compares with the pixels in other neighborhoods. Second, LBP encodes a little information about the relationship

of local texture with the features, such as edges, peaks and valleys. To solve these two problems, this dissertation proposes a new Feature Local Binary Patterns (FLBP) texture descriptor that compares a pixel with the pixels in its own neighborhood as well as in other neighborhoods, and encodes the information of both local texture and features. The features encoded in FLBP are broadly defined by any features which meet the requirements of specific applications, such as the edges, the intensity peaks or valleys, the Gabor wavelet features (Liu and Wechsler, 2002), (Liu, 2004) and the color features (Z. Liu and C. Liu, 2008a), (Z. Liu and C. Liu, 2008b), (Yang and Liu, 2007), (Yang and Liu, 2008). As the FLBP method encodes both local and feature information, the performance of FLBP depends on the extraction of the feature pixels. To improve FLBP performance, a new feature pixel extraction method, the LBP with Relative Biased Threshold (LRBT) method is present in this dissertation.

The FLBP is applied to eye detection using the BioID and FERET databases. The experimental results show that:

1. The FLBP method significantly improves upon the LBP method in terms of both eye detection rate and eye center localization accuracy.
2. The new LRBT feature pixel extraction method helps improve the FLBP eye detection performance when compared with other feature pixel extraction methods.
3. The FLBP method displays superior representational power and flexibility to the LBP method due to the introduction of feature pixels as well as its parameters.
4. In comparison with the state of the art methods, the FLBP method achieves the highest accuracy of eye center localization.

1.2 Local Quaternary Patterns and Feature Local Quaternary Patterns

Tan and Triggs (2007, 2010) argued that LBP tends to be sensitive to noise, especially in near-uniform image regions, because it thresholds exactly at the value of the central

pixel. To solve the problem, they proposed three-valued codes, called Local Ternary Patterns (LTP). In LTP, neighbor pixels are compared with an interval [-r, +r] around the value of the center pixel. A neighbor pixel is assigned 1, 0 or -1, if its value is above +r, in the interval [-r, +r] or below –r, respectively. Because the radius r is not changed with the gray scale, the LTP is no longer a strictly gray-scale invariant texture description, and is less tolerance against illumination than LBP. Similar to the text unit method, LTP has 6561 possible values as well, which not only poses a computational challenge but also leads to sparse histograms. To solve these problems, a coding scheme is introduced to split a LTP code into two binary codes, the positive one (PLTP) and the negative one (NLTP). Therefore, the total number of possible values of two split binary codes is reduced to 512. LTP doubles the size of feature dimensions and histograms. Some of experiments show that LTP and LBP achieved similar results for face and facial expression recognition, although LTP has a higher computational cost than LBP (Tan & Triggs, 2007, 2010), (Gritti, 2008).

To improve the performance of LTP, this dissertation proposes another new local texture descriptor, Local Quaternary Patterns (LQP) and its extension, Feature Local Quaternary Patterns (FLQP). LQP encodes four relationships of local texture, and therefore, it includes more information of local texture than the LBP and LTP which encodes two, and three relationships, respectively. LQP has 65535 (4^8) possible values. To reduce the size of feature dimensions and histograms of LQP, a coding scheme is introduced to split each LQP code into two binary codes, the upper LQP (ULQP) and the lower LQP (LLQP). After splitting, the possible LQP values are reduced to 512. FLQP is the extension of LQP using the same approach of FLBP. FLQP can compare a pixel with

the pixels in its own neighborhood as well as in other neighborhoods, and encodes the information of both local texture and features. FLQP also has 65535 possible values. To reduce the size of feature dimensions and histograms, an FLQP code can be split into two binary codes as well, the upper FLQP (UFLQP) and the lower FLQP (LFLQP).

To demonstrate their feasibility, the proposed LQP and FLQP methods are applied to eye detection on the BioID database. Experimental results show that both FLQP and LQP achieve better eye detection performance than Feature Local Ternary Patterns (FLTP), LTP, FLBP and LBP. The FLQP method achieves the highest eye detection rates.

1.3 Overview of Dissertation

The remaining part of the dissertation is organized as follows. Chapter 2 first reviews the origin, applications and extensions of LBP, and then discusses the objective, performance and extensions of LTP. Last the chapter reviews the recent works and techniques for eye detection. Chapter 3 reviews the definitions of LBP, distance transform and distance vector, and then introduces FLBP. The three special cases of FLBP which are LBP, FLBP1 and FLBP2 are also descripts in the chapter. Chapter 4 first reviews the LTP and its code schema, and then introduces the LQP and it extension, FLQP. The new code schemas to reduce the dimension of LQP and FLQP are presented in the chapter. Chapter 5 descripts the application of FLBP and FLQP to eye detection. A new feature pixel extraction method, LBP with Relative Biased Threshold (LRBT) is introduced. The system architecture of the FLBP-based and FLQP-based eye detection method is descripted. A fast algorithm that is used to computer FLBP histogram and similarity is explained. The FLBP application on gradient images is discussed. Chapter 6 discusses the

experimental results of FLBP-based eye detection method. In chapter 6 the performance of the FLBP method is compared with the LBP method, and the methods using other local texture descriptors. The performance of the FLBP method in terms of feature pixels and parameters is assessed. An enhanced eye detection method is introduced and its performance is compared with other state of the art eye detection methods. Chapter 7 discusses the experimental results of LQP-based and FLQP-based eye detection methods. First the performance of LQP-based and FLQP-based methods is assessed, and then the performance of LTP-Based and FLTP-based method is assessed. Last the performance of the LBP, FLBP, LTP, FLTP, LQP and FLQP eye detection methods is comparatively assessed. Chapter 8 summarizes the dissertation and discusses the future work.

CHAPTER 2

BACKGROUND

2.1 Local Binary Patterns

The local binary pattern (LBP) was originally designed for texture description (Ojala et al., 1994), (Ojala et al., 1996), (Ojala et al., 2002). LBP assigns a label to every pixel of an image by compared with its eight neighbors in a 3 x 3 neighborhood. Two possible values: 0 or 1 is assigned to each neighbor whose value is "less than" or "greater than or equal to" the value of the center pixel, respectively. For each given pixel, a binary LBP code is obtained by concatenating the binary values of its eight neighbors in the 3 x 3 neighborhood. The corresponding decimal value of the binary code is used to label the given pixel. As a result, there are 256 (2^8) possible value in total. The most important properties of the LBP operator are its tolerance against illumination and computational simplicity, which makes it possible to analyze images in real-world in real-time.

The LBP has been widely applied in many applications. Face recognition is one of the most popular and successful applications in recent years. Ahonen et al. (2004, 2006) presented a facial image representation based on local binary pattern (LBP). The face image is divided into several local regions from which the local LBP histograms are extracted, and then concatenated them into a feature vector to be used as a face descriptor. The performance of the proposed method was assessed in the face recognition problem. The weighted Chi square distance and nearest neighbor (NN) classifier are used as similarity measure between corresponding LBP histograms of two face images. Their

method was tested on the FERET database and yields the recognition rates of 97%, 79%, 66% and 64% on the fb, fc, dup I and dup II sets, respectively. The experimental results showed that their approach outperforms the PCA, the elastic bunch graph matching (EBGM), and the Bayesian intra- and extra-personal classifier. G. Zhang et al. (2004) presented an approach for face recognition by boosting statistical local features based classifiers. The face image is scanned with a scalable sub-window from which the LBP histograms are obtained to describe the local features of a face image. The AdaBoost algorithm is used to learn a similarity of every face image pairs. The proposed method was tested on the fb set of FERET database. W. Zhang et al. (2005a) proposed a local Gabor binary pattern histogram sequence (LGBPHS) for face recognition. In their approach, a face image is modeled by concatenating the histograms of all the local regions of all the local Gabor magnitude binary pattern maps. For recognition, histogram intersection is used to measure the similarity of different LGBPHSs and the nearest neighborhood is exploited for final classification. They further proposed to assign different weights for each histogram piece when measuring two LGBPHSs. The proposed method was tested on the AR and FERET face databases. W. Zhang et al. (2005b) proposed Multi-resolution Histograms of Local Variation Patterns (MHLVP) to recognize faces. For a face image, multiple Gabor feature maps (GFM) are computed by convolving the image with the multi-scale and multi-orientation Gabor filters. Each GFM is then divided into small non-overlapped regions from which LBP histograms are extracted and concatenated into a feature histogram for GFM. Moreover, the feature histograms extracted from all GFM are concatenated into a single feature histogram as the final facial representation of the given face image. Histogram intersection is used as

the similarity matching between the histograms of two face images. Their method is tested on the fb, fc, dup I and dup II sets of FERET database. J. Zhao et al. (2005) presented a LBP based Kernel Fisher Discriminant Analysis (KFDA) approach by integrating the LBP descriptor of face images and the KFDA method for face classifier. They introduced the kernel function by using Chi square statistic distance and RBF as inner product for KFDA classifier. They tested their method on the FRGC database. Hadid et al. (2006a. 2007) introduced VLBP to extract and use the local facial dynamics for a spatio-temporal face recognition from video. AdaBoost was applied to learn the specific facial dynamics of each person, while ignoring intrapersonal temporal information, such as facial expressions. Yao et al. (2007) used Local Gabor Binary Pattern Histogram (LGBPH) features for face representation, and adopts RankBoost to select the most discriminative features for face recognition. Their approach was tested on the FERET databases. Chan et al. (2007) proposed a discriminative face representation derived by the Linear Discriminant Analysis (LDA) of multi-scale local binary pattern histograms for face recognition. The face image is first partitioned into several non-overlapping regions. In each region, multi-scale local binary uniform pattern histograms are extracted and concatenated into a regional feature. The features are then projected on the LDA space to be used as a discriminative facial descriptor. The method is tested on the FERET and XM2VTS databases. Li et al. (2006, 2007) and D. Huang (2007) applied LBP to near-IR (NIR) facial images for face recognition. LBP feature has also be applied to 3-D face recognition (Li et al, 2005), (X. Huang et al, 2006), (Nanni and Lumini, 2007). Yang and Wang (2007) presented a LBP-based face recognition method with Hamming distance constraint. By assuming that the illumination, pose or expression

changes of a face image are some kinds of "noise", they introduced the Hamming distance in channel coding to LBP so as to decrease the error rate caused by these noise disturbances. Experimental results on FRGC show that their method improves the recognition performance than the traditional LBP-based face recognition methods when face images are under uncontrolled circumstances. W. Zhang et al. (2008) argued that Gabor phases are also useful for face recognition by applying LBP on Gabor phases face image. Their experimental results show that the Gabor phases are quite compensatory to the magnitude information, since higher classification accuracy is achieved by combining Gabor phases and magnitudes. Lei et al. (2008) presented a face representation and recognition approach. The face image is first decomposed by multi-scale and multi-orientation Gabor filters. The Gabor magnitude responses are reformulated as a 3rd-order volume and then apply LBP analysis on three orthogonal planes of the Gabor volume, named GV-LBPTOP. Further, a computationally effective version, E-GV-LBP, is proposed to depict the neighboring changes in spatial, frequency and orientation domains simultaneously. Z. Liu and C. Liu (2010) presented a novel face recognition method by means of fusing color, local spatial and global frequency information. Specifically, the proposed method fuses the multiple features derived from a hybrid color space, the Gabor image representation, the local binary patterns (LBP), and the discrete cosine transform (DCT) of the input image. First, a hybrid color space, the RCrQ color space, is constructed by combining the R component image of the RGB color space and the chromatic component images, Cr and Q, of the YCbCr and YIQ color spaces, respectively. Second, three effective image encoding methods are proposed for the component images in the RCrQ hybrid color space to extract features: (i) a patch-based

Gabor image representation for the R component image, (ii) a multi-resolution LBP feature fusion scheme for the Cr component image, and (iii) a component-based DCT multiple face encoding for the Q component image. Experiments on the FRGC database show that the proposed method improves face recognition performance significantly.

LBP has also been used for face detection. Hadid *et al*. (2004) proposed a face detection method that is based on LBP and consists of dividing the facial image into a set of regions from which LBP feature histograms are computed and concatenated into a single histogram. The approach uses a second degree polynomial kernel SVM for classification. They tested their method on the MIT-CMU database. H. Zhang and D. Zhao (2004) presented a face detection approach in color images using LBP. First, five measurements, *Y*, *R*, *G*, *B*, and θ, in the RGB and YUV color space are extracted from the original images. LBP spatial histograms are calculated on the five color measurements. Based on the spatial histogram representation, discriminating features are extracted for face detection. A hierarchical classifier combining histogram matching algorithm and support vector machine is utilized to identify face and non-face. Hadid *et al*. (2006b) proposed an approach which combines the advantages of both color and gray scale based methods to detect faces in natural and unconstrained environments. Their method first preprocesses the images using skin modeling in order to determine the potential skin regions. Thus, a scanning of the whole image when searching for faces is avoided. Then, they apply an exhaustive search in and around the detected skin regions using a gray scale based approach. The experimental results show that the proposed approach inherits the speed from the color based methods and the efficiency from the gray scale based ones. Jin et al. (2006) presented a face detection approach using improved local binary

patterns (ILBP) as facial representation. ILBP feature is an improvement of LBP feature that considers both local shape and texture information instead of raw grayscale information. They model the face and non-face class using multivariable Gaussian model and classify them under Bayesian framework. They tested their method on The Yale B and MIT-CMU database. L. Zhang et al. (2007) presented Multi-block Local Binary Patterns (MB-LBP) for face detection. Based on the MB-LBP features, a boosting-based learning method is developed to achieve the goal of face detection. Their experiments show the weak classifiers based on MB-LBP are more discriminative than Haar-like features and original LBP features. Pan et al. (2013) proposed heterogeneous feature descriptors for face detection. A face is represented by the Generalized Haar-like (GH) descriptor, Multi-Block Local Binary Patterns (MB-LBP) descriptor and Speeded-Up Robust Features (SURF) descriptor. The approach uses Adaboost leaning algorithm for classification.

Another application of LBP is Facial expression analysis. Feng et al. (2004a, 2004b) introduced a coarse-to-fine classification scheme to recognize facial expressions with the LBP histogram as face representation. In the coarse stage, the seven class problem is reduced to a two-class one. In the fine classification stage, a K-nearest neighbor classifier fulfills final classification. The method is tested on the JAFFE database. Feng et al. (2005) proposed an approach to recognize facial expression. The LBP are used to represent the facial images. The linear programming (LP) technique is adopted to classify seven facial expressions. He et al. (2005) applied LBP on four kinds of frequency images decomposed by Gabor wavelets for facial expression recognition. Their experiments show that their approach improves the performance of facial

expression recognition. Liao et al. (2006) proposed facial expression recognition approach based on texture features and global appearance features. The first feature set is obtained by using the extended local binary patterns in both intensity and gradient maps and computing the Tsallis entropy of the Gabor filtered responses. The second set of features is obtained by performing null-space based linear discriminant analysis on the training face images. The proposed method is evaluated on the JAFFE database. G. Zhao et al. (2007a) proposed an approach for recognizing dynamic textures and its simplifications and extensions to facial image analysis. The textures are modeled with volume local binary patterns (VLBP), which are an extension of the LBP operator. To make the approach computationally simple, LBP-TOP is then considered. A block-based method is also proposed to deal with specific dynamic events, such as facial expressions. A recognition rate of 96.26% was achieved on the Cohn–Kanade database. Cao and Tong (2008) proposed a method to combine LBP and embedded hidden markov model (EHMM) for facial expression recognition. Shan et al. (2005a, 2005b, 2005c, 2008 and 2009) empirically evaluated facial representation using LBP for facial expression recognition. Different machine learning methods are systematically examined on several databases. The results show that LBP features are efficient for facial expression recognition. They further formulated Boosted-LBP to extract the most discriminant LBP features, and the best recognition performance is obtained by using SVM classifiers with Boosted-LBP features. They investigated LBP features for low-resolution facial expression recognition. Their experiments show that LBP features perform stably and robustly over a useful range of low resolutions of face images, and yield promising performance in compressed low-resolution video sequences captured in real-world

environments. Moore and Bowden (2011) investigated the effects of pose on facial expression recognition using LBP and some extensions including multi-scale LBP (LBP^{ms}) and local gabor binary patterns (LGBP) on BU3DFE and multi-pie database. Results in their paper show that LGBPs outperform other features.

In addition to facial image analysis, LBP has been exploited in other applications. Banerji et al. (2011, 2013) proposed a new color multi-mask LBP for texture and scene classification. They further proposed a novel Three Dimensional Local Binary Patterns (3D-LBP) feature for color image. The proposed new LBP features combining with other features achieve better classification performance than other popular image descriptors. Sinha et al. (2012) proposed novel color Gabor-LBP-PHOG (GLP) descriptors for object and scene image classification. X. Nanni and Lumini (2008) presented an approach for pedestrian detection. They designed an ensemble of classifiers that employ LBP, Laplacian EigenMaps, and Gabor filters feature representation schemes of the pedestrian images. X. Wang et al. (2009) propose a human detection approach capable of handling partial occlusion by combining Histograms of Oriented Gradients (HOG) and LBP as the features. Liao et al. (2009) proposes an approach for texture classification using dominant local binary patterns (DLBP). Heikkilä and Pietikäinen (2006) presented a texture-based method for modeling the background and detecting moving objects from a video sequence. Each pixel is modeled as a group of LBP histograms that are calculated over a circular region around the pixel. Turtinen et al. (2006) studied the combined use of LBP texture features and the Isomap dimensionality reduction method for analyzing trans-illuminated paper textures. Oliver (2007) et al. (2007) proposed an approach for false positive reduction in the field of mammographic mass detection using LBP. Yuan et al.

(2011) proposed an image retrieval system based on bag-of-features (BoF) model by integrating scale invariant feature transform (SIFT) and LBP.

Many extensions of the original LBP have been proposed to improve the performance. Jin et al. (2006) argued that the original LBP might not include all the local structure information as the central pixel is not considered in the LBP coding. They presented an improved LBP (ILBP) for face detection, which compares all the pixels including the center pixel in a 3 × 3 neighborhood with the mean of the pixels in the same neighborhood. As a result, the ILBP can represent 511 patterns (29-1, as all zeros and all ones are the same). The extended local binary pattern (ELBP) (X. Huang, 2006), (D. Huang, 2007) is presented to not only compare the central pixel with its neighbors, but also encode their gray-value differences (GDs). The ELBP consists of several LBP codes at multiple layers. The first layer of ELBP is actually the original LBP code that encodes the sign of GD. The following layers of ELBP encode the absolute value of GD. Each absolute GD value is first encoded in its binary representation, and then all the binary values at a given layer form an additional LBP. Modify Local Binary Pattern (MLBP) (Pham-Ngo and Jo, 2006) is introduced for face detection by adding a set of spatial templates. Instead of comparing with each pixel of its neighborhood, the central pixel compares with two pixels in the neighborhood which are paired according to the spatial templates. Eight main spatial templates are defined in MLBP. Each of the spatial templates corresponds to one binary digit. If the value of center pixel is greater than the values of both pixels in a pair, their corresponding binary digit is assigned to 1, otherwise 0. A Multi-Block LBP (MB-LBP) is introduced for face recognition (Liao and Li, 2007) and face detection (L. Zhang et al, 2007). MB-LBP compares the average intensity of the

central sub-region with its neighboring sub-regions. The original LBP can be regarded as a special case of the MB-LBP, where the central and neighboring sub-regions contain only one pixel. The neighboring pixels in the original LBP are defined on a circle. An Elongated LBP (Liao and Chung, 2007) with neighboring pixels lying on an ellipse is introduced for face recognition. The experimental results demonstrate that the Elongated LBP outperforms the original LBP for face recognition. Fu and Wei (2008) introduced the Centralized Binary Patterns (CBP). CBP compares two neighbor pixels at the same diameter of the circle, and also compares the central pixel with the mean of all the pixels (including the central pixel) in the neighborhood. CBP needs only five binary digits which represent the relationships of four pairs of the neighbor pixels on the same diameter and the central pixel with the mean of all the pixels. The experiments for facial expression recognition show that CBP has better performance than LBP although it includes less relationships of local texture. Guo et al. (2010) proposed a complete LBP (CLBP) which is similar to ELBP. Unlike the binary bit coding schema used by ELBP, CLBP compares the absolute value of GD with the given central pixel again to generate an LBP code. B. Zhang and Gao (2010) introduced Local Derivative Pattern (LDP). LDP is a general framework to encode directional pattern features based on local derivative variations. Murala and Maheshwari (2012) introduced local tetra patterns (LTrP). LTrP encodes the relationship between the center pixel and its neighbors, based on the directions that are calculated using the first-order derivatives in vertical and horizontal directions.

2.2 Local Ternary Patterns

Tan and Triggs (2007, 2010) argued that LBP tends to be sensitive to noise, especially in near-uniform image regions. They introduced the three-valued code, LTP to solve the problem. In LTP, neighbor pixels are compared with an interval [-r, +r] around the value of the center pixel. A neighbor pixel is assigned 1, 0 or -1, if its value is above +r, in the interval [-r, +r] or below –r, respectively. LTP has 6561 ($3^{8)}$ possible values which not only poses a computational challenge but also leads to sparse histograms. To solve these problems, a coding scheme is introduced to split a LTP code into two binary codes, the positive one (PLTP) and the negative one (NLTP). Therefore, the total number of possible values of two split binary codes is reduced to 512.

They compared the performance of LBP and LTP on face recognition using different image preprocessing methods. Their results show that LTP yields best results using their proposed preprocessing method. However, their experiments also shows that the LBP archives better results than LTP using some other competing preprocessing methods. Gritti et al. (2008) compared the performance of different local texture features, including LBP and LTP for facial expression recognition. Their results show that LBP archived the best overall performance.

The performance of LTP depends on r, the radius of the interval around the value of the central pixel. It is a challenging task to find a best r. Akhloufi and Bendada (2010) proposed the Local Adaptive Ternary Pattern (LATP). LATP computes r using the mean and the standard deviation of the local region. The results show LATP performs better than LTP in face recognition. Liao et al. (2010) proposed the Scale Invariant Local Ternary Pattern (SILTP). In SILTP r is determined by the value of center pixel and is

grey scale invariant. The results show that SILTP is effective for handling illumination variations.

2.3 Eye Detection

Eye detection, an example of facial landmark detection, plays an important role in designing an automatic face recognition system. Eyes have some unique geometric and photometric characteristics, which provide important and reliable information for their localization. Even though a lot of research has been carried out and some progress has been reported, eye detection remains a challenging research topic due to the difficult factors caused by occlusion, closed eye, illumination variation, eye size and orientations, etc. Three major types of approaches for eye detection are template-based, distinctive feature-based and photometric appearance-based approaches.

The template-based method usually constitutes two components: a geometric eye model and a similarity measure. The geometric eye models are constructed from either the local point features of the eye and face region or from their contours. In template-base method, different segments of an input image are compared with those in the template, usually using a similarity measure to evaluate the similarity of the counterpart. Yuille et al. (1992) proposed a deformable template for face features, where an eye is described by a parameterized template. Specifically, an energy function is first defined to link the edges, peaks, and valleys in an image to the properties of the template. The template then interacts dynamically with the image by altering its parameter values to minimize the energy function, and by doing so deforms itself for the best fit. However, this method is not only time consuming, but critically relies on the initial position of the template. If the initial position of the template is above the eyebrow, for example, the method fails to

detect the eye. Lam and Yan (1996) extend Yuille's method for extracting eye features by using corner locations inside the eye windows as initialization points. The detected eye corners are used to reduce the number of iterations in the optimization of the deformable template. Further improvement of the method by applying some eye features in the initialization stage was also reported by Xie et al. (1994), L. Zhang (1996), Kampmann and Zhang (1998).

The common features in the distinctive feature-based approaches include edge, intensity of iris, as well as color distribution. Feng and Yuen (1998, 2001) described an eye model that consists of six landmarks corresponding to the eye corner points, which are located based on a variance projection function or VPF. Zhou and Geng (2004) extended the VPF to a generalized projection function (GPF). Their experiments show that the hybrid projection function, which is a special case of GPF, is better than VPF, while VPF is better than the integral projection function. Kawato et al. (2000, 2002) proposed a method that extracts the center point between the two eyes. Based on the observation that the between-eye area is dark on its left and right (eyes and eyebrows) and bright on the upper side (forehead) and the lower side (nose bridge), they proposed a circle-frequency filter to locate the candidate points. Sirohey et al. (2001, 2002) presented methods for eye detection using linear and non-linear filters. The linear filter contains the Gabor wavelets with four orientations for detecting the edges of an eye's sclera, and a Gaussian filter for detecting the dark circle of the iris. The nonlinear filter is used to detect the left and right corners of an eye in a color image. Kawaguchi and Rizon (2003) proposed a method for locating the iris of an eye using both intensity and edge information. Other methods (Wu and Zhou, 2003), (Han et al. 2002) first extract the

intensity valleys as the potential eye-analogue segments. A pair of eye-analogue segments is then detected as eyes if its placement is most consistent with the anthropological characteristic of human eyes. Khosravi and Safabakhsh (2008) proposed an approach that uses a morphological method for extracting an eye strip, where the iris is located through template matching by means of an adaptive half circle template.

The photometric appearance-based approaches usually collect a large amount of training data representing the eyes of different subjects, with different face orientations and under different illumination conditions. A classifier or regression model is then constructed for eye detection. The Eigen analysis has been applied in eye detection (Pentland et al., 1994), (Ryu and Oh, 2001), (W. Huang and Mariani, 2000), (Hillman et al., 2003). Pentland et al. (1994) extended the eigenfaces technique to the description and coding of facial features, yielding eigeneyes, eigennoses, and eigenmouths. Asteriadis et al. (2009) proposed a method for detecting eye and mouth using distance vector field. Recently, Chen and Liu (2010 presented an eye detection method using color information and wavelet features together with a new efficient Support Vector Machine (eSVM)

CHAPTER 3

FEATURE LOCAL BINARY PATTERNS

The proposed Feature Local Binary Patterns (FLBP) encodes the information of both local texture and features. The features are broadly defined by any features which meet the requirements of specific applications, such as the edges, the intensity peaks or valleys, the Gabor wavelet features, the color features. This chapter first reviews LBP, the concepts of the distance transform and distance vector, and then presents FLBP.

3.1 Local Binary Patterns

Local binary patterns, or LBP, define a gray-scale invariant texture description by comparing a center pixel which is used as a threshold with those pixels in its local neighborhood (Ojala et al. 1994, 1996, 2002). Specifically, for a 3 × 3 neighborhood of a pixel $\mathbf{p} = [x, y]^t$, each neighbor is labeled by a number from 0 to 7 as shown in Figure 3.1. The neighbors of the pixel **p** thus may be defined as follows:

$$\mathbf{N}(\mathbf{p}, i) = [x_i,\ y_i]^t, \quad i = 0, 1, 2, \ldots, 7 \tag{3.1}$$

where i is the number used to label the neighbor. The value of the LBP code of the pixel **p** is calculated as follows:

$$LBP(\mathbf{p}) = \sum_{i=0}^{7} 2^i S\{\, G[\mathbf{N}(\mathbf{p}, i)] - \ G(\mathbf{p})\} \tag{3.2}$$

where $G(\mathbf{p})$ and $G[\mathbf{N}(\mathbf{p}, i)]$ are the gray level of the pixel **p** and its neighbor $\mathbf{N}(\mathbf{p}, i)$, respectively. S is a threshold function that is defined as follows:

$$S(x_i - x_c) = \begin{cases} 1, & \text{if } x_i \geq x_c; \\ 0, & \text{otherwise.} \end{cases} \tag{3.3}$$

7	6	5
0	**p**	4
1	2	3

Figure 3.1 The 3 × 3 neighborhood of a pixel **p** and the label of its neighbors.

LBP can achieve gray-scale invariance because only the signs of the differences between the center pixel and its neighbors rather than their exact values are used to define the LBP code. Figure 3.2 shows an example of computing the LBP code. The left 3 × 3 matrix displays a neighborhood of a center pixel whose gray level is 4. After thresholding, the right 3 × 3 matrix reveals the signs of the differences between the center pixel and its neighbors. The binary LBP code is 11010011, which corresponds to 211 in decimal.

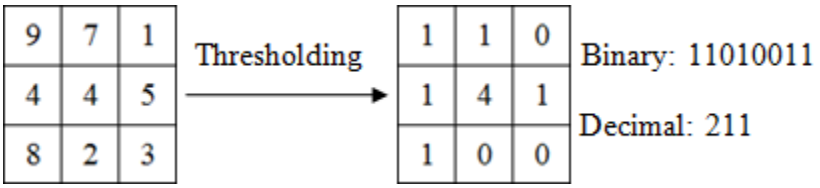

Figure 3.2 An example of the LBP computation.

3.2 Distance Transform and Distance Vector

The features in FLBP are broadly defined. Different features could be used by different pattern recognition tasks. For a certain type of features, many feature pixels can be extracted from an image. FLBP uses distance transform and distance vector to locate a feature pixel for an image pixel.

A Feature extracted from an image can be represented by a binary image. In a binary image, each pixel assumes one of two discrete values: 0 or 1. While pixels of value 0 are called the background pixels, pixels of 1 are called feature pixels. For a given metric δ, the distance transform of an image is an assignment to each pixel **p** of the distance between **p** and the nearest feature pixel **q**:

$$D(\mathbf{p}) = \delta(\mathbf{p}, \mathbf{q}) \tag{3.4}$$

$$\mathbf{q} = \arg \min_{\mathbf{r} \in F} \delta(\mathbf{p}, \mathbf{r}) \tag{3.5}$$

where F is the set of all feature pixels of the binary image, and the distance map D is called the distance transform. Since the Euclidean distance is widely used in many image applications, several algorithms with linear time complexity have been developed for the fast computation of the Euclidean distance transform (Maurer et al., 2011), (Costa, 2008). One shortcoming of the distance transform is that it does not contain the exact location of the nearest feature pixels. To overcome this shortcoming, a new concept of Distance Vector Field (DVF) is presented by assigning to each pixel **p** of a vector **dv**

which points to its nearest feature point **q (**Danielson, 1980). Specifically, for a given distance metric δ, the DVF of an image may be defined as follows:

$$\mathbf{dv}(\mathbf{p}) = \mathbf{q} - \mathbf{p} \tag{3.6}$$

Figure 3.3 shows an example of a binary image, its Distance Vector Field (DVF), and the Euclidean distance transform. Note that the upper left pixel has coordinates (1, 1) in a Cartesian coordinate system with a horizontal axis pointing to the right and a vertical axis pointing downwards. In particular, the binary image in Figure 3.3(a) has only one feature pixel at the location (2, 2). Figure 3.3(b) displays the DVF where the numbers are derived using Equation 3.6, and Figure 3.3(c) shows the Euclidean distance transform where the numbers are calculated using Equations 3.4 and 3.5.

0	0	0	0
0	1	0	0
0	0	0	0

(a)

1,1	0,1	-1,1	-2,1
1,0	0,0	-1,0	-2,0
1,-1	0,-1	-1,-1	-2,-1

(b)

1.4	1.0	1.4	2.2
1.0	0.0	1.0	2.0
1.4	1.0	1.4	2.2

(c)

Figure 3.3 (a) An example of a binary image. (b) The Distance Vector Field (DVF). (c) The Euclidean distance transform.

3.3 Feature Local Binary Patterns — the General Form (FLBP)

In order to define the general form of FLBP, the concepts of True Center (TC) and Virtual Center (VC) are introduced as follows:

Definition 1: True Center (TC) is the center pixel of a given neighborhood.

Definition 2: Virtual Center (VC) is a pixel used to replace the center pixel of a given neighborhood.

Let **p** and **q** represent a pixel and its nearest feature pixel, respectively. Let **dv** be the distance vector pointing from **p** to **q** as defined by Equation 3.6. Note that **dv** is used to replace **dv**(**p**) for simplicity. Let $\mathbf{C}_t(\mathbf{p})$ and $\mathbf{C}_v(\mathbf{p})$ be the TC and VC of **p**, respectively. The TC, which may be any pixel on the path from **p** to **q**, is defined as follows:

$$\mathbf{C}_t(\mathbf{p}) = \mathbf{p} + \alpha_t \mathbf{dv} \tag{3.7}$$

where $\alpha_t \in [0, 1]$ is a parameter that controls the location of the TC. When $\alpha_t = 0$, the TC is **p**; when $\alpha_t = 1$, the TC is **q**; and when $0 < \alpha_t < 1$, the TC is a pixel on the path between **p** and **q**. Similarly, the VC, which may be any pixel on the path from **p** to **q** as well, is defined as follows:

$$\mathbf{C}_v(\mathbf{p}) = \mathbf{p} + \alpha_v \mathbf{dv} \tag{3.8}$$

where $\alpha_v \in [0, 1]$ is a parameter that controls the location of the VC. When $\alpha_v = 0$, the VC is **p**; when $\alpha_v = 1$, the VC is **q**; and when $0 < \alpha_v < 1$, the VC is a pixel on the path between **p** and **q**.

The general form of FLBP is defined as follows:

$$FLBP(\mathbf{p}) = \sum_{i=0}^{7} 2^i S\{ G[\mathbf{N}(\mathbf{C}_t(\mathbf{p}), i)] - G[\mathbf{C}_v(\mathbf{p})] \} \tag{3.9}$$

where $\mathbf{N}(\mathbf{C}_t(\mathbf{p}), i)$ represents the neighbors of the TC. $G[\mathbf{C}_v(\mathbf{p})]$ and $G[\mathbf{N}(\mathbf{C}_t(\mathbf{p}), i)]$ are the gray levels of the VC and the neighbors of the TC, respectively. S is a threshold function. Equation 3.3 provides one definition of the function. Another definition of the threshold function introduces a fixed bias b (Kumar, 2009):

$$S(x_i - x_c) = \begin{cases} 1, & \text{if } x_i \geq x_c + b; \\ 0, & \text{otherwise.} \end{cases} \tag{3.10}$$

To increase flexibility, this dissertation introduces a threshold function using a relative bias:

$$S(x_i - x_c) = \begin{cases} 1, & \text{if } x_i \geq (1 + \beta)x_c; \\ 0, & \text{otherwise.} \end{cases} \tag{3.11}$$

where β is a parameter that controls the contribution of x_c to the bias.

9	7	1
4	4	5
8	2	3

(a)

1	0	0
0		0
1	0	0

(b)

1	1	0
0		1
1	0	0

(c)

1	1	0
0		0
1	0	0

(d)

Figure 3.4 (a) A 3 × 3 image. (b) The LBP thresholding result using a fixed bias (b = 4) threshold function. (c) The LBP thresholding result using a relative bias (β = 0.1) threshold function. (d) The LBP thresholding result using a relative bias (β = 0.3) threshold function.

Figure 3.4 shows the different LBP thresholding results when different threshold functions are applied. In particular, Figure 3.4(a) displays a 3 × 3 image, and Figure

3.4(b), (c), and (d) exhibit the LBP thresholding results using a fixed bias (b = 4) threshold function (Equation 3.10), a relative bias (β = 0.1) threshold function (Equation 3.11), and a relative bias (β = 0.3) threshold function (Equation 3.11), respectively.

Next is an example of the computation of FLBP code. Figure 3.5(a) shows a grayscale image. The upper left pixel is assumed at location (1, 1) in a Cartesian coordinate system with a horizontal axis pointing to the right and a vertical axis pointing downwards. As discussed before, the feature pixels in FLBP are broadly defined. In this example, for simplicity, the pixel at the coordinates (6, 6) is randomly picked as the only feature pixel. The corresponding binary feature image of Figure 3.5(a) is shown in Figure 3.5(b). Because the pixel at the coordinates (6, 6) in Figure 3.5(a) is the only pixel, the pixel becomes the only feature pixel in the binary image shown in Figure 3.5(b). Not surprisingly this feature pixel becomes the nearest one for all the pixels in Figure 3.5(a).

70	10	92	1	3	2	7
91	50	45	66	1	4	9
30	56	30	77	10	2	8
1	58	62	64	20	31	1
2	1	91	34	60	26	52
4	3	4	22	28	90	61
9	5	8	1	20	10	40

(a)

0	0	0	0	0	0	0
0	0	0	0	0	0	0
0	0	0	0	0	0	0
0	0	0	0	0	0	0
0	0	0	0	0	0	0
0	0	0	0	0	1	0
0	0	0	0	0	0	0

(b)

Figure 3.5 (a) A grayscale image used in the examples of FLBP computation. (b) The binary feature image derived by extracting feature pixel from Figure 5(a).

Figure 3.5(a) shows the computation of the FLBP code of the pixel **p** at coordinates (2, 2). First, the **dv** pointing from **p** to its nearest feature pixel **q** is computed. Given $\mathbf{p} = [2, 2]^t$, and $\mathbf{q} = [6, 6]^t$, $\mathbf{dv} = \mathbf{q} - \mathbf{p}$ is equal to $[4, 4]^t$. On the path pointed by the **dv**, the locations of TC and VC which are controlled by the parameters α_t and α_v can be

determined. After TC and VC are located, the FLBP code can be computed. Figure 3.6 shows two examples of the computation of FLBP with different locations of TC and VC. In Figure 3.6(a) given $\alpha_t = 0.75$ and $\alpha_v = 0.25$, $\mathbf{C}_t(\mathbf{p}) = \mathbf{p} + \alpha_t\mathbf{dv}$ is equal to $[5, 5]^t$, and $\mathbf{C}_v(\mathbf{p}) = \mathbf{p} + \alpha_v\mathbf{dv}$ is equal to $[3, 3]^t$. Therefore, the TC is the pixel at location (5, 5) and the VC is the pixel at location (3, 3). According to Equation 3.9, the binary FLBP code: $FLBP(2, 2) = 10101001$ is obtained by replacing the gray level 60 of the TC by the gray level 30 of the VC as the new threshed of the neighbors of the TC. Figure 3.6(b) shows another example of the $FLBP(2, 2)$ computation when $\alpha_t = 0.25$, and $\alpha_v = 0.75$. Similarly, the TC is the pixel at location (3, 3) and the VC is the pixel at location (5, 5). The binary FLBP code becomes: $FLBP(2, 2) = 00111100$.

FLBP has the following special cases:

- LBP is a special case of FLBP.

  When $\alpha_v = \alpha_t = 0$, the VC and TC coincide with the center pixel **p**, and FLBP becomes LBP, where no feature pixels are involved. LBP compares the center pixel **p**, with its own neighbors.

- FLBP Form 1 — FLBP1.

  When $\alpha_v = 0$, pixel **p** becomes the VC, and the TC may be any pixel on the distance vector **dv**. FLBP1 compares the center pixel **p** which is used as the threshold, with the neighbors of the TC.

- FLBP Form 2 — FLBP2.

  When $\alpha_t = 0$, pixel **p** becomes the TC, and the VC may be any pixel on the distance vector **dv**. FLBP2 compares the VC which is used as the threshold, with the neighbors of the center pixel **p**.

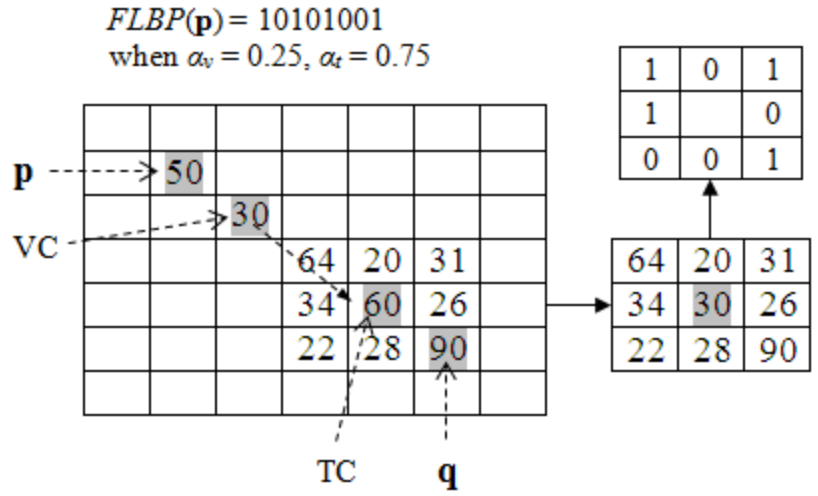

(a)

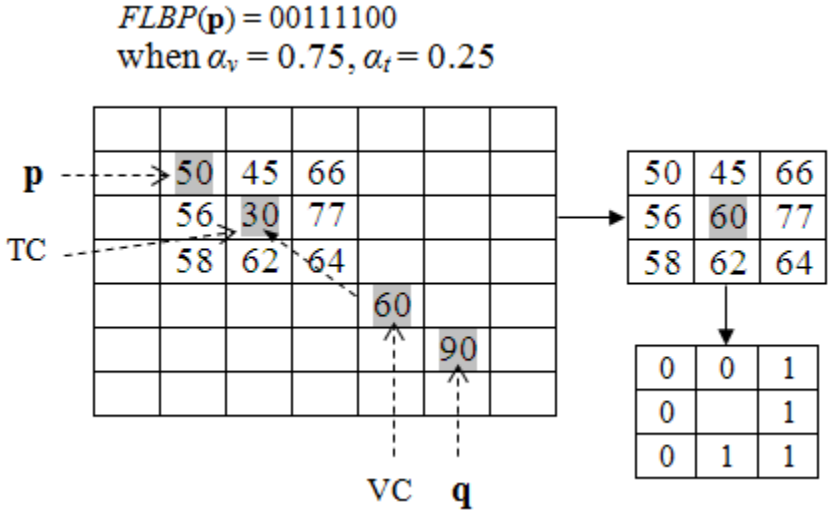

(b)

Figure 3.6 The computation of FLBP for the pixel at (2, 2). (a) An example when TC (α_t = 0.75) is at (5, 5) and VC (α_v = 0.25) is at (3, 3) (b) An example when TC (α_t = 0.25) is at (3, 3) and VC (α_v = 0.75) is at (5, 5).

3.4 Feature Local Binary Patterns—Form 1 (FLBP1)

FLBP1, which is a special case of FLBP, when α_v = 0, may be defined as follows:

$$FLBP1(\mathbf{p}) = \sum_{i=0}^{7} 2^i S\{\, G[\mathbf{N}(\mathbf{C}_t(\mathbf{p}), i)] - \, G(\mathbf{p}) \,\} \tag{3.12}$$

where $G(\mathbf{p})$ and $G[\mathbf{N}(\mathbf{C}_t(\mathbf{p}), i)]$ are the gray levels of the center pixel **p** and the neighbors of the TC, respectively. Equation 3.12 shows that FLBP1 compares the center pixel **p** with the neighbors of the TC, which may be any pixel on the distance vector **dv**.

Figure 3.7 illustrates the computation of FLBP1 using the same grayscale image and binary feature image shown in Figure 3.5. Figure 3.7(a) shows an example of FLBP1 at (2, 2) when $\alpha_t = 1$. The TC becomes the feature pixel **q** at (6, 6) when $\alpha_t = 1$. The binary FLBP1 code becomes: *FLBP1*(2, 2) = 10110000. Figure 3.7(b) shows another example of FLBP1 at (2, 2) when $\alpha_t = 0.5$. $\mathbf{C}_t(\mathbf{p}) = \mathbf{p} + \alpha_t\mathbf{dv}$ is equal to $[4, 4]^t$. As a result, the TC is the pixel at location (4, 4). The binary FLBP1 code becomes*: FLBP1(2, 2)* = 01001011.

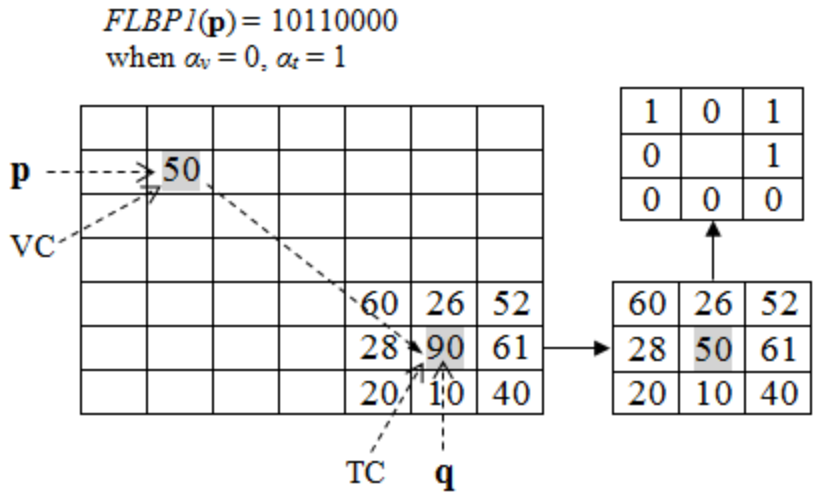

(a)

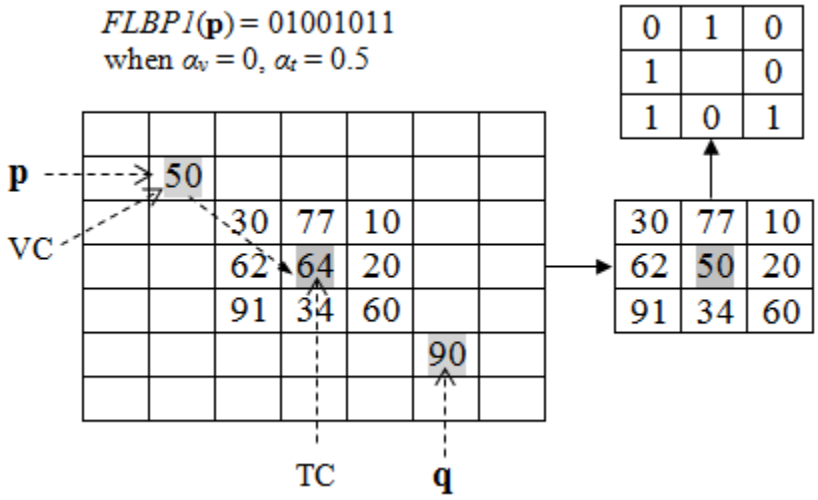

(b)

Figure 3.7 The computation of FLBP1 for the pixel at (2, 2). (a) An example when TC (α_t = 1) is at (6, 6). (b) An example when TC (α_t = 0.5) is at (4, 4).

3.5 Feature Local Binary Patterns—Form 2 (FLBP2)

FLBP2, which is another special case of FLBP, when α_t = 0, may be defined as follows:

$$FLBP2(\mathbf{p}) = \sum_{i=0}^{7} 2^i S\{\, G[\mathbf{N}(\mathbf{p}, i)] - \, G[\mathbf{C}_v(\mathbf{p})] \,\} \tag{3.13}$$

where $G[\mathbf{C}_v(\mathbf{p})]$ and $G[\mathbf{N}(\mathbf{p}, i)]$ are the gray levels of the VC and the neighbors of the center pixel **p**, respectively. Equation 3.13 shows that FLBP2 compares the VC, which may be any pixel on the distance vector **dv**, with the neighbors of the center pixel **p**.

Figure 3.8 illustrates the computation of FLBP2 using the same grayscale image and binary feature image shown in Figure 3.5. Figure 3.8(a) shows an example of FLBP2 at (2, 2) when α_v = 1. The VC becomes the feature pixel **q** when α_v = 1. The binary FLBP2 code becomes: *FLBP2*(2, 2) = 00100001. Figure 3.8(b) shows another example of FLBP2 when α_v = 0.5. $\mathbf{C}v(\mathbf{p}) = \mathbf{p} + \alpha_v\mathbf{dv}$ is equal to $[4, 4]^t$. As a result, the VC is at location (4, 4). The binary FLBP2 code becomes: *FLBP2*(2, 2) = 10100001.

Figure 3.9 shows an example of the FLBP representation of a face image. The traditional LBP representation is also included for comparison. Specifically, Figure 3.9(a) and (b) display a face image and its binary feature image derived using the Canny edge detector. Figure 3.9(c) shows the LBP representation of the face image of Figure 3.9(a). Figure 3.9(d), (e), (f), and (g) exhibit the FLBP1 representations when α_t = 0.25, 0.5, 0.75, 1, respectively. Figure 3.9(h), (i), (j), and (k) show the FLBP2 representations when α_v = 0.25, 0.5, 0.75, 1, respectively.

Figure 3.9 shows that LBP has only one face representation, and FLBP can have many different face representations using different parameter values. The feature pixels used in the FLBP are broadly defined. Different feature pixels also lead to different FLBP representations. Different FLBP representations can serve different purposes for texture description and pattern recognition. FLBP encodes much richer information than LBP

does. Not only does FLBP encode both local and feature information, but it also enhances its representational power and flexibility by incorporating a number of parameters, such as the CT parameter α_t, the VT parameter α_v, as well as the relative bias parameter β.

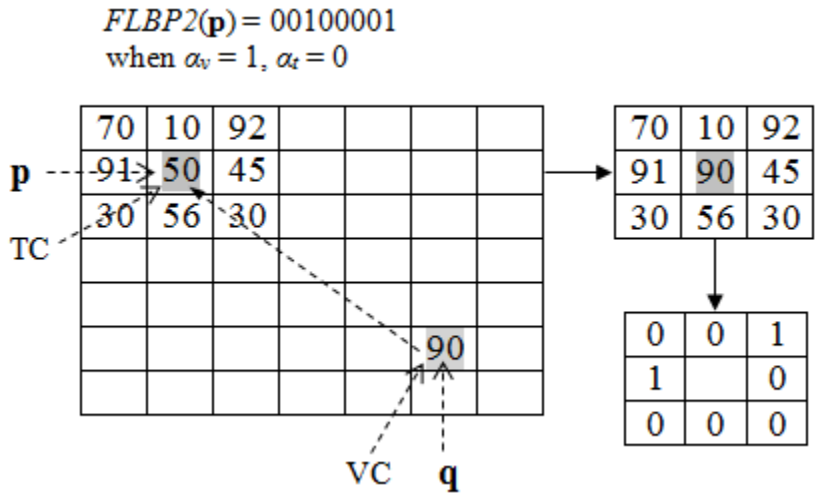

(a)

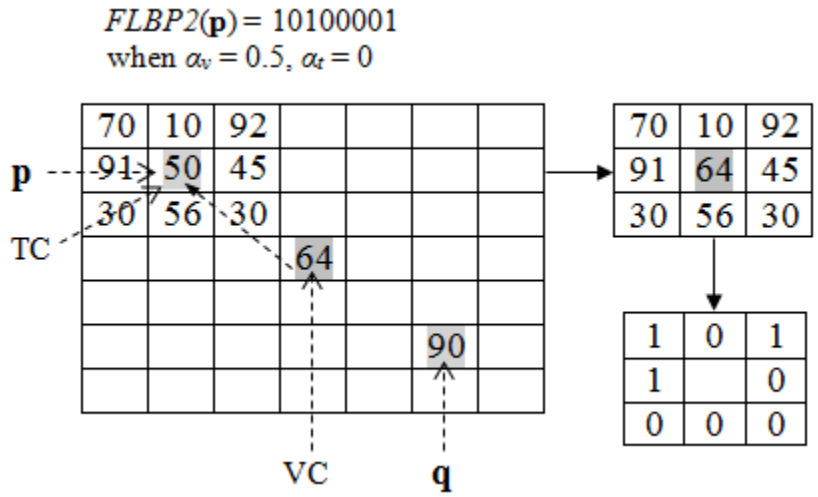

(b)

Figure 3.8 The computation of FLBP2 for the pixel at (2, 2) (a) An example when VC (α_v = 1) is at (6, 6). (b) An example when VC (α_v = 0.5) is at (4, 4).

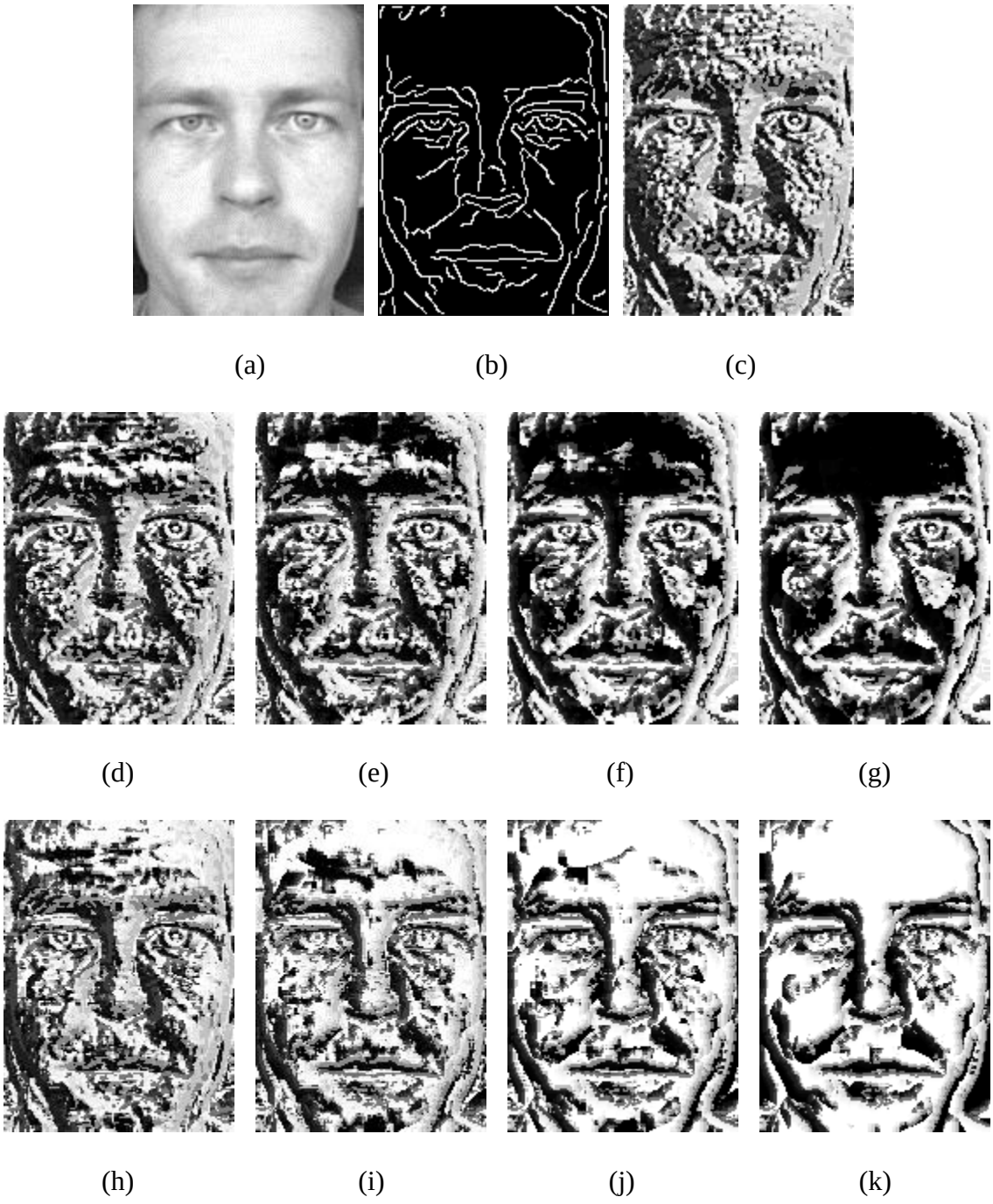

Figure 3.9 (a) A face image. (b) The binary feature image of Figure 9(a) derived using the Canny edge detector. (c) The LBP representation of the face image. (d)–(g) The FLBP1 representations when α_t = 0.25, 0.5, 0.75, 1, respectively. (h)–(k) The FLBP2 representations when α_v = 0.25, 0.5, 0.75, 1, respectively.

CHAPTER 4

LOCAL QUATERNARY PATTERNS AND FEATURE LOCAL QUATERNARY PATTERNS

This chapter first reviews LTP, and then introduces the new local texture descriptor, Local Quaternary Patterns (LQP) and its extension, Feature Local Quaternary Patterns (FLQP). LQP, which encodes four relationships of local texture, includes more information of local texture than the Local Binary Patterns (LBP) and Local Ternary Patterns (LTP). FLQP which encodes both local and feature information is expected to perform better than LQP for texture description and pattern recognition.

4.1 Local Ternary Pattern

Tan and Triggs (2010) introduced Local Ternary Pattern or LTP operator. In LTP the threshold function is defined as follows:

$$S_{ltp}(g_i, g_c, r) = \begin{cases} 1, & \text{if } g_i \geq g_c + r \\ 0, & \text{if } |g_i - g_c| < r \\ -1, & \text{if } g_i \leq g_c - r \end{cases} \tag{4.1}$$

where *r* is the radius of the interval around the grey level of the central pixel. Figure 4.1 shows an example of the computation of LTP. The grey level of the central pixel is 40 and *r* is 5. A neighbor pixel is assigned to 1, 0 or -1, if its grey level is greater than or equal to 45, between 44 and 36, or less than or equal to 35, respectively. The total number of the possible LTP codes is 6561, which leads to a large size for the feature

dimension and sparse histograms of the LTP codes. To solve the problem, an LTP code is split into two binary codes: the positive and negative halves as shown in Figure 4.1. The positive half of LTP (PLTP) is obtained by replacing -1 with 0. The negative half of LTP (NLTP) is obtained by first replacing the 1 with 0 and then changing -1 to 1. Thus an LTP code can be represent by two binary codes. As a result, the total number of the split LTP codes is reduced to 512.

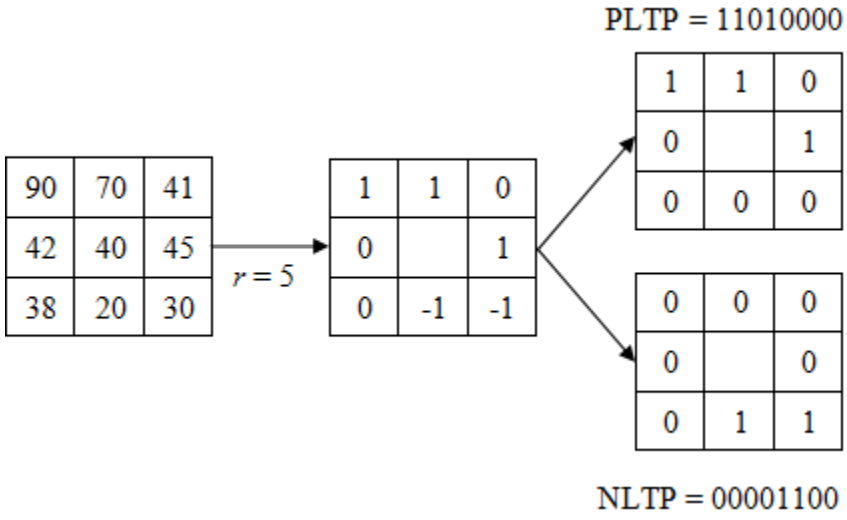

Figure 4.1 Computing the LTP and splitting it to two binary codes, PLTP and NLTP.

4.2 Local Quaternary Patterns

The new Local Quaternary Patterns (LQP) encodes four relationships of local texture, and therefore, it includes more information of local texture than LBP and LTP. The threshold function of LQP is defined using two binary digits as follows:

$$S_{lqp}(g_i, g_c, r) = \begin{cases} 11, & \text{if } g_i \geq g_c + r \\ 10, & \text{if } g_c \leq g_i < g_c + r \\ 01, & \text{if } g_c - r \leq g_i < g_c \\ 00, & \text{if } g_i < g_c - r \end{cases} \quad (4.2)$$

where r is the radius of the interval around the value of the central pixel and may be defined as follows.

$$r = c + \tau g_c \quad (4.3)$$

Where c is a constant and τ is a parameter to control the contribution of g_c to r. To reduce the total number of codes, an LQP code can be split into two binary codes, the upper and lower halves as shown in Figure 4.2. The upper half of LQP (ULQP) is obtained by extracting the first digit of LQP code. The lower half of LTP (LLQP) is obtained by extracting the second digit of LQP code. Thus the total number of LQP codes is reduced to 512.

From Equation 4.2 the threshold functions of ULQP and LLQP, S_{ulqp} and S_{llqp} can be derived as follows:

$$S_{ulqp}(g_i, g_c) = S_{lbp}(g_i, g_c) \quad (4.4)$$

$$S_{llqp}(g_i, g_c, r) = \begin{cases} 1, & \text{if } g_i \geq g_c + (-1)^{[1-S_{lbp}(g_i, g_c)]} r; \\ 0, & \text{otherwise.} \end{cases} \quad (4.5)$$

The threshold function of ULQP S_{ulqp} is equal to the threshold function of LBP and is not depend on the r. The ULQP and LLQP are defined as follows:

$$ULQP(\mathbf{p}) = LBP(\mathbf{p}) \tag{4.6}$$

$$LLQP(\mathbf{p}) = \sum_{i=0}^{7} 2^i S_{llqp}\{ G[\mathbf{N}(\mathbf{p}, i)], G(\mathbf{p}), r \} \tag{4.7}$$

Note that the ULQP is the same as the LBP which is defined by Equation 3.2. Figure 4.2 shows an example of the computation of the LQP. The grey level of the central pixel is 40 and r is 5. The ULQP code is 11110001. For LLQP, a pixel is assigned 1 if it is greater than or equal to 45, or it is less than 40 and greater than or equal to 35, otherwise is assigned 0. The LLQP code is 11010010.

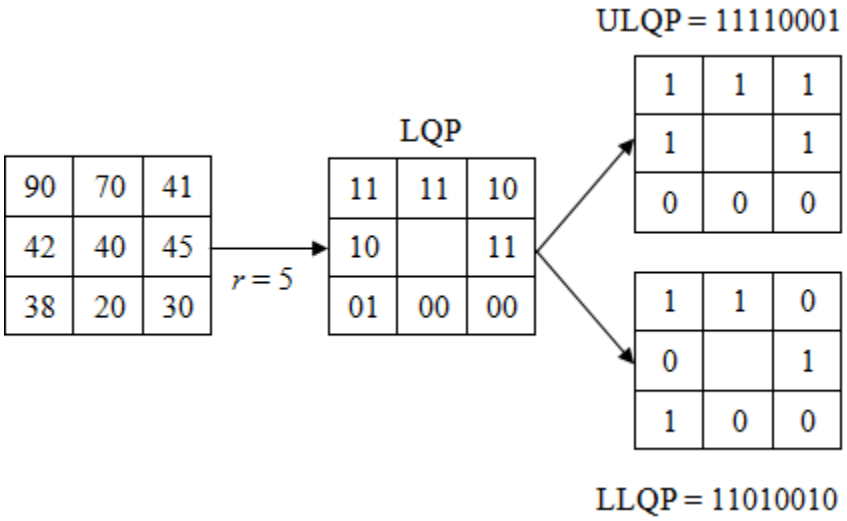

Figure 4.2 Computing the LQP and splitting it to two binary codes ULQP and LLQP.

4.3 Feature Local Quaternary Patterns

LQP can be extended to FLQP using the method of FLBP introduced in chapter 3. To reduce the total number of codes, an FLQP code can be split into two binary codes, the upper half of FLQP (UFLQP) and the lower half of FLQP (LFLQP) using the threshold functions defined in Equations. 4.4 and 4.5, respectively. The UFLQP is equivalent to the FLBP which is defined by Equation 3.9. The general form of UFLQP and LFLQP is defined below:

$$UFLQP(\mathbf{p}) = FLBP(\mathbf{p}) \tag{4.8}$$

$$LFLQP(\mathbf{p}) = \sum_{i=0}^{7} 2^i S_{llqp}\{ G[\mathbf{N}(\mathbf{C}_t(\mathbf{p}), i)], G[\mathbf{C}_v(\mathbf{p})], r \} \tag{4.9}$$

Figure 4.3 shows the FLQP computation of the pixel **p** at coordinates (2, 2) when r = 5. The grayscale image and the feature binary image are the same as those in Figure 3.5. First, the **dv** pointing from **p** to its nearest feature pixel **q** is computed. Given **p** = $[2, 2]^t$, and **q** = $[6, 6]^t$, **dv** = **q** − **p** is equal to $[4, 4]^t$. On the path pointed by the **dv**, the locations of TC and VC which are controlled by the parameters α_t and α_v can be determined. In Figure 4.3(a) given α_t = 0.75 and α_v = 0.25, $\mathbf{C}_t(\mathbf{p})$ = **p** + α_t**dv** is equal to $[5, 5]^t$, and $\mathbf{C}_v(\mathbf{p})$ = **p** + α_v**dv** is equal to $[3, 3]^t$. Therefore, the TC is the pixel at location (5, 5) and the VC is the pixel at location (3, 3). After replacing the grey level 60 of TC by the grey level 30 of VC, UFLQP(2, 2) is equal to 10101001 which is equal to FLBP, and

LFLQP(2, 2) is equal to 1001110. Figure 4.3(b) shows the FLQP computation of the pixel **p** at (2, 2) when $\alpha_v = 0.75$, and $\alpha_t = 0.25$. Using the same method as the example in Figure 4.3(a), UFLQP(2, 2) and LFLQP(2, 2) are obtained as 00111100 and 00110011, respectively.

Figure 4.4 shows an example of the FLQP and LQP representations of a face image when $r = 10$. The face image and the binary feature image derived by Canny edge detector are the same as Figure 3.9(a) and Figure 3.9(b). Figure 4.4(a) shows the LLQP image. The ULQP image is the same as LBP image in Figure 3.9(c). Figure 4.4(b) - (e) show LFLQP images when $\alpha_t = 0.25, 0.5, 0.75, 1$, respectively, and $\alpha_v = 0$. Their corresponding UFLQP are the same as Figure 3.9(d) – (g). Figure 4.4(f) - (i) show LFLQP images when $\alpha_v = 0.25, 0.5, 0.75, 1$, respectively, and $\alpha_t = 0$. Their corresponding UFLQP are the same as Figure 3.9(h) – (k).

Figure 4.5 shows another example of the FLQP representations when $r = 0.1g_c$. The face image and the binary feature image derived by Canny-Edge detector are the same as Figure 3.9(a) and Figure 3.9(b). Figure 4.5(a) shows the LLQP image. The ULQP image is the same as LBP image in Figure 3.9(c). Figure 4.5(b) - (e) show LFLQP images when $\alpha_t = 0.25, 0.5, 0.75, 1$, respectively, and $\alpha_v = 0$. Their corresponding UFLQP are the same as Figure 3.9(d) – (g). Figure 4.5(f) - (i) show LFLQP images when $\alpha_v = 0.25, 0.5, 0.75, 1$, respectively, and $\alpha_t = 0$. Their corresponding UFLQP are the same as Figure 3.9(h) – (k).

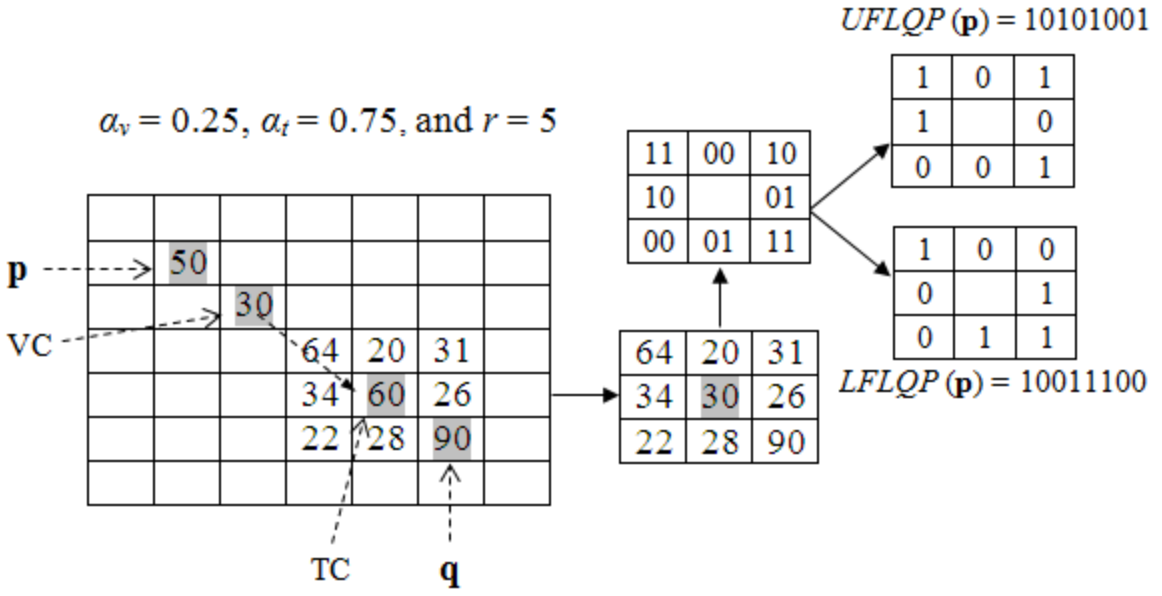

(a)

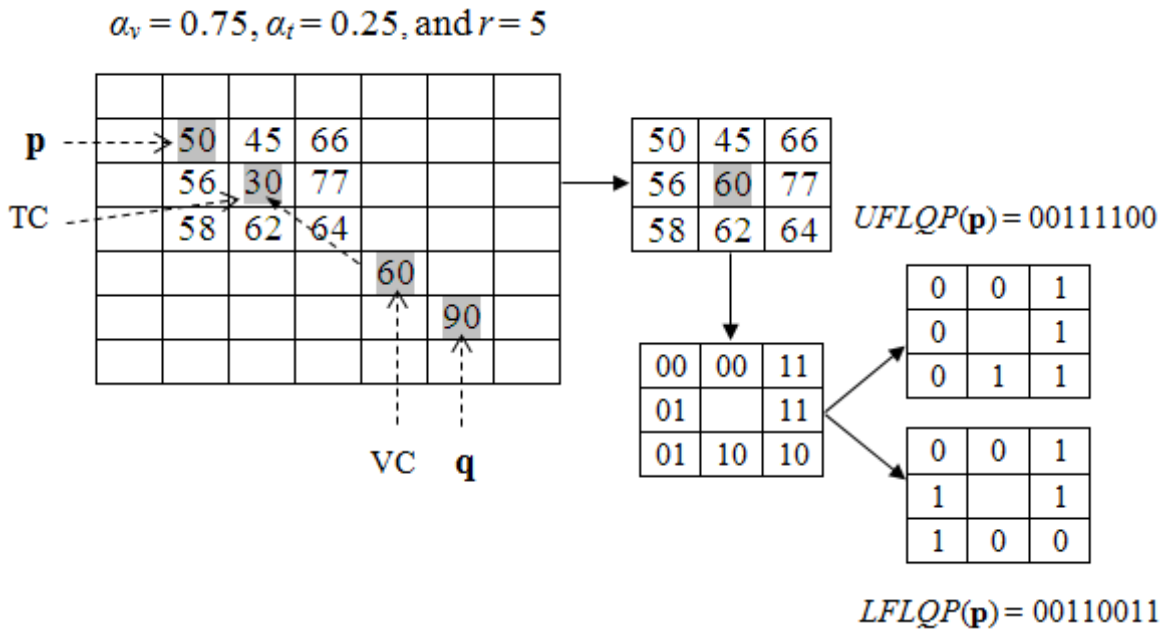

(b)

Figure 4.3 The computation of FLQP (a) The TC (α_t = 0.75), the VC (α_v = 0.25), r = 5, and the LFLQP code for the pixel at (2, 2). (b) The TC (α_t = 0.25), the VC (α_v = 0.75), r = 5 and the LFLQP code for the pixel at (2, 2).

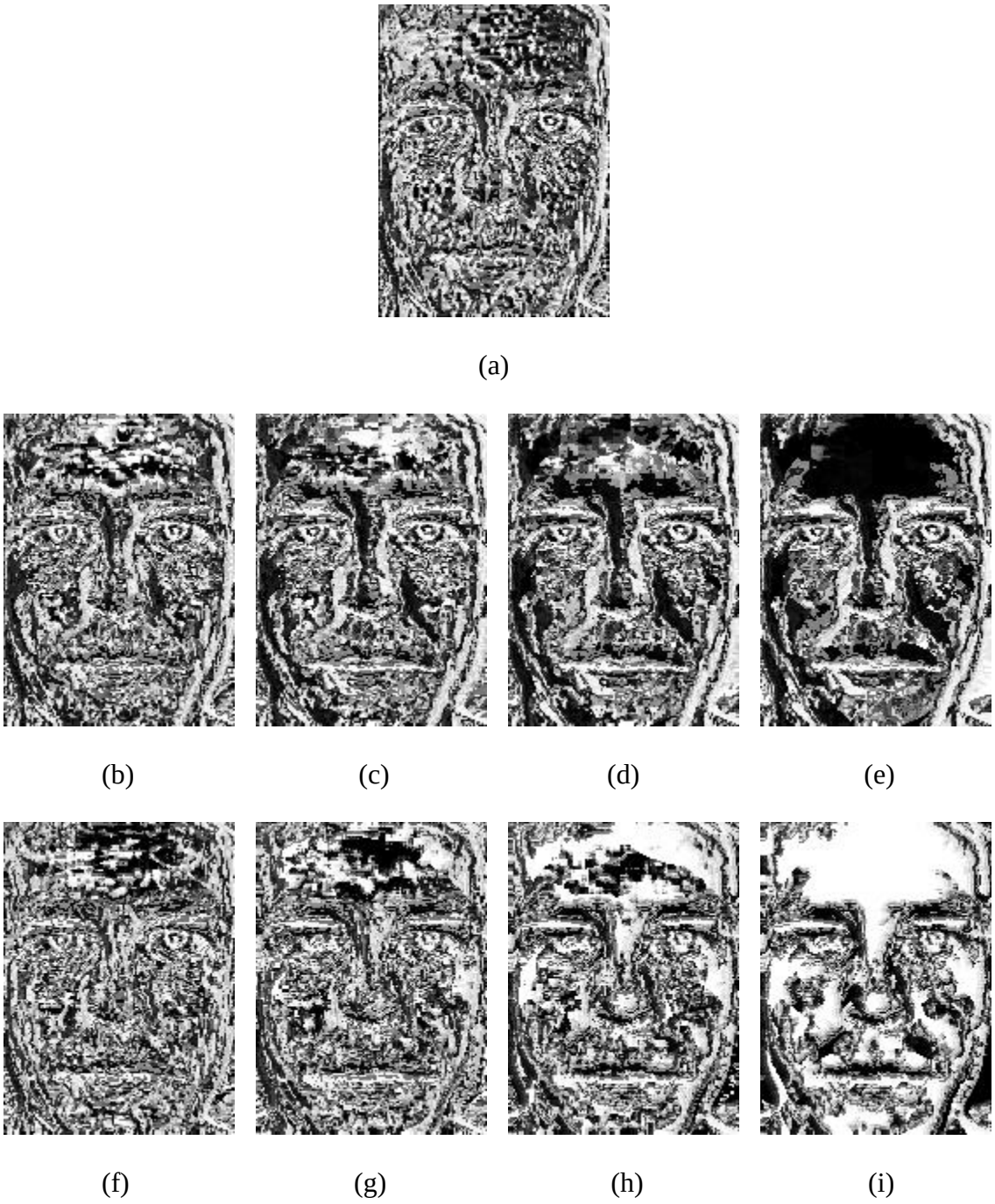

(a)

(b) (c) (d) (e)

(f) (g) (h) (i)

Figure 4.4 The FLQP representations of a face image when r = 10 (a) The LLQP image (b) - (e) The LFLQP images when α_t = 0.25, 0.5, 0.75, 1, respectively, and α_v = 0 (f) - (i) The LFLQP images when α_v = 0.25, 0.5, 0.75, 1, respectively, and α_t = 0.

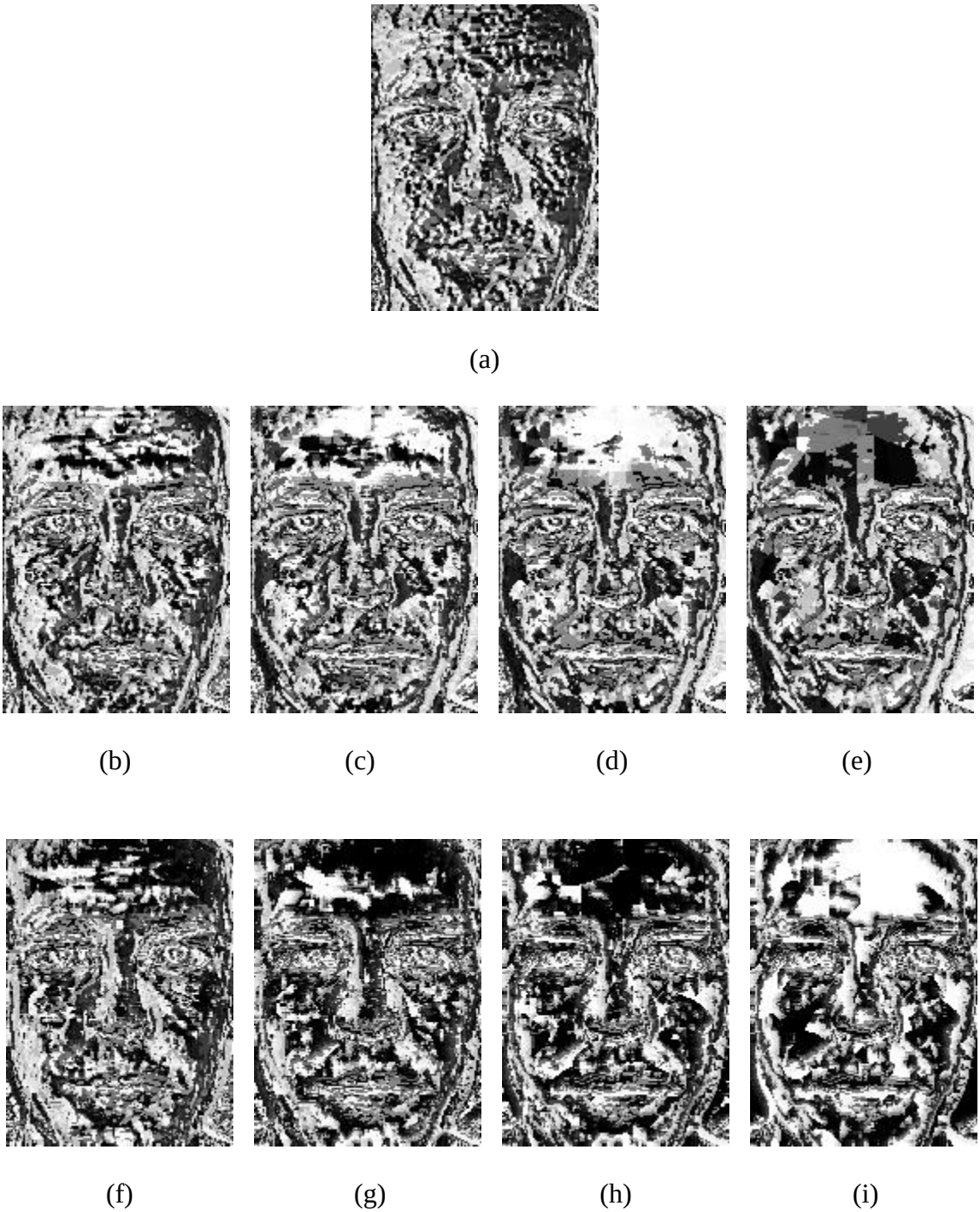

(a)

(b) (c) (d) (e)

(f) (g) (h) (i)

Figure 4.5 The FLQP representations of a face image when $r = 0.1g_c$ (a) The LLQP image (b) - (e) The LFLQP images when α_t = 0.25, 0.5, 0.75, 1, respectively, and $\alpha_v = 0$ (f) - (i) The LFLQP images when α_v = 0.25, 0.5, 0.75, 1, respectively, and $\alpha_t = 0$

CHAPTER 5

APPLICATION OF FLBP AND FLQP TO EYE DETECTION

Eye detection has broad applications in automated facial recognition, where a face can be located first by applying, for example, the Bayesian Discriminating Features (BDF) method (Liu, 2003, 2004, 2006, 2007, 2008), (Liu and Yang, 2009). After a face is located in an image, the eyes on the face can be accurately detected by the application of the FLBP and FLQP methods. This chapter first introduces a new feature pixel extraction method, the LBP with Relative Bias Thresholding (LRBT) method, and then descripts the system architecture of eye detection method and the histogram and similarity computation for the eye detection method.

5.1 A New Feature Pixel Extraction Method — LBP with Relative Bias Thresholding

As the FLBP and FLQP methods encode both local and feature information, the performance of FLBP and FLQP depend on the extraction of the feature pixels. For eye detection, the shape of eye constitutes one of the most prominent features. To amplify such information around the eye region, this dissertation presents a new feature pixel extraction method, the LBP with Relative Bias Thresholding (LRBT) method. In particular, the LRBT method first computes the LBP representation using the relative bias threshold function of Equation 3.11 with a given β. An LBP image is then defined by the LBP representation. The LRBT method converts the LBP image to a binary LRBT feature image, whose feature pixels correspond to those whose LBP code is greater than 0, and the background pixels correspond to the pixels in the LBP image with the LBP

code 0. Note that different binary LRBT feature images can be generated with different β values.

Figure 5.1 shows the LBP images and the corresponding binary LRBT feature images of the face image shown in Figure 3.9(a). Specifically, Figure 5.1(a), (b), and (c) display the LBP images when β = 0.05, 0.1, 0.2, respectively. Figure 5.1(d), (e), and (f) exhibit the binary LRBT feature images when β = 0.05, 0.1, 0.2, respectively.

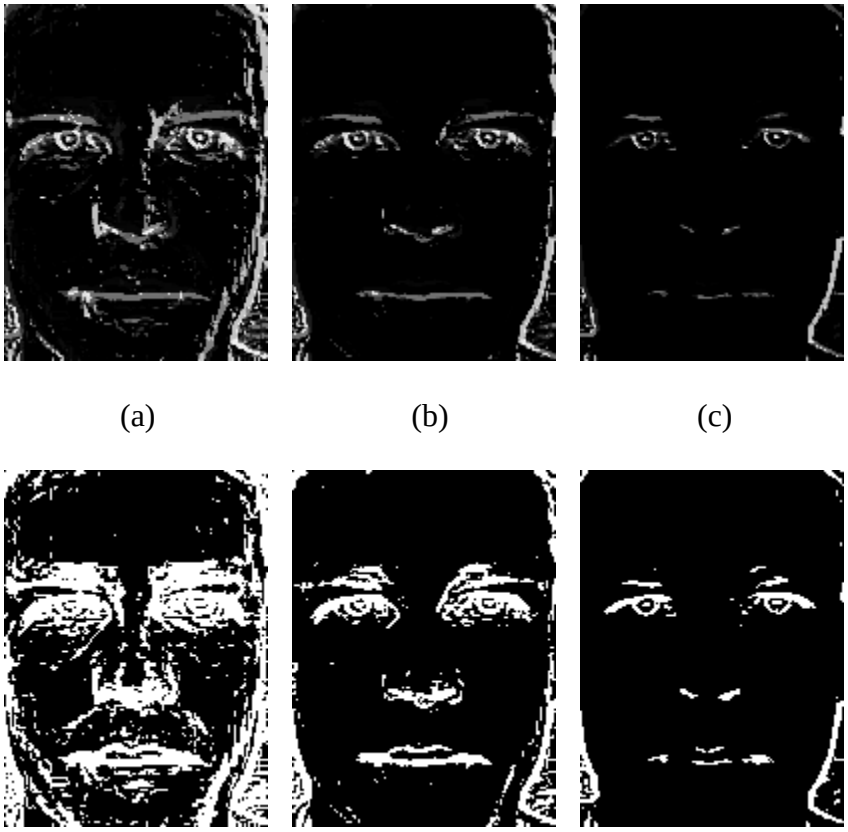

Figure 5.1 LBP images and the corresponding binary LRBT feature images of a face image. (a)–(c) The LBP images when β = 0.05, 0.1, 0.2, respectively. (d)–(f) The binary LRBT feature images when β = 0.05, 0.1, 0.2, respectively.

Figure 5.2 shows the FLBP1 and FLBP2 representations of the face image that applies the binary LRBT feature image shown in Figure 5.1(e) when $\beta = 0.1$. Specifically, Figure 5.2(a), (b), (c), and (d) display the FLBP1 representations when α_t = 0.25, 0.5, 0.75, 1, respectively. Figure 5.2(e), (f), (g), and (h) exhibit the FLBP2 representations when α_v = 0.25, 0.5, 0.75, 1, respectively.

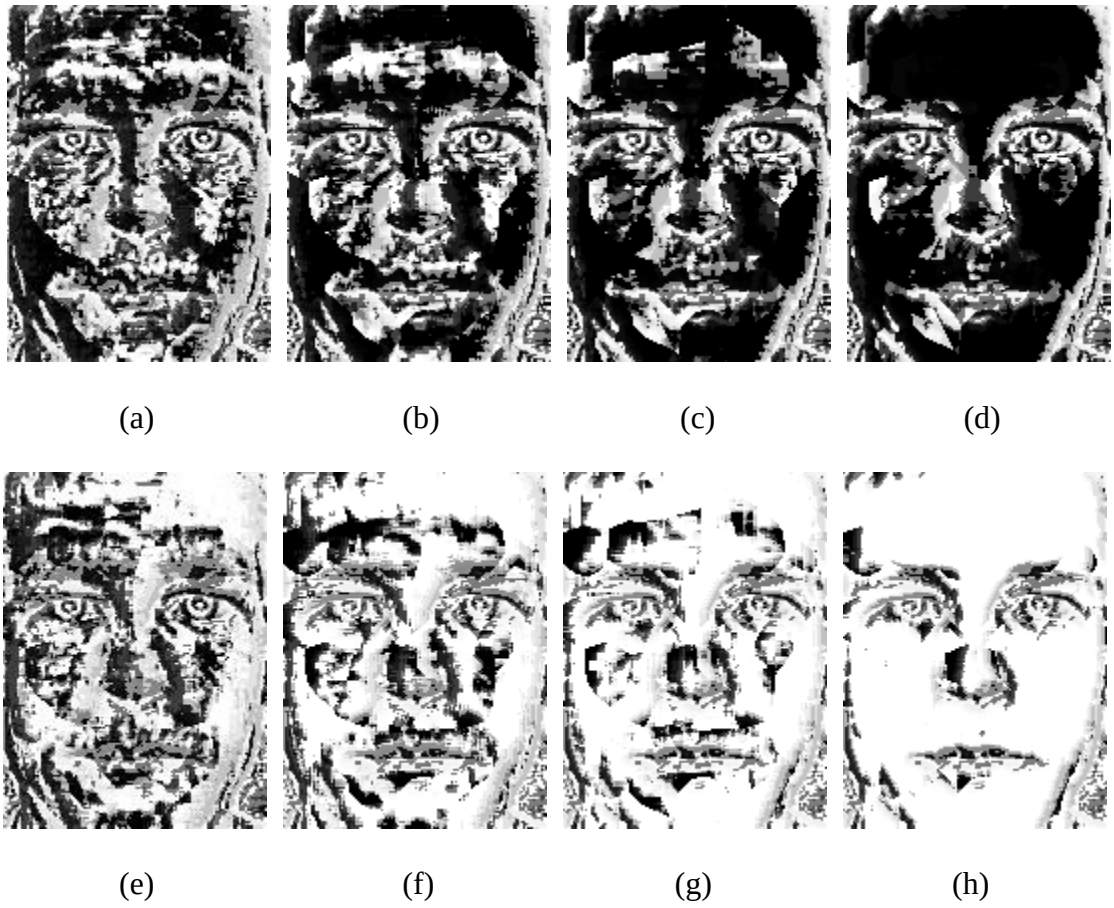

Figure 5.2 The FLBP1 and FLBP2 representations of a face image using the binary LRBT feature pixels when $\beta = 0.1$. (a)–(d) The FLBP1 images when α_t = 0.25, 0.5, 0.75, 1, respectively. (e)–(h) The FLBP2 images when α_v = 0.25, 0.5, 0.75, 1, respectively.

5.2 The FLBP-Based Eye Detection Method

5.2.1 System Architecture of Eye Detection Method

Figure 5.3 shows the system architecture of our FLBP-based eye detection method that consists of three major steps. First, a binary feature image, which contains the feature pixels of the grayscale face image, is derived by applying the LBP with Relative Biased Threshold (LRBT) method. Second, the FLBP representation of the face image is formed based on the grayscale image and a distance vector field or DVF. DVF is obtained by computing the distance vector between each pixel and its nearest feature pixel defined in the binary image. Finally, for eye detection, an eye template is first constructed from a number of training eye samples. The eye template is defined by the mean FLBP histograms of the training eye samples. Each eye candidate is compared with the eye template based on the FLBP histogram and a similarity measure, whose computation is implemented by a fast algorithm. The eye candidate with the largest similarity is selected as the detected eye center.

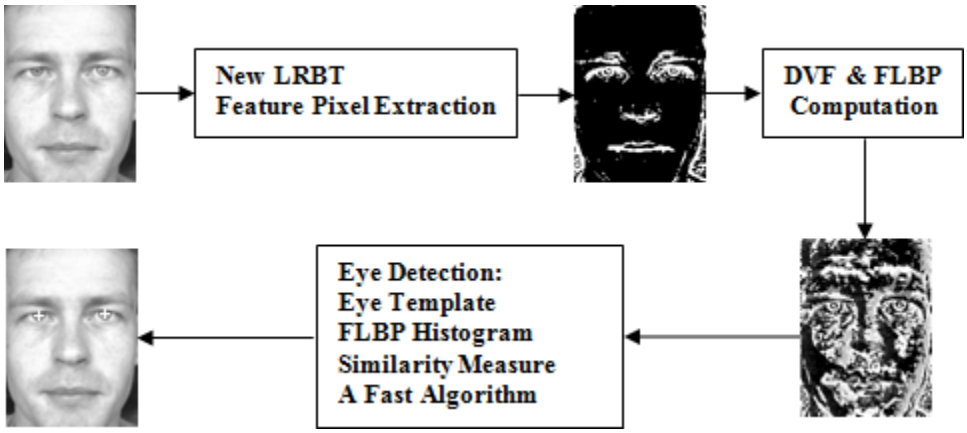

Figure 5.3 The system architecture of the FLBP-based eye detection method.

5.2.2 Histogram and Similarity Computation

This section discusses the FLBP histogram and similarity computation for the eye detection method. Let the eye template and an eye candidate window be divided into a grid of $r \times c$ cells. A FLBP histogram of a cell is formed by the FLBP codes of the pixels in the cell. The eye template is defined by the $r \times c$ mean FLBP histograms of the training eye samples. Let T and C represent the eye template and eye candidate windows, respectively. The following similarity measure $M(C, T)$ is applied to compare T and C:

$$M(C,T) = -\sum_{i=1}^{g}\sum_{j=1}^{b}\frac{\left(C_{i,j} - T_{i,j}\right)^2}{C_{i,j} + T_{i,j}} \tag{5.1}$$

where $C_{i,j}$ represents the j-th bin of the FLBP histogram of the i-th cell of the eye candidate window, $T_{i,j}$ represents the j-th bin of the FLBP histogram of the i-th cell of the eye template, $g = rc$ is the total number of cells of the $r \times c$ grid, and b is the number of bins of a histogram.

An exhaustive search of eye location may compare an eye candidate window centered at every pixel in a face image with the eye template. The pixel whose eye candidate window has the largest similarity value with the eye template is the location of the detected eye. Let the spatial resolution of the face image and the eye template be $m \times n$ and $w \times h$, respectively. The FLBP-based eye detection method includes three steps. The time complexity of extracting LRBT feature in the first step, and deriving the DVF and computing FLBP in the second step is O(mn). The complexity of computing the FLBP histogram and similarity for an eye candidate window in the third step is O(wh)

and O(*gb*), respectively. As a result, the total time for searching a face image is O(*whmn*) and O(*gbmn*) for FLBP histogram and similarity computation, respectively. Because O(*mn*) is smaller than O(*whmn*) and O(*gbmn*), the time complexity of the FLBP method is the larger one of O(*whmn*) and O(*gbmn*).

To reduce the computational complexity of FLBP histogram and similarity computation a fast method is used for the eye detection. Figure 5.4 shows a search region, which contains an eye candidate window with a spatial resolution of $w \times h$, the top left pixel at (x_1, y_1), and the lower right pixel at (x_w, y_h). For simplicity, an eye candidate window is represented by the upper left pixel. Suppose the FLBP histogram and similarity for window at (x_1, y_1) have been computed, and then the eye template is moved to the next column to compare the next eye candidate window at $(x_1 + 1, y_1)$ with the eye template. Now the difference between these two eye candidate windows resides in column x_1 and column $x_w + 1$. If column x_1 is removed from and column $x_w + 1$ is added to window (x_1, y_1), the new window is window $(x_1 + 1, y_1)$. Since the FLBP histogram and similarity for window (x_1, y_1) is already computed, the new results for window $(x_1 + 1, y_1)$ can be obtained by examining the difference between columns x_1 and $x_w + 1$.

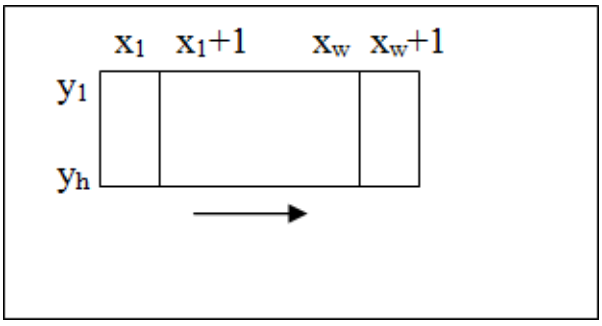

Figure 5.4 A search region that contains an eye candidate window with a spatial resolution of $w \times h$, the top left pixel at (x_1, y_1), and the lower right pixel at (x_w, y_h).

The fast computation method works as follows.

First, assign the FLBP histogram and similarity of window (x_1, y_1) to window (x_1 + 1, y_1).

Second, update the FLBP histogram for window (x_1 + 1, y_1) as follows: (i) for each pixel in column x_1, reduce 1 from the histogram bin corresponding to its FLBP code; and (ii) for each pixel in column x_1 + 1, add 1 to the histogram bin corresponding to its FLBP code. The time complexity for FLBP histogram computation is now reduced to O(h) from O(wh).

Third, update the similarity for window (x_1 + 1, y_1) as follows: (i) save the similarity values for every histogram bin of window (x_1, y_1); (ii) for every histogram bin that has been updated, subtract the old similarity value, recalculate the similarity value, and add the new value to the similarity.

The time complexity for similarity computation is now reduced to O(h) from O(b), as h, which is the height of the eye candidate window, is much smaller than b, which is the number of bins of the histogram. Note that the reduced time complexity is independent of b. The significance of the fast method is that it runs equally fast no matter it is applied to the three-level texture analysis method with 6561 histogram bins or the LBP method with 256 histogram bins.

The eye candidate window in Figure 5.4 is not divided into a grid. If the eye template and an eye candidate window are divided into a grid of $r \times c$ cells, the time complexities for FLBP histogram and similarity computation using the fast method are both O(ch) which are smaller than O(wh) and O(rcb), the time complexity of FLBP

histogram and similarity computation using the exhaustive search, respectively. Using the fast method, the total time for searching an $m \times n$ face image is O(*chmn*) for both FLBP histogram and similarity computation. Therefore, the time complexity of the FLBP method is also O(*chmn*).

This dissertation comparatively assesses the LBP and FLBP on the eye detection. The LBP method uses less time than the FLBP method because it does not include the computation of LRBT feature extraction and DVF. However, the time complexity of the LBP method is determined by the histogram and similarity computation. Because the histogram and similarity computation of the LBP method is the same as the computation of the FLBP method, the time complexity of the LBP method is the same as the time complexity of the FLBP method.

Figure 5.4 shows that the eye candidate window moves horizontally to the next column. If the eye candidate window moves vertically, the fast method works as well by examining the difference between the rows y_1 and $y_h + 1$. The time complexity for FLBP histogram and similarity computation is O(*w*), where *w* is usually not equal to *h*. If *w* is greater than *h*, moving the window row by row is faster, otherwise, moving the window column by column is faster.

Viola and Jones (2004) introduced the integral image to rapidly computer the sum of the pixels within arbitrary rectangular regions. The integral image at location (*x*, *y*) contains the sum of the pixels above and to the left of (*x*, *y*). The integral image can be computed in one pass over the original image. The sum of the pixels on a rectangular region can be computed using the four integral image values at the corners of the rectangular region. The integral image has been extended to extract histogram from a

rectangular region by building an integral image for each bin of the histogram. The time complexity to compute a histogram in a rectangular regions is O(*b*) which is larger than O(*h*) the time complexity of the method used in FLBP eye detection. However, for an object detection task where *b* is smaller than the *h* and *w* the integral image should be used. For example, one experiment conducted in this dissertation is to test each method by computing the histogram of each 64 x 64 candidate window on a 384 x 286 image using MATLAB codes. The average CPU time spent are 7.33, 2.93, 0.21 and 0.17 seconds by the conventional method, the integral image of 256 bins histogram, the method used in FLBP eye detection and the integral image of 16 bins histogram, respectively. A system with different software and hardware could have different CPU time. This experiment is to demonstrate that an appropriate method should be chosen based on the number of bins and the dimensions of the candidate window.

5.3 The FLQP-based Eye Detection Method

Figure 5.5 shows the system architecture of FLQP-based eye detection method that consists of three major steps. The first step is same as the FLBP-based eye detection method. A binary feature image is derived from the grayscale face image by applying LRBT method. In the Second step, the FLQP code is computed based on the grayscale image and a distance vector field or DVF. The FLQP code is then split to two binary codes, from which two images, UFLQP and LFLQP images are formed. Finally, each eye candidate is compared with the eye template based on the UFLQP and LFLQP histograms and similarity measures. The eye template is defined by UFLQP and LFLQP mean histograms of the training eye samples. The similarity measure to compare the UFLQP and LFLQP histograms of an eye template and an eye candidate is defined by

Equation 5.1. The final similarity measure is the sum of similarity values of the UFLQP and LFLQP histograms. The eye candidate with the largest final similarity is selected as the detected eye center.

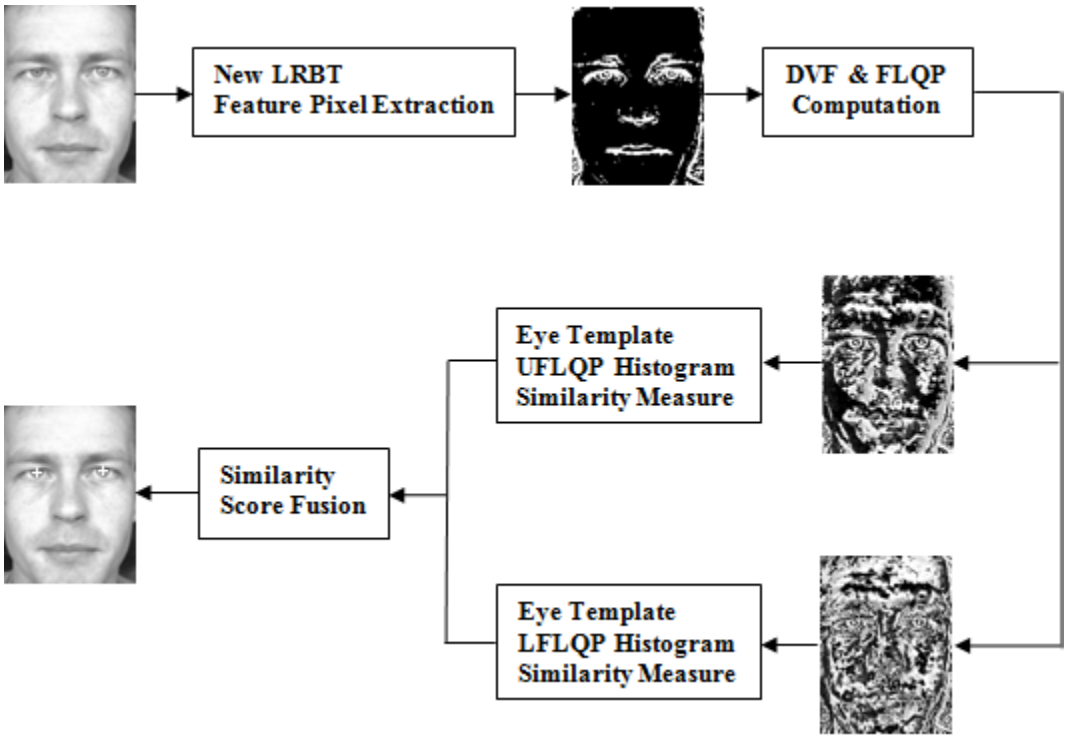

Figure 5.5 The system architecture of the FLQP-based eye detection method.

5.4 FLBP Application on Gradient Images

In addition to apply FLBP on grayscale image, this dissertation also applies FLBP on gradient images. The gradient of a grayscale image I can be derived by convolving with a filter as follows:

$$G_x = K_x * I, \qquad G_y = K_y * I \tag{5.2}$$

where G_x and G_y are the gradient components in horizontal and vertical directions, respectively. K_x and K_y are the filter kernel in horizontal and vertical directions, respectively. * denotes convolution operation. The gradient magnitude image can be created as follows:

$$|\nabla I| = \sqrt{{G_x}^2 + {G_y}^2}) \tag{5.3}$$

The gradient direction image can be created as follows:

$$\theta = \arctan\frac{G_y}{G_x} \tag{5.4}$$

One of the common filters is Sobel filter which uses the following kernel:

$$K_x = \begin{bmatrix} -1 & 0 & 1 \\ -2 & 0 & 2 \\ -1 & 0 & 1 \end{bmatrix}, \qquad K_y = \begin{bmatrix} -1 & -2 & -1 \\ 0 & 0 & 0 \\ 1 & 2 & 1 \end{bmatrix} \tag{5.5}$$

This dissertation designs a new filter which computes the gradient along the two diagonal directions and projects to the horizontal and vertical directions. The kernel of the new filter is defined as follows:

$$K_{x'} = \begin{bmatrix} 0 & \cos(\pi/4) & 1 \\ -\cos(\pi/4) & 0 & \cos(\pi/4) \\ -1 & -\cos(\pi/4) & 0 \end{bmatrix},$$
$$K_{y'} = \begin{bmatrix} -1 & -\cos(\pi/4) & 0 \\ -\cos(\pi/4) & 0 & \cos(\pi/4) \\ 0 & \cos(\pi/4) & 1 \end{bmatrix} \quad (5.6)$$

where *x'* and *y'* represent the two diagonal directions. The experimental results show the new filter achieves better performance than the Sobal filter in the FLBP eye detection method.

The system architecture to detect eye from the gradient images is similar to the one shown in Figure 5.3. First the LRBT features are extracted from the grayscale image. Second the DVF is obtained using the extracted LRBT features binary image. Two FLBP representations of a face image are formed from the gradient magnitude and direction images. Finally, each eye candidate is compared with the eye template based on the FLBP histograms of the gradient magnitude and direction images. The similarity measure is defined by Equation 5.1. The eye candidate with the largest similarity is selected as the detected eye center.

CHAPTER 6

EXPERIMENTAL RESULTS OF FLBP-BASED METHOD

The FLBP-based method is assessed using the public BioID and color FERET databases. The BioID database contains 1,521 grayscale frontal face images with spatial resolution of 384 × 286. The images in the BioID database, which are formed in real world conditions, pose challenges to eye detection, such as illumination variations, eye glasses, and closed eyes. Figure 6.1 shows some examples of the face images in the BioID database. The facial images are cropped and normalized to the size of 132 × 178.

Figure 6.1 The examples of the face images in the BioID database.

Source: BioID AG. https://www.bioid.com/

All 1,986 color frontal face images with spatial resolution of 512 × 768 from the *fa* and *fb* sets of the FERET database are used in our experiments. All color images are converted to grayscale images. The facial images are cropped and normalized to the size of 132 × 178. Figure 6.2 shows some examples of the face images in the FERET database.

Figure 6.2 The examples of the face images in the FERET database.
Source: http://www.nist.gov/itl/iad/ig/feret.cfm.

To construct the eye template, 70 pairs of eye samples that are not from the BioID and FERET databases are collected. As only the right eye template is constructed due to the symmetry between right and left eyes, the 70 left eyes are flipped horizontally to double the number of the right eye samples. To detect the left eye, first the face image is

flipped horizontally, and then detect eye in the flipped image by comparing it with the right eye template. Figure 6.3 shows some right eye samples that are cropped to size of 37 × 17.

Figure 6.3 The right eye samples that are cropped to 37×17.

Eye detection performance is measured by the relative distance error in two forms. The first form measures the performance of each individual eye and is defined as follows:

$$\gamma = \frac{d_1}{d_2} \tag{6.1}$$

where d_1 is the Euclidean distance between the detected eye center and the ground truth eye center, and d_2 is the interocular distance — the distance between the two ground truth eye centers. The detected eye center is considered inside the eye region, inside the iris, and inside the pupil, when $\gamma \leq 0.25, 0.1, 0.05$, respectively. The second form measures the performance of a pair of eyes by the worse eye and is defined as follows:

$$\gamma_p = \max(\gamma_l, \gamma_r) \tag{6.2}$$

where γ_l and γ_r are the γ of the left and right eyes, respectively. The success rate for $\gamma \leq 0.25, 0.1, 0.05$, $\gamma_p \leq 0.25, 0.1, 0.05$ and the average γ and γ_p are used to assess the performance of the eye detection method.

6.1 Assessment of Neighborhood Size

As the FLBP method may apply a neighborhood of different size, first the effect of neighborhood size on eye detection performance is assessed on the BioID database. In particular, Figures 3.1 and 6.4 show the 3 × 3 and 5 × 5 neighborhood, respectively. Note that in the 5 × 5 neighborhood, only the labeled neighbors with numbers from 0 to 7 are used to compute the FLBP code. Table 6.1 shows the success rates for $\gamma \leq 0.25, 0.1, 0.05$ and the average γ of eye detection using the FLBP1, FLBP2, and LBP methods corresponding to the 3 × 3 and 5 × 5 neighborhood. Table 6.2 shows the success rates for $\gamma_p \leq 0.25, 0.1, 0.05$ and the average γ_p of eye detection using the FLBP1, FLBP2, and LBP methods corresponding to the 3 × 3 and 5 × 5 neighborhood. The grid size of the eye candidate windows and the eye template is 3 × 4 for all the methods. The feature pixels for the FLBP1 and FLBP2 methods are from the binary LRBT feature image. Both Table 6.1 and Table 6.2 reveal that the eye detection performance corresponding to the 5 × 5 neighborhood is better than the 3 × 3 neighborhood. Therefore, the 5×5 neighborhood is applied for the remaining experiments.

7		6		5
0		**p**		4
1		2		3

Figure 6.4 The 5 × 5 neighborhood of the center pixel and the labels of its neighbors.

Table 6.1 The Success Rates for $\gamma \leq 0.25$, 0.1, 0.05 and the Average γ of the FLBP1, FLBP2, and LBP Eye Detection Methods using the 3 × 3 and 5 × 5 Neighborhoods

Method		**Size**	$\gamma \leq 0.25$	$\gamma \leq 0.1$	$\gamma \leq 0.05$	**Average γ**
FLBP1	$\beta = 0.1$, $\alpha_t = 1$	5 × 5	97.86	93.23	85.57	0.0442
		3 × 3	96.35	92.60	79.91	0.0542
	$\beta = 0.2$, $\alpha_t = 0.25$	5 × 5	97.67	93.98	86.52	0.0427
		3 × 3	97.53	94.71	84.78	0.0460
FLBP2	$\beta = 0.1$, $\alpha_v = 1$	5 × 5	93.33	89.05	83.10	0.0560
		3 × 3	89.58	84.71	74.75	0.0787
	$\beta = 0.2$, $\alpha_v = 0.25$	5 × 5	98.65	95.23	87.84	0.0385
		3 × 3	96.38	92.41	83.10	0.0543
LBP		5 × 5	92.34	90.34	83.14	0.0812
		3 × 3	90.57	87.18	75.48	0.0990

Table 6.2 The Success Rates for $\gamma_p \leq 0.25$, 0.1, 0.05 and the Average γ_p of the FLBP1, FLBP2, and LBP Eye Detection Methods using the 3 × 3 and 5 × 5 Neighborhoods

Method		**Size**	$\gamma_p \leq 0.25$	$\gamma_p \leq 0.1$	$\gamma_p \leq 0.05$	**Average γ_p**
FLBP1	$\beta = 0.1$, $\alpha_t = 1$	5 × 5	96.58	88.95	77.25	0.0605
		3 × 3	94.15	88.30	67.39	0.0755
	$\beta = 0.2$, $\alpha_t = 0.25$	5 × 5	96.25	90.14	78.44	0.0583
		3 × 3	96.25	91.65	75.35	0.0626
FLBP2	$\beta = 0.1$, $\alpha_v = 1$	5 × 5	89.09	83.30	74.36	0.0785
		3 × 3	83.69	76.07	61.60	0.1124
	$\beta = 0.2$, $\alpha_v = 0.25$	5 × 5	97.83	92.44	80.14	0.0513
		3 × 3	94.15	87.84	72.72	0.0767
LBP		5 × 5	87.44	84.62	73.37	0.1207
		3 × 3	85.73	79.88	61.67	0.1418

6.2 Assessment of Grid Size

The effect of the grid size of the eye candidate window on eye detection performance is assessed next on the BioID database. The eye candidate window is divided into three different grids which are 3 × 3, 3 × 4, and 4 × 4 grids shown in Figure 6.5.

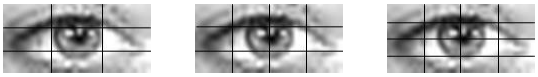

(a) (b) (c)

Figure 6.5 The eye window grids (a) The 3 × 3 grid. (b) The 3 × 4 grid. (c) The 4 × 4 grid.

The FLBP1, FLBP2 and LBP methods are implemented using these three different grids for eye detection. The feature pixels for the FLBP1 and FLBP2 methods are from the binary LRBT feature image. Table 6.3 shows the success rates for $\gamma \leq 0.25$, 0.1, 0.05 and the average γ of eye detection of the FLBP1, FLBP2, and LBP methods using the 3 × 3, 3 × 4, and 4 × 4 grids. Table 6.4 shows the success rates for $\gamma_p \leq 0.25$, 0.1, 0.05 and the average γ_p of eye detection of the FLBP1, FLBP2, and LBP methods using the 3 × 3, 3 × 4, and 4 × 4 grids. The results show that the 3 × 4 grid yields the best overall eye detection performance. Therefore, the 3 × 4 grid is applied for the remaining experiments.

Table 6.3 The Success Rates for $\gamma \leq 0.25$, 0.1, 0.05 and the Average γ of the FLBP1, FLBP2, and LBP Eye Detection Methods using the 3 × 3, 3 × 4, and 4 × 4 Grids

Method		**Grid**	$\gamma \leq 0.25$	$\gamma \leq 0.1$	$\gamma \leq 0.05$	**Average γ**
FLBP1	$\beta = 0.1$, $\alpha_t = 1$	3×3	97.70	89.71	74.52	0.0516
		3×4	97.86	93.23	85.57	0.0442
		4×4	96.88	92.44	84.35	0.0478
	$\beta = 0.2$, $\alpha_t = 0.25$	3×3	97.53	89.94	74.19	0.0522
		3×4	97.67	93.98	86.52	0.0427
		4×4	97.57	93.75	85.54	0.0444
FLBP2	$\beta = 0.1$, $\alpha_v = 1$	3×3	93.69	85.80	70.97	0.0684
		3×4	93.33	89.05	83.10	0.0560
		4×4	91.85	87.38	80.80	0.0634
	$\beta = 0.2$, $\alpha_v = 0.25$	3×3	98.19	90.53	75.51	0.0494
		3×4	98.65	95.23	87.84	0.0385
		4×4	98.46	94.74	86.26	0.0402
LBP		3×3	91.35	85.96	70.02	0.0952
		3×4	92.34	90.34	83.14	0.0812
		4×4	91.91	89.71	81.95	0.0835

Table 6.4 The Success Rates for $\gamma_p \leq 0.25$, 0.1, 0.05 and the Average γ_p of the FLBP1, FLBP2, and LBP Eye Detection Methods using the 3 × 3, 3 × 4, and 4 × 4 Grids

Method		**Grid**	$\gamma_p \leq 0.25$	$\gamma_p \leq 0.1$	$\gamma \leq 0.05$	**Average γ_p**
FLBP1	$\beta = 0.1$, $\alpha_t = 1$	3×3	96.25	83.50	61.87	0.0699
		3×4	96.58	88.95	77.25	0.0605
		4×4	94.94	87.84	75.61	0.0652
	$\beta = 0.2$, $\alpha_t = 0.25$	3×3	96.12	84.68	62.00	0.0698
		3×4	96.25	90.14	78.44	0.0583
		4×4	96.06	89.81	76.86	0.0607
FLBP2	$\beta = 0.1$, $\alpha_v = 1$	3×3	89.88	78.11	56.54	0.0947
		3×4	89.09	83.30	74.36	0.0785
		4×4	86.79	81.13	71.07	0.0889
	$\beta = 0.2$, $\alpha_v = 0.25$	3×3	97.11	84.75	61.87	0.0669
		3×4	97.83	92.44	80.14	0.0513
		4×4	97.44	91.26	77.45	0.0541
LBP		3×3	85.73	77.65	55.36	0.1415
		3×4	87.44	84.62	73.37	0.1207
		4×4	86.85	83.76	71.47	0.1240

6.3 Comparative Assessment of FLBP and LBP

After determining the best neighborhood size and grid size, the eye detection performance of FLBP and LBP methods are comparatively assessed on the BioID database. Many face images on the BioID database wear eyeglasses or close eyes. The performance of FLBP and LBP methods is assessed using the controlled and uncontrolled face image sets. The uncontrolled set includes all face images. The controlled set includes only the face images which are eye opening and without eyeglasses.

6.3.1 Using the Uncontrolled Face Image Set

The uncontrolled face image set includes all 1521 face images in the BioID database. Tables 6.5 and 6.6 show the success rates of the FLBP1, FLBP2, and LBP eye detection methods for $\gamma \leq 0.25, 0.1, 0.05$ and $\gamma_p \leq 0.25, 0.1, 0.05$ using the uncontrolled face image set, respectively. The feature pixels for the FLBP1 and FLBP2 methods are from the binary LRBT feature image. Three FLBP1 and FLBP2 experiments are selected to compare with the LBP method. Each of the FLBP1 or FLBP2 experiments has either one of the highest success rates for γ or $\gamma_p \leq 0.25, 0.1, 0.05$ or one of the top three highest success rate for γ or $\gamma_p \leq 0.05$.

In particular, Table 6.5 reveals that the success rates of both FLBP1 and FLBP2 when $\gamma \leq 0.25, 0.1$ and 0.05 are around 98%, 95% and 87%, respectively. In comparison, the success rates of LBP are about 92%, 90% and 84% which are lower than the success rates achieved by either FLBP1 or FLBP2. Table 6.6 also shows that the success rates or $\gamma_p \leq 0.25, 0.1, 0.05$ of both FLBP1 and FLBP2 are higher than the success rates of the LBP method. Therefore, the experimental results show that FLBP achieves better eye detection performance than LBP.

Figures 6.6 and 6.7 are the graphs of the success rates of the FLBP and LBP for γ and γ_p from 0.05 to 0.5, respectively. The FLBP shown in the graph is the FLBP2 when $\beta = 0.2$, $\alpha_v = 0.25$ which has the highest success rates among all methods in table 6.5 and 6.6. Figures 6.6 and 6.7 show that the success rates of the FLBP method reach 100% as the γ and γ_p increase, while the success rates of the LBP method are lower than 95% and 90% for γ and γ_p, respectively. The gap between the two curves increases when the γ and

γ_p increase. This indicates that the success rate of FLBP increases faster than the success rate of LBP when the γ and γ_p increase.

Table 6.5 The Success Rates for $\gamma \leq 0.25, 0.1, 0.05$ of the FLBP1, FLBP2, and LBP Eye Detection Methods using the Uncontrolled Face Image Set

Method		$\gamma \leq 0.25$	$\gamma \leq 0.1$	$\gamma \leq 0.05$
FLBP1	LRBT, $\beta = 0.2$, $\alpha_t = 0.12$	97.86	**95.10**	**87.41**
	LRBT, $\beta = 0.1$, $\alpha_t = 0.25$	98.03	94.74	87.21
	LRBT, $\beta = 0.15$, $\alpha_t = 0.25$	**98.13**	93.75	86.00
FLBP2	LRBT, $\beta = 0.2$, $\alpha_v = 0.25$	**98.65**	**95.23**	**87.84**
	LRBT, $\beta = 0.15$, $\alpha_v = 0.25$	98.55	95.04	87.51
	LRBT, $\beta = 0.25$, $\alpha_v = 0.25$	98.62	94.44	87.08
LBP		92.34	90.34	83.14

Table 6.6 The Success Rates for $\gamma_p \leq 0.25, 0.1, 0.05$ of the FLBP1, FLBP2, and LBP Eye Detection Methods using the Uncontrolled Face Image Set

Method		$\gamma_p \leq 0.25$	$\gamma_p \leq 0.1$	$\gamma_p \leq 0.05$
FLBP1	LRBT, $\beta = 0.2$, $\alpha_t = 0.12$	96.52	**92.31**	**80.00**
	LRBT, $\beta = 0.1$, $\alpha_t = 0.25$	96.78	91.91	79.88
	LRBT, $\beta = 0.15$, $\alpha_t = 0.25$	**96.97**	89.94	77.78
FLBP2	LRBT, $\beta = 0.2$, $\alpha_v = 0.25$	**97.83**	**92.44**	**80.14**
	LRBT, $\beta = 0.15$, $\alpha_v = 0.25$	97.57	91.65	80.01
	LRBT, $\beta = 0.25$, $\alpha_v = 0.25$	97.70	90.92	79.22
LBP		87.44	84.62	73.37

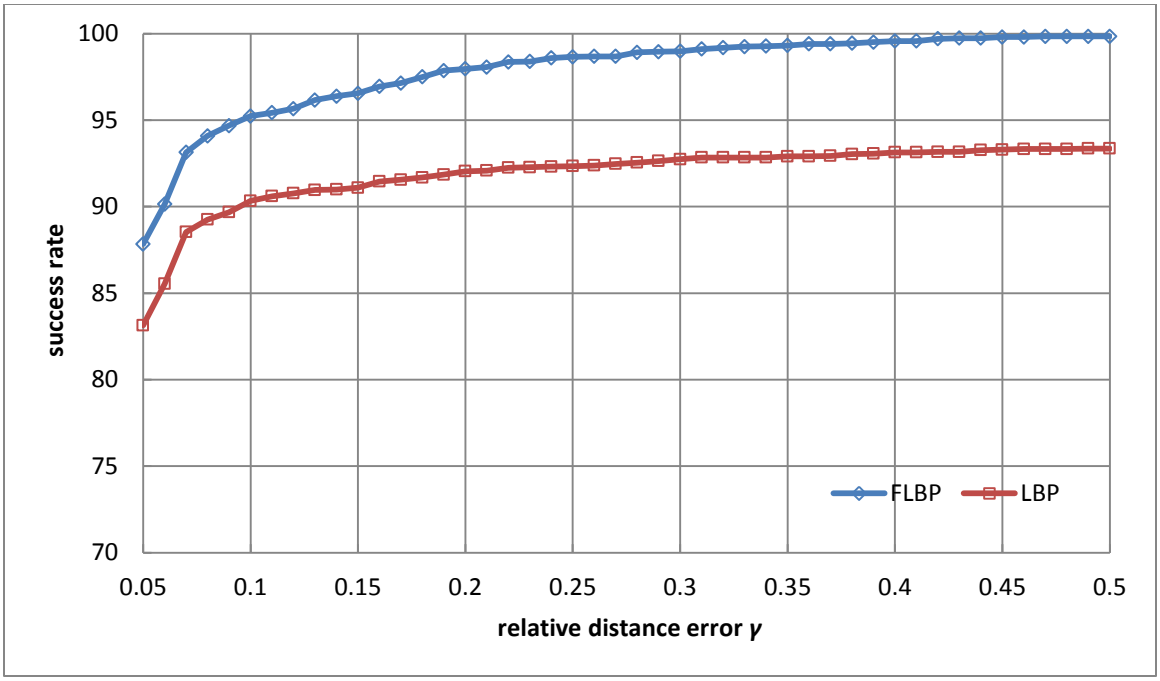

Figure 6.6 The success rate of the FLBP (LRBT, β = 0.2, α_t = 0, α_v = 0.25) and LBP method for various γ using the uncontrolled face image set.

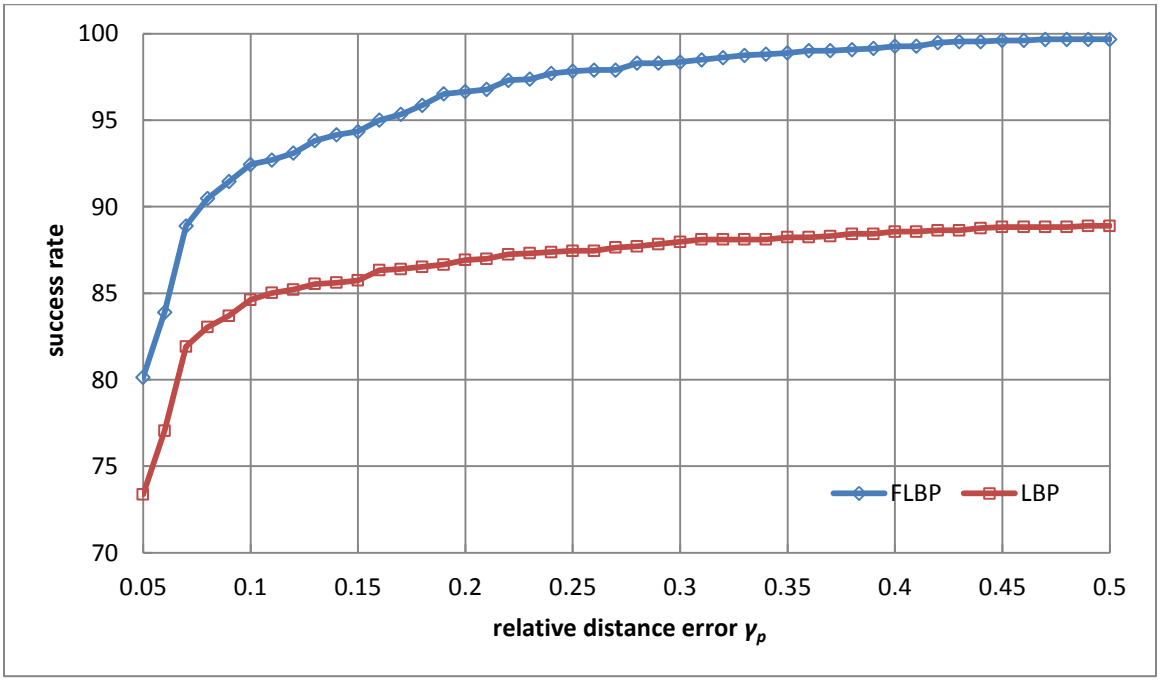

Figure 6.7 The success rate of the FLBP (LRBT, β = 0.2, α_t = 0, α_v = 0.25) and LBP method for various γ_p using the uncontrolled face image set.

Table 6.7 shows the average γ and γ_p of the FLBP1, FLBP2 and LBP methods. The feature pixels for FLBP1 and FLBP2 are derived by the LRBT method. The three FLBP1 and FLBP2 methods with lowest average γ and γ_p are selected to compare with the LBP method. Table 6.7 reveals that the average γ of FLBP1 and FLBP2 are less than 0.04, which means that the average detected eye center is inside the pupil. In comparison, the average γ of LBP is 0.081, which means that the average detected eye center is outside the pupil. Table 6.7 also shows that the average γ_p of FLBP1 and FLBP2 are around 0.05, which means that the average detected worse eye center is close to the pupil. In comparison, the average γ_p of LBP is larger than 0.1, which means that the average detected worse eye center is outside the iris. As a result, the experimental results lead to the finding that FLBP locates the eye center more accurately than LBP method.

Table 6.7 The Average γ and γ_p of Eye Detection of the FLBP1, FLBP2, and LBP Methods using the Uncontrolled Face Image Set

Method		**Average γ**	**Average γ_p**
FLBP1	LRBT, $\beta = 0.1$, $\alpha_t = 0.25$	**0.0416**	**0.0555**
	LRBT, $\beta = 0.15$, $\alpha_t = 0.25$	0.0422	0.0570
	LRBT, $\beta = 0.15$, $\alpha_t = 0.12$	0.0424	0.0569
FLBP2	LRBT, $\beta = 0.2$, $\alpha_v = 0.25$	**0.0385**	**0.0513**
	LRBT, $\beta = 0.15$, $\alpha_v = 0.25$	0.0392	0.0526
	LRBT, $\beta = 0.25$, $\alpha_v = 0.25$	0.0397	0.0534
LBP		0.0812	0.1207

The relative distance error γ_p measures the performance using the worse eye. If the right and left eyes of a person are identical, the success rate for γ_p should be the same as the success rate for γ. The physical difference between the right and left eyes of a person is usually small. The appearance of the right and left eyes on an image could have large

difference due to the illumination and pose variations. Therefore, the success rate for γ_p is lower than the success rate for γ. Table 6.8 shows the difference between success rate for γ and success rate for γ_p and the percentage of average γ_p increased from average γ. The FLBP1 and FLBP2 methods with lowest average γ are selected to compare with LBP method. Table 6.8 shows that the success rates for γ_p of the FLBP1 and FLBP2 methods drop less than the success rates for γ_p of the LBP method, and the average γ_p of the FLBP1 and FLBP2 methods increase less than the average γ_p of the LBP method. This finding indicates that FLBP method is less sensitive to the appearance change which might be caused by the illumination and pose variations than the LBP method.

Table 6.8 The Difference between Success Rate for γ and Success Rate for γ_p and the Percentage of Average γ_p Increased from Average γ of the FLBP1, FLBP2, and LBP Methods using the Uncontrolled Face Image Set

Method	**success rate for γ - success rate for γ_p**			**$(\gamma_p - \gamma)/\gamma$ (Average)**
	≤ 0.25	**≤ 0.1**	**≤ 0.05**	
FLBP1, LRBT, $\beta = 0.1$, $\alpha_t = 0.25$	1.25	2.83	7.33	33.41
FLBP2, LRBT, $\beta = 0.2$, $\alpha_v = 0.25$	0.82	2.79	7.70	33.25
LBP	4.9	5.72	9.77	48.65

6.3.2 Using the Controlled Face Image Set

The controlled face image set excludes 512 face images which are either wear eyeglasses or close eyes. Therefore, there are total 1009 face images in the set. Tables 6.9 and 6.10 show the success rates of the FLBP1, FLBP2, and LBP eye detection methods for $\gamma \leq$ 0.25, 0.1, 0.05 and $\gamma_p \leq 0.25, 0.1, 0.05$ using the controlled face image set, respectively. The feature pixels for the FLBP1 and FLBP2 methods are from the binary LRBT feature image. Three FLBP1 and FLBP2 methods are selected to compare with the LBP method.

Each of the FLBP1 or FLBP2 method has either one of the highest success rates for γ or $\gamma_p \leq 0.25, 0.1, 0.05$ or one of the top three highest success rate for γ or $\gamma_p \leq 0.05$.

Table 6.9 The Success Rates for $\gamma \leq 0.25, 0.1, 0.05$ of the FLBP1, FLBP2, and LBP Eye Detection Methods using the Controlled Face Image Set

Method		$\gamma \leq 0.25$	$\gamma \leq 0.1$	$\gamma \leq 0.05$
FLBP1	LRBT, $\beta = 0.25$, $\alpha_t = 0.25$	99.41	98.22	**93.61**
	LRBT, $\beta = 0.2$, $\alpha_t = 0.25$	99.45	**98.46**	93.51
	LRBT, $\beta = 0.15$, $\alpha_t = 0.25$	**99.50**	98.22	93.06
FLBP2	LRBT, $\beta = 0.2$, $\alpha_v = 0.25$	**99.70**	**98.36**	**93.76**
	LRBT, $\beta = 0.25$, $\alpha_v = 0.25$	**99.70**	98.12	93.61
	LRBT, $\beta = 0.15$, $\alpha_v = 0.25$	99.55	98.12	93.71
LBP		95.59	94.75	89.94

Table 6.10 The Success Rates for $\gamma_p \leq 0.25, 0.1, 0.05$ of the FLBP1, FLBP2, and LBP Eye Detection Methods using the Controlled Face Image Set

Method		$\gamma_p \leq 0.25$	$\gamma_p \leq 0.1$	$\gamma_p \leq 0.05$
FLBP1	LRBT, $\beta = 0.25$, $\alpha_t = 0.25$	98.91	96.63	**89.20**
	LRBT, $\beta = 0.1$, $\alpha_t = 0.25$	**99.11**	96.93	89.10
	LRBT, $\beta = 0.2$, $\alpha_t = 1$	98.12	**97.42**	87.71
FLBP2	LRBT, $\beta = 0.15$, $\alpha_v = 0.25$	99.11	96.53	**89.79**
	LRBT, $\beta = 0.2$, $\alpha_v = 0.25$	**99.41**	**97.03**	89.10
	LRBT, $\beta = 0.25$, $\alpha_v = 0.25$	99.41	96.53	88.60
LBP		92.57	91.18	83.55

Table 6.9 shows that the success rates of both FLBP1 and FLBP2 when $\gamma \leq 0.25$, 0.1 and 0.05 are around 99%, 98% and 93%, respectively. The success rates of LBP are around 95%, 94% and 90% which are lower than the success rates achieved by either

FLBP1 or FLBP2. Table 6.10 shows that the success rates of both FLBP1 and FLBP2 when $\gamma_p \leq 0.25$, 0.1 and 0.05 are around 99%, 97% and 89%, respectively. The success rates of LBP are around 92%, 91% and 83% which are lower than the success rates achieved by either FLBP1 or FLBP2. The experimental results show that FLBP achieves better eye detection performance than LBP using the controlled face image set.

Figures 6.8 and 6.9 are the graphs of the success rates of the FLBP and LBP for γ and γ_p from 0.05 to 0.5 using the controlled face image set. The FLBP shown in the graph is the FLBP2 when $\beta = 0.2$, $\alpha_v = 0.25$. Figures 6.8 and 6.9 show that the success rates of the FLBP method reach 100% as the γ and γ_p increase, while the success rates of the LBP method reaches to around 96% and 93% for γ and γ_p, respectively.

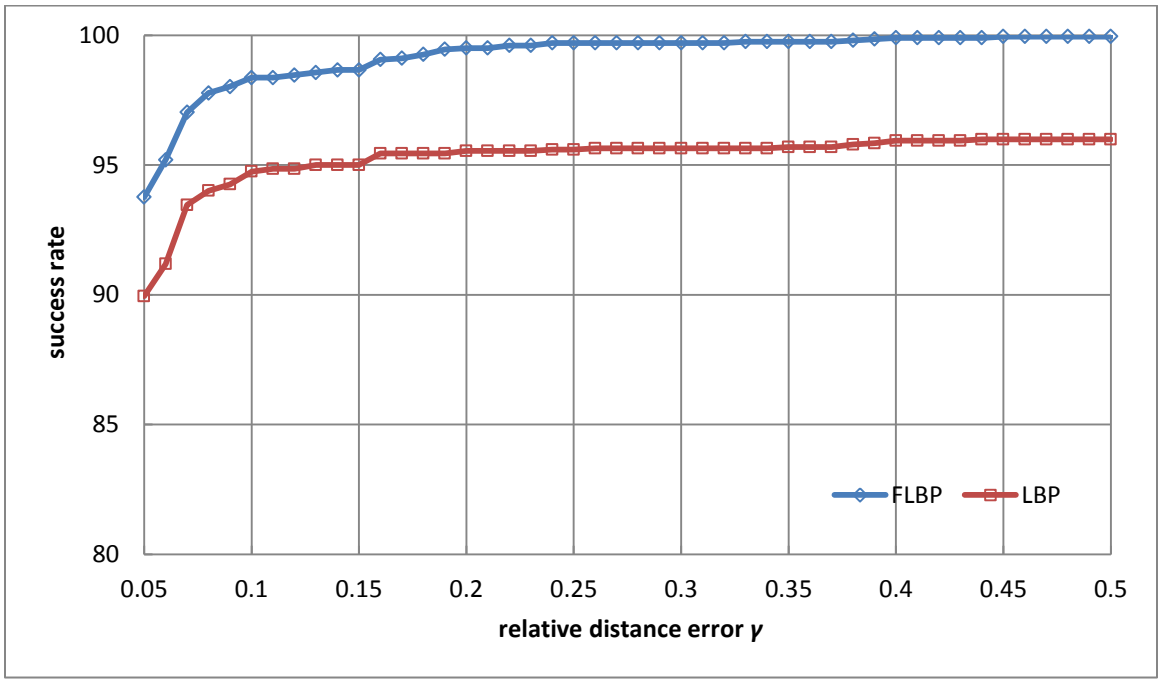

Figure 6.8 The success rate of the FLBP (LRBT, $\beta = 0.2$, $\alpha_t = 0$, $\alpha_v = 0.25$) and LBP method for various γ using the controlled face image set.

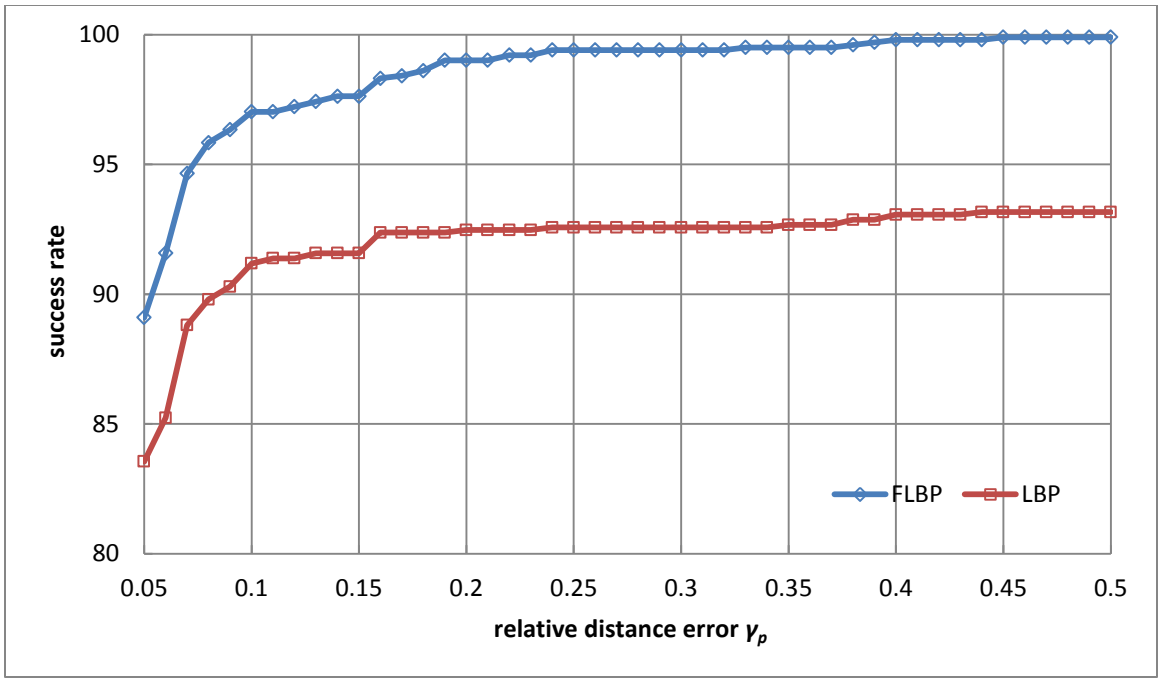

Figure 6.9 The success rate of the FLBP (LRBT, β = 0.2, α_t = 0, α_v = 0.25) and LBP method for various γ_p using the controlled face image set.

Tables 6.11 and 6.12 show the average γ and γ_p of the FLBP1, FLBP2 and LBP methods using the controlled face image set, respectively. The three FLBP1 and FLBP2 methods with lowest average γ and γ_p are selected to compare with the LBP method. Table 6.11 reveals that the average γ of FLBP1 and FLBP2 are around 0.03, which means that the average detected eye center is inside the pupil, and the average γ of LBP is more than 0.05, which means that the average detected eye center is outside the pupil. Table 6.12 shows that the average γ_p of FLBP1 and FLBP2 are around 0.04, which means that the average detected worse eye center is inside the pupil, and the average γ_p of LBP is 0.0856, which means that the average detected worse eye center is outside the pupil. The experimental results show that FLBP locates the eye center more accurately than LBP method using the controlled face image set.

Table 6.11 The Average γ of Eye Detection of the FLBP1, FLBP2, and LBP Methods using the Controlled Face Image Set

Method		Average γ
FLBP1	LRBT, β = 0.2, α_t = 0.25	**0.0298**
	LRBT, β = 0.25, α_t = 0.25	0.0300
	LRBT, β = 0.15, α_t = 0.25	0.0308
FLBP2	LRBT, β = 0.25, α_v = 0.25	**0.0294**
	LRBT, β = 0.2, α_v = 0.25	0.0297
	LRBT, β = 0.15, α_v = 0.25	0.0306
LBP		0.0579

Table 6.12 The Average γ_p of Eye Detection of the FLBP1, FLBP2, and LBP Methods using the Controlled Face Image Set

Method		Average γ_p
FLBP1	LRBT, β = 0.2, α_t = 0.25	**0.0395**
	LRBT, β = 0.25, α_t = 0.25	0.0399
	LRBT, β = 0.15, α_t = 0.25	0.0405
FLBP2	LRBT, β = 0.25, α_v = 0.25	**0.0388**
	LRBT, β = 0.2, α_v = 0.25	0.0390
	LRBT, β = 0.15, α_v = 0.25	0.0403
LBP		0.0856

Table 6.13 shows the difference between success rate for γ and success rate for γ_p and the percentage of average γ_p increased from average γ using controlled face image set. The FLBP1 and FLBP2 methods with lowest average γ are selected to compare with LBP method. Table 6.13 shows that the success rates for γ_p of the FLBP1 and FLBP2 methods drop less than the success rates for γ_p of the LBP method, and the average γ_p of the FLBP1 and FLBP2 methods increase less than the average γ_p of the LBP method.

This finding agrees with the results using uncontrolled face set that FLBP method is less sensitive to the appearance change which might be caused by the illumination and pose variations than the LBP method.

Table 6.13 The Difference between Success Rate for γ and Success Rate for γ_p and the Percentage of Average γ_p Increased from Average γ of the FLBP1, FLBP2, and LBP Methods using the Controlled Face Image Set

Method	**success rate for γ - success rate for γ_p**			**$(\gamma_p - \gamma)/\gamma$ (Average)**
	≤ 0.25	**≤ 0.1**	**≤ 0.05**	
FLBP1, LRBT, $\beta = 0.2$, $\alpha_t = 0.25$	0.44	1.33	4.91	32.55
FLBP2, LRBT, $\beta = 0.2$, $\alpha_v = 0.25$	0.29	1.33	4.66	31.31
LBP	3.02	3.57	6.39	47.84

6.4 Flexibility of the FLBP Method

Compared to LBP, the FLBP method is more flexible due to the introduction of feature pixels as well as its parameters. Next the flexibility of the FLBP method in terms of feature pixels and parameters is assessed on the BioID database.

6.4.1 Feature Pixels

The performance of FLBP depends on the extraction of the feature pixels. Table 6.14 shows the success rates for $\gamma \leq 0.25, 0.1, 0.05$ and the average γ of the FLBP1 and FLBP2 eye detection methods using different feature pixels. Table 6.15 shows the success rates for $\gamma_p \leq 0.25, 0.1, 0.05$ and the average γ_p of the FLBP1 and FLBP2 eye detection methods using different feature pixels. The feature pixels shown in the tables are derived by the LRBT method, the Canny edge detector, and the LBP with Fixed Biased Threshold (LFBT) method which is similar to LRBT method but using the fixed bias

threshold function defined by Equation 3.10. The experiments with the lowest average γ and γ_p in each feature extraction method are selected to make the comparison. The results in Tables 6.14 and 6.15 show that the FLBP method using LRBT feature achieves the best eye detection performance, and the FLBP method using Canny Edge Pixels has the worst performance.

Table 6.14 The Eye Detection Success Rates for $\gamma \leq 0.25$, 0.1, 0.05 and the Average γ of the FLBP1, FLBP2 Methods using Different Feature Pixels

Method		**$\gamma \leq 0.25$**	**$\gamma \leq 0.1$**	**$\gamma \leq 0.05$**	**Average γ**
FLBP1	LRBT, $\beta = 0.1$, $\alpha_t = 0.25$	98.03	94.74	87.21	0.0416
	LFBT, $b = 15$, $\alpha_t = 0.25$	98.22	94.28	86.36	0.0419
	Canny Edge Pixels, $\alpha_t = 0.12$	97.80	94.67	86.65	0.0438
FLBP2	LRBT, $\beta = 0.2$, $\alpha_v = 0.25$	98.65	95.23	87.84	0.0385
	LFBT, $b = 20$, $\alpha_v = 0.25$	98.52	94.94	86.88	0.0396
	Canny Edge Pixels, $\alpha_v = 0.25$	97.63	94.41	86.16	0.0431

Table 6.15 The Eye Detection Success Rates for $\gamma_p \leq 0.25$, 0.1, 0.05 and the Average γ_p of the FLBP1, FLBP2 Methods using Different Feature Pixels

Method		**$\gamma_p \leq 0.25$**	**$\gamma_p \leq 0.1$**	**$\gamma_p \leq 0.05$**	**Average γ_p**
FLBP1	LRBT, $\beta = 0.1$, $\alpha_t = 0.25$	96.78	91.91	79.88	0.0555
	LFBT, $b = 15$, $\alpha_t = 0.25$	97.17	90.73	78.24	0.0563
	Canny Edge Pixels, $\alpha_t = 0.12$	96.52	91.52	78.57	0.0596
FLBP2	LRBT, $\beta = 0.2$, $\alpha_v = 0.25$	97.83	92.44	80.14	0.0513
	LFBT, $b = 20$, $\alpha_v = 0.25$	97.70	91.52	79.09	0.0524
	Canny Edge Pixels, $\alpha_v = 0.25$	95.99	90.73	77.91	0.0590

6.4.2 Parameters

Tables 6.16 and 6.17 show the eye detection success rate for $\gamma \leq 0.25$, 0.1, 0.05 and average γ of the FLBP1 and FLBP2 methods, respectively. Tables 6.18 and 6.19 show the eye detection success rate for $\gamma_p \leq 0.25$, 0.1, 0.05 and average γ_p of the FLBP1 and FLBP2 methods, respectively. The ranks in the tables are derived by sorting the average γ or γ_p in ascending order. The feature pixels are derived by the LRBT method. The LRBT method applies five β values: 0.05, 0.1, 0.15, 0.2 and 0.25. The FLBP parameters α_t and α_v in the experiments are from the following set: {0.12, 0.25, 0.5, and 1}.

The relative bias parameter β in the LRBT method should assume an appropriate value that is neither too small nor too large. If β is too small, more noise pixels will be included as feature pixels, which is detrimental to either feature pixel extraction or FLBP code derivation. If β is too large, more meaningful feature pixels will be filtered out, whose effect is also harmful for feature pixel extraction and FLBP code generation. Our experimental results show that the empirical values of 0.1, 0.15 and 0.2 for β help most methods achieve good eye detection performance. The results also reveal that when β = 0.05, good eye detection performance is achieved for large values of α_t or α_v.

The locations of the true center and the virtual center are controlled by the parameter α_t and α_v, respectively. The larger value the parameters assume, the closer the true center or virtual center gets to the nearest feature pixel. When comparing the average γ in Tables 6.16 and 6.17, one can see that both FLBP1 and FLBP2 obtain the smallest error when α_t or α_v = 0.25, except for LRBT with β = 0.05 (this situation will be discussed in the next paragraph). When α_t (or α_v) gets smaller or larger than 0.25, the results become worse. As the FLBP method encodes the information from both the local

texture and the feature pixels, a proper balance should be kept in order to reach the best performance. When α_t (or α_v) is smaller than 0.25, FLBP contains more information from the local texture than the feature pixels. When α_t (or α_v) is larger than 0.25, FLBP encodes more information from the feature pixels than from the local texture. When α_t (or α_v) = 0.25, FLBP optimally encodes the information from both the local texture and the feature pixels, and the FLBP method achieves the best eye detection performance.

For LRBT with β = 0.05, Tables 6.16 – 6.19 show that both FLBP1 and FLBP2 obtain the smallest average relative distance error γ and γ_p when α_t = 1 for FLBP1 and α_v = 1 for FLBP2. When α_t (or α_v) gets smaller, the results become worse. Note that when β = 0.05, which is the smallest among the four β values in our experiments, more feature pixels are extracted. As a result, the distance vectors to the nearest feature pixel are smaller than those corresponding to a larger β value. In order to achieve the balanced information encoding from both the local texture and the feature pixels, α_t (or α_v) should be large according to Equations. 3.7 and 3.8

Table 6.16 The Eye Detection Success Rates for $\gamma \leq 0.25$, 0.1, 0.05 and the Average γ of the FLBP1 Methods using Different Parameter Values

Method		**FLBP1**				
β	α_t	$\gamma \leq 0.25$	$\gamma \leq 0.1$	$\gamma \leq 0.05$	**Average γ**	**Rank**
0.05	0.12	94.38	92.14	84.42	0.0665	19
	0.25	97.01	94.05	86.00	0.0491	14
	0.5	97.30	93.95	85.67	0.0463	12
	1	97.76	94.18	85.70	0.0440	9
0.1	0.12	97.63	94.64	86.59	0.0450	11
	0.25	98.03	94.74	87.21	**0.0416**	**1**
	0.5	97.70	93.82	85.73	0.0432	8
	1	97.86	93.23	85.57	0.0442	10
0.15	0.12	98.03	95.00	87.15	0.0424	3
	0.25	**98.13**	93.75	86.00	0.0422	2
	0.5	96.81	91.88	84.45	0.0480	13
	1	96.32	89.12	82.02	0.0544	16
0.2	0.12	97.86	**95.10**	**87.41**	0.0428	6
	0.25	97.67	93.98	86.52	0.0427	5
	0.5	96.29	90.01	82.58	0.0534	15
	1	95.36	86.92	79.29	0.0622	18
0.25	0.12	97.99	94.84	87.28	0.0429	7
	0.25	98.09	93.85	85.83	0.0426	4
	0.5	95.73	88.66	81.66	0.0562	17
	1	92.44	83.43	75.21	0.0785	20

Table 6.17 The Eye Detection Success Rates for $\gamma \leq 0.25$, 0.1, 0.05 and the Average γ of the FLBP2 Methods using Different Parameter Values

Method		**FLBP2**				
β	α_v	$\gamma \leq 0.25$	$\gamma \leq 0.1$	$\gamma \leq 0.05$	**Average γ**	**Rank**
0.05	0.12	93.79	91.62	84.19	0.0705	17
	0.25	95.63	93.13	85.47	0.0577	15
	0.5	95.89	92.04	85.77	0.0538	12
	1	96.91	93.43	86.49	0.0447	8
0.1	0.12	97.30	94.31	86.26	0.0473	10
	0.25	97.90	94.67	86.88	0.0426	7
	0.5	96.81	92.83	86.49	0.0451	9
	1	93.33	89.05	83.10	0.0560	14
0.15	0.12	97.93	94.97	86.62	0.0425	6
	0.25	98.55	95.04	87.51	0.0392	2
	0.5	95.92	92.37	86.19	0.0474	11
	1	88.89	83.07	76.33	0.0748	18
0.2	0.12	98.16	95.04	86.72	0.0414	5
	0.25	**98.65**	**95.23**	**87.84**	**0.0385**	**1**
	0.5	94.61	89.58	84.22	0.0542	13
	1	84.45	77.84	70.74	0.0931	19
0.25	0.12	98.16	94.84	86.65	0.0412	4
	0.25	98.62	94.44	87.08	0.0397	3
	0.5	93.23	87.77	82.18	0.0626	16
	1	80.14	73.64	67.49	0.1108	20

Table 6.18 The Eye Detection Success Rates for $\gamma_p \leq 0.25$, 0.1, 0.05 and the Average γ_p of the FLBP1 Methods using Different Parameter Values

Method		**FLBP1**				
β	α_t	$\gamma_p \leq 0.25$	$\gamma_p \leq 0.1$	$\gamma_p \leq 0.05$	**Average γ_p**	**Rank**
0.05	0.12	90.47	87.25	75.48	0.0989	19
	0.25	94.94	90.47	77.51	0.0690	14
	0.5	95.66	89.94	76.53	0.0644	12
	1	96.32	90.47	76.73	0.0600	9
0.1	0.12	96.32	91.52	78.37	0.0607	11
	0.25	96.78	91.91	79.88	**0.0555**	**1**
	0.5	96.25	90.20	77.25	0.0588	8
	1	96.58	88.95	77.25	0.0605	10
0.15	0.12	96.84	92.18	79.22	0.0569	2
	0.25	**96.97**	89.94	77.78	0.0570	3
	0.5	94.61	87.31	76.99	0.0659	13
	1	93.82	83.89	74.16	0.0737	15
0.2	0.12	96.52	**92.31**	**80.00**	0.0581	4
	0.25	96.25	90.14	78.44	0.0583	5
	0.5	93.62	85.14	73.90	0.0741	16
	1	94.39	82.58	70.94	0.0827	18
0.25	0.12	96.84	91.78	79.42	0.0585	6
	0.25	96.58	90.27	77.84	0.0585	6
	0.5	92.83	83.17	73.31	0.0775	17
	1	87.97	77.91	65.68	0.1071	20

Table 6.19 The Eye Detection Success Rates for $\gamma_p \leq 0.25$, 0.1, 0.05 and the Average γ_p of the FLBP2 Methods using Different Parameter Values

Method		**FLBP2**				
β	α_v	$\gamma_p \leq 0.25$	$\gamma_p \leq 0.1$	$\gamma \leq 0.05$	**Average γ_p**	**Rank**
0.05	0.12	89.48	86.32	75.02	0.1057	18
	0.25	92.90	89.28	77.25	0.0819	15
	0.5	93.16	87.7	77.71	0.0776	13
	1	95.00	88.89	78.17	0.0623	8
0.1	0.12	95.73	90.99	78.04	0.0644	10
	0.25	96.65	91.58	78.83	0.0576	6
	0.5	94.61	88.17	78.70	0.0631	9
	1	89.09	83.30	74.36	0.0785	14
0.15	0.12	96.52	91.98	78.30	0.0579	7
	0.25	97.57	91.65	80.01	0.0526	2
	0.5	93.29	87.90	78.90	0.0664	11
	1	83.50	76.07	65.81	0.1022	17
0.2	0.12	96.98	92.11	78.57	0.0557	5
	0.25	**97.83**	**92.44**	**80.14**	**0.0513**	**1**
	0.5	90.86	84.16	76.27	0.0769	12
	1	77.19	69.23	59.57	0.1281	19
0.25	0.12	96.98	91.58	78.63	0.0556	4
	0.25	97.70	90.92	79.22	0.0534	3
	0.5	88.82	82.51	74.36	0.0876	16
	1	71.14	65.02	56.34	0.1510	20

6.5 Comparison FLBP with Other Local Feature Descriptors

This dissertation compares FLBP with the Histograms of Oriented Gradient (HOG) descriptor (Dalal and Triggs, 2005) and two LBP variants, Local Derivative Pattern (LDP) (B. Zhang and Gao, 2010) and Local Quantized Patterns (Hussain and Triggs, 2012) on eye detection in the BioID database. Tables 6.16 – 6.19 show that the FLBP experiment when α_v = 0.25, α_t = 0 and β = 0.2, archives the lowest average γ and γ_p among all FLBP experiments, therefore, the FLBP method with these parameter values is chosen to compare with the methods using other local feature descriptors.

6.5.1 FLBP vs. HOG

The idea behind the Histogram of Oriented Gradient descriptors (HOG) is that local object appearance and shape within an image can be described by the distribution of intensity gradients or edge directions. The implementation of HOG is achieved by dividing the image into small connected regions, called cells, and for each cell compiling a histogram of gradient directions or edge orientations for the pixels within the cell. The combination of these histograms then represents the descriptor. For improved accuracy, the local histograms can be contrast-normalized by calculating a measure of the intensity across a larger region of the image, called a block, and then using this value to normalize all cells within the block. This normalization results in better invariance to changes in illumination or shadowing.

Tables 6.20 and 6.21 show the success rates for γ and $\gamma_p \leq 0.25, 0.1, 0.05$ and the average γ and γ_p of eye detection using the FLBP and HOG methods, respectively. The numbers of orientation bins of HOG in the table are 9 and 18. The results show that the FLBP method achieves better performance than HOG method.

Table 6.20 The Eye Detection Success Rates for $\gamma \leq 0.25, 0.1, 0.05$ and the Average γ of the FLBP and HOG Methods

Method		**$\gamma \leq 0.25$**	**$\gamma \leq 0.1$**	**$\gamma \leq 0.05$**	**Average γ**
HOG	9 orientation bins	91.72	87.51	77.81	0.0737
	18 orientation bins	92.31	87.87	76.43	0.0690
FLBP, LRBT, $\beta = 0.2$, $\alpha_t = 0$, $\alpha_v = 0.25$		**98.65**	**95.23**	**87.84**	**0.0385**

Table 6.21 The Eye Detection Success Rates for $\gamma_p \leq 0.25, 0.1, 0.05$ and the Average γ_p of the FLBP and HOG Methods

Method		**$\gamma_p \leq 0.25$**	**$\gamma_p \leq 0.1$**	**$\gamma_p \leq 0.05$**	**Average γ_p**
HOG	9 orientation bins	86.46	80.60	66.47	0.1092
	18 orientation bins	87.38	81.46	65.22	0.0991
FLBP, LRBT, $\beta = 0.2$, $\alpha_t = 0$, $\alpha_v = 0.25$		**97.83**	**92.44**	**80.14**	**0.0513**

6.5.2 FLBP vs. LDP

LDP is a general framework to encode directional pattern features based on local derivative variations. For a given an image, LDP first computer the N^{th}- Order derivatives along 0^o, 45^o, 90^o and 135^o directions to generate four N^{th}- Order derivatives images. The four 8-bit directional N^{th}- Order LDPs can be computed using the threshold function defined as follows:

$$S(x_i, x_c) = \begin{cases} 0, & \text{if } x_i * x_c > 0\,; \\ 1, & \text{otherwise.} \end{cases} \tag{6.3}$$

Finally, the N^{th}- Order LDP is defined as the concatenation of the four 8-bit directional LDPs.

The 2nd-order and 3rd-order LDP are used in the experiments. LDP is also extended to the Feature LDP (FLDP) using the same approach that extends LBP to

FLBP. The parameters of LDP used in the experiment are the same as those used by the FLBP method. Tables 6.22 and 6.23 show the success rates for γ and $\gamma_p \leq 0.25$, 0.1, 0.05 and the average γ and γ_p of eye detection using the FLBP, LDP and FLDP methods, respectively. The experimental results in these tables lead to the following findings.

- The FLBP method has the best performance among all methods.
- The 2nd-order LDP methods perform better than 3rd-order LDP methods
- The FLDP methods perform better their corresponding LDP methods.

Table 6.22 The Eye Detection Success Rates for $\gamma \leq 0.25$, 0.1, 0.05 and the Average γ of the FLBP, LDP and FLDP Methods

Method	$\gamma \leq 0.25$	$\gamma \leq 0.1$	$\gamma \leq 0.05$	**Average γ**
LDP^2	88.89	82.22	69.13	0.1060
FLDP^2, $\beta = 0.2$, $\alpha_t = 0$, $\alpha_v = 0.25$	93.23	85.86	73.18	0.0736
LDP^3	63.48	50.36	36.26	0.2865
FLDP^3, $\beta = 0.2$, $\alpha_t = 0$, $\alpha_v = 0.25$	72.62	58.61	43.16	0.2218
FLBP, $\beta = 0.2$, $\alpha_t = 0$, $\alpha_v = 0.25$	**98.65**	**95.23**	**87.84**	**0.0385**

Table 6.23 The Eye Detection Success Rates for $\gamma_p \leq 0.25$, 0.1, 0.05 and the Average γ_p of the FLBP, LDP and FLDP Methods

Method	$\gamma_p \leq 0.25$	$\gamma_p \leq 0.1$	$\gamma_p \leq 0.05$	**Average γ_p**
LDP^2	84.48	73.77	55.62	0.1437
FLDP^2, $\beta = 0.2$, $\alpha_t = 0$, $\alpha_v = 0.25$	89.81	78.24	59.63	0.1107
LDP^3	51.28	37.21	22.16	0.3771
FLDP^3, $\beta = 0.2$, $\alpha_t = 0$, $\alpha_v = 0.25$	62.59	46.81	29.85	0.2909
FLBP, $\beta = 0.2$, $\alpha_t = 0$, $\alpha_v = 0.25$	**97.83**	**92.44**	**80.14**	**0.0513**

6.5.3 FLBP vs. LQtP

LQtP is a generalized form of local patterns that uses many different neighborhood geometries. The binary coding LQtP with the H_7, V_7, HV_7 and DA_7 neighborhood shapes which are shown in Figure 6.10 are used in our experiments. LQtP is extended to the Feature LQtP (FLQtP) using the same approach that extends LBP to FLBP. The parameters of LDP used in the experiment are the same as those used by the FLBP method.

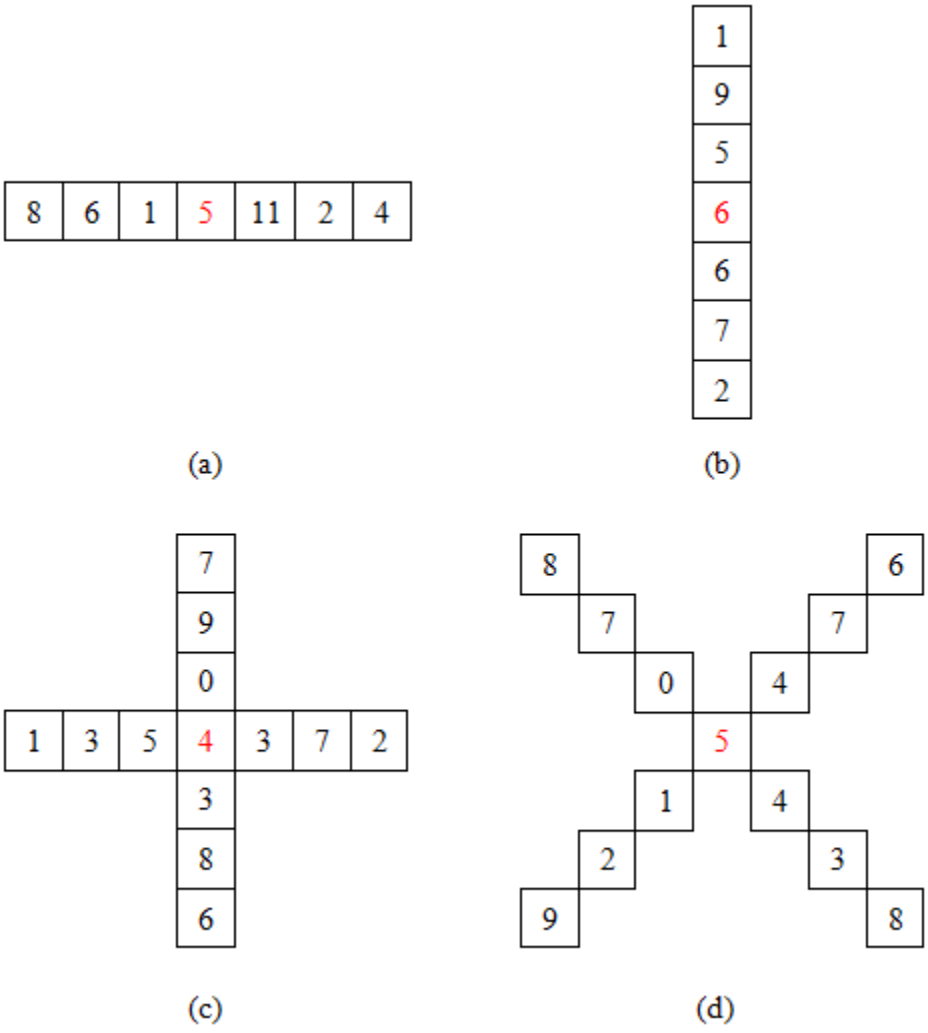

Figure 6.10 The local pattern neighborhoods (a) Horizontal (H_7), (b) Vertical (V_7), (c) Horizontal-Vertical (HV_7), and (d) Diagonal-Antidiagonal (DA_7).

Tables 6.24 and 6.25 show the success rates for γ and $\gamma_p \leq 0.25, 0.1, 0.05$ and the average γ and γ_p of eye detection using the FLBP, LQtP and FLQtP methods, respectively. The experimental results in these tables lead to the following findings.

- The FLBP method has the best performance among all methods.
- The FLQtP methods perform better their corresponding LQtP methods.
- LQtP-HV_7 and LQtP-DA_7 have the better results than LQtP-H_7 and LQtP-V_7. However, the dimensions of LQtP-HV_7 and LQtP-DA_7 (2^{12}) are higher than the dimensions of LQtP-H_7 and LQtP-V_7 (2^6) and FLBP (2^{10}).

Table 6.24 The Eye Detection Success Rates for $\gamma \leq 0.25, 0.1, 0.05$ and the Average γ of the FLBP, LQtP and FLQtP Methods

Method	$\gamma \leq 0.25$	$\gamma \leq 0.1$	$\gamma \leq 0.05$	**Average γ**
LQtP-H_7	61.05	50.46	37.80	0.2813
FLQtP-H_7, $\beta = 0.2$, $\alpha_t = 0$, $\alpha_v = 0.25$	87.31	75.74	64.07	0.1195
LQtP-V_7	69.17	49.34	35.63	0.2291
FLQtP-V_7, $\beta = 0.2$, $\alpha_t = 0$, $\alpha_v = 0.25$	92.37	74.03	60.19	0.0941
LQtP-DA_7	92.44	88.43	81.43	0.0762
FLQtP-DA_7, $\beta = 0.2$, $\alpha_t = 0$, $\alpha_v = 0.25$	96.19	90.86	84.16	0.0485
LQtP-HV_7	94.64	89.91	80.80	0.0634
FLQtP-HV_7, $\beta = 0.2$, $\alpha_t = 0$, $\alpha_v = 0.25$	97.53	91.22	85.14	0.0466
FLBP, $\beta = 0.2$, $\alpha_t = 0$, $\alpha_v = 0.25$	**98.65**	**95.23**	**87.84**	**0.0385**

Table 6.25 The Eye Detection Success Rates for $\gamma_p \leq 0.25, 0.1, 0.05$ and the Average γ_p of the FLBP, LQtP and FLQtP Methods

Method	$\gamma_p \leq 0.25$	$\gamma_p \leq 0.1$	$\gamma_p \leq 0.05$	Average γ_p
LQtP-H_7	45.30	35.04	20.78	0.3855
FLQtP-H_7, $\beta = 0.2$, $\alpha_t = 0$, $\alpha_v = 0.25$	80.80	66.86	50.82	0.1655
LQtP-V_7	54.70	32.61	19.72	0.3189
FLQtP-V_7, $\beta = 0.2$, $\alpha_t = 0$, $\alpha_v = 0.25$	87.31	62.98	44.84	0.1331
LQtP-DA_7	87.51	82.12	71.53	0.1129
FLQtP-DA_7, $\beta = 0.2$, $\alpha_t = 0$, $\alpha_v = 0.25$	93.36	85.67	76.20	0.0686
LQtP-HV_7	90.53	84.22	70.35	0.0940
FLQtP-HV_7, $\beta = 0.2$, $\alpha_t = 0$, $\alpha_v = 0.25$	96.06	86.98	77.32	0.0635
FLBP, $\beta = 0.2$, $\alpha_t = 0$, $\alpha_v = 0.25$	**97.83**	**92.44**	**80.14**	**0.0513**

6.6 Fusion of FLBP on Grayscale and Gradient Images

The fusion of the FLBP methods on grayscale and gradient images for eye detection is explored in this dissertation. The similarity measures are fused at decision level by the simple sum rule. Sobel kernel defined by Equation 5.5 and the kernel defined by Equation 5.6 are used to compute the gradient. The experimental results show the FLBP method when $\alpha_v = 0.25$, $\alpha_t = 0$ and $\beta = 0.2$, archives the best performance on grayscale, therefore, the FLBP method with these parameter values is chose for on gradient images.

Tables 6.26 and 6.27 show the success rates for γ and $\gamma_p \leq 0.25, 0.1, 0.05$ and the average γ and γ_p of the LBP and FLBP eye detection methods on gradient (Sobel kernel) and grayscale images, respectively. Tables 6.28 and 6.29 show the success rates for γ and $\gamma_p \leq 0.25, 0.1, 0.05$ and the average γ and γ_p of the LBP and FLBP eye detection methods on gradient (kernel defined by Equation 5.6) and grayscale images, respectively. The

method names, GD, GM and GS in tables represent the FLBP methods on gradient direction, gradient magnitude and grayscale images, respectively. The + sign denotes the fusion of the FLBP on different images. The results show that the method fusing the grayscale, gradient magnitude and direction images improves eye detection performance and the kernel defined by Equation 5.6 performs better than Sobel kenel.

Table 6.26 The Eye Detection Success Rates for $\gamma \leq 0.25$, 0.1, 0.05 and the Average γ of the LBP and FLBP Methods Applied on Gradient Images (Sobel Kernel), Grayscale Images and the Fusion of Gradient and Grayscale Image

Method		$\gamma \leq 0.25$	$\gamma \leq 0.1$	$\gamma \leq 0.05$	**Average γ**
GD	**LBP**	77.41	70.38	52.24	0.1868
	FLBP	88.30	79.55	39.58	0.1180
GM	**LBP**	91.16	88.53	77.84	0.0896
	FLBP	94.97	90.14	77.45	0.0590
GD+GM	**LBP**	92.77	90.70	79.19	0.0816
	FLBP	96.75	93.49	80.21	0.0514
GS	**LBP**	92.34	90.34	83.14	0.0812
	FLBP	98.65	95.23	87.84	0.0385
GD+GM+GS	**LBP**	96.06	95.50	88.69	0.0532
	FLBP	**98.75**	**97.53**	**90.27**	**0.0333**

Table 6.27 The Eye Detection Success Rates for $\gamma_p \leq 0.25$, 0.1, 0.05 and the Average γ_p of the LBP and FLBP Methods Applied on Gradient Images (Sobel Kernel), Grayscale Images and the Fusion of Gradient and Grayscale Images

Method		$\gamma_p \leq 0.25$	$\gamma_p \leq 0.1$	$\gamma_p \leq 0.05$	**Average γ_p**
GD	**LBP**	67.13	58.25	35.77	0.2666
	FLBP	81.92	69.10	39.58	0.1723
GM	**LBP**	85.67	81.99	66.60	0.1357
	FLBP	91.91	85.08	65.22	0.0835
GD+GM	**LBP**	88.76	85.80	68.64	0.1189
	FLBP	94.54	89.35	68.57	0.0738
GS	**LBP**	87.44	84.62	73.37	0.1207
	FLBP	97.83	92.44	80.14	0.0513
GD+GM+GS	**LBP**	93.75	92.97	82.25	0.0748
	FLBP	**98.09**	**96.06**	**83.96**	**0.0438**

Table 6.28 The Eye Detection Success Rates for $\gamma \leq 0.25$, 0.1, 0.05 and the Average γ of the LBP and FLBP Methods Applied on Gradient Images (the New Kernel), Grayscale Images and the Fusion of Gradient and Grayscale Images

Method		$\gamma \leq 0.25$	$\gamma \leq 0.1$	$\gamma \leq 0.05$	**Average γ**
GD	**LBP**	71.96	67.00	51.02	0.2155
	FLBP	82.35	76.43	59.24	0.1570
GM	**LBP**	91.78	89.05	78.01	0.0849
	FLBP	95.10	90.34	77.78	0.0573
GD+GM	**LBP**	92.21	90.37	79.98	0.0829
	FLBP	96.09	93.33	82.51	0.0542
GS	**LBP**	92.34	90.34	83.14	0.0812
	FLBP	98.65	95.23	87.84	0.0385
GD+GM+GS	**LBP**	95.92	95.23	89.84	0.0537
	FLBP	**98.65**	**97.73**	**91.29**	**0.0328**

Table 6.29 The Eye Detection Success Rates for $\gamma_p \leq 0.25$, 0.1, 0.05 and the Average γ_p of the LBP and FLBP Methods Applied on Gradient Images (the New Kernel), Grayscale Images and the Fusion of Gradient and Grayscale Images

Method		$\gamma_p \leq 0.25$	$\gamma_p \leq 0.1$	$\gamma_p \leq 0.05$	**Average γ_p**
GD	**LBP**	59.57	53.58	33.07	0.3122
	FLBP	73.90	66.01	42.54	0.2260
GM	**LBP**	86.72	82.84	66.60	0.1290
	FLBP	91.72	85.14	65.75	0.0817
GD+GM	**LBP**	87.38	84.75	68.64	0.1259
	FLBP	93.49	89.35	71.93	0.0791
GS	**LBP**	87.44	84.62	73.37	0.1207
	FLBP	97.83	92.44	80.14	0.0513
GD+GM+GS	**LBP**	93.43	92.31	83.76	0.0779
	FLBP	**97.96**	**96.32**	**85.34**	**0.0436**

6.7 The Enhanced Eye Detection Method

To further improve the performance, two enhancements are implemented to the eye detection methods. In tables 6.26 - 6.29, all methods use the same parameter values for the FLBP on grayscale image and gradient images. The first enhancement is to use the different parameter values between the grayscale image and the gradient images. The experimental results indicate the performance can be improved if different parameter values are chosen appropriately.

The second enhancement is based on the fact that the iris is the darkest area in the eye region and the eye center is also the center of an iris. After a pixel p is initially detected as the eye center by the similarity measure, *M* defined by Equation 5.1, the eye center is adjusted in the 3 × 3 neighbor of p. First for each pixel in the 3 × 3 neighbor of

p, the sum of the intensity values of all pixels inside a 10 × 10 window around the pixel is calculated, and then the sum is multiplied by *M*, the similarity measure of the pixel. The pixel with the smallest product will be selected as the new eye center.

The enhanced method is tested on both the BioID and FERET database. Table 6.30 shows the success rates and average γ of an enhanced GD+GM+GS method on the BioID and FERET databases. The values of α_v, α_t and β for GS are 0.25, 0, 0.2, respectively. The values of α_v, α_t and β for GM and GD are 0, 0.12 and 0.1, respectively. The results on the BioID database show the enhanced FLBP method archives the best performance among all FLBP methods introduced in the dissertation. Especially, the success rate for γ and $\gamma_p \leq 0.05$ are significantly increased and average γ and γ_p are significantly decreased. The enhanced method on the FERET database also shows the good results. The graphs in Figures 6.11 and 6.12 show the success rates of the enhanced FLBP method for various γ and γ_p on the BioID and FERET databases, respectively.

Table 6.30 The Eye Detection Success Rates for $\gamma \leq 0.25$, 0.1, 0.05 and the Average γ of the Enhanced GD+GM+GS Method on the BioID and FERET Databases

Database	$\gamma \leq 0.25$	$\gamma \leq 0.1$	$\gamma \leq 0.05$	**Average γ**
BioID	98.82	97.93	94.38	0.0281
FERET	99.27	98.87	94.11	0.0275

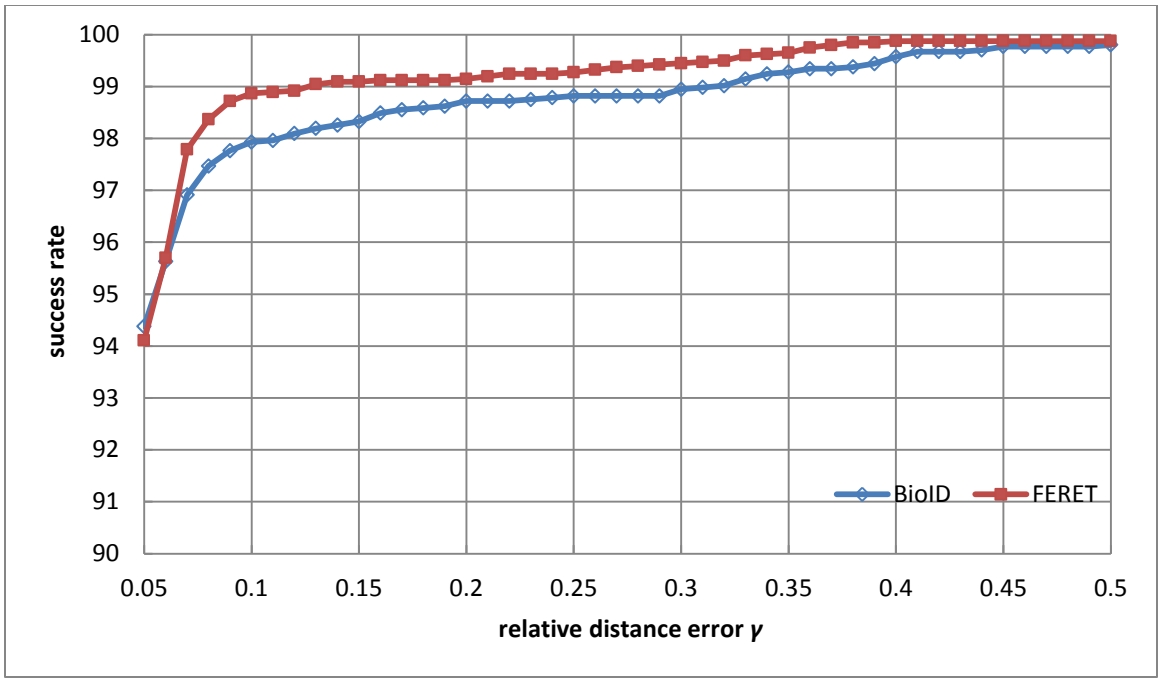

Figure 6.11 The eye detection success rates of the enhanced FLBP method for various γ on the BioID and FERET database.

Table 6.31 The Eye Detection Success Rates for $\gamma_p \leq 0.25$, 0.1, 0.05 and the Average γ_p of the Enhanced GD+GM+GS Method on the BioID and FERET Databases

Database	$\gamma_p \leq 0.25$	$\gamma_p \leq 0.1$	$\gamma_p \leq 0.05$	**Average γ_p**
BioID	98.16	96.65	90.99	0.0381
FERET	98.69	97.94	90.48	0.0363

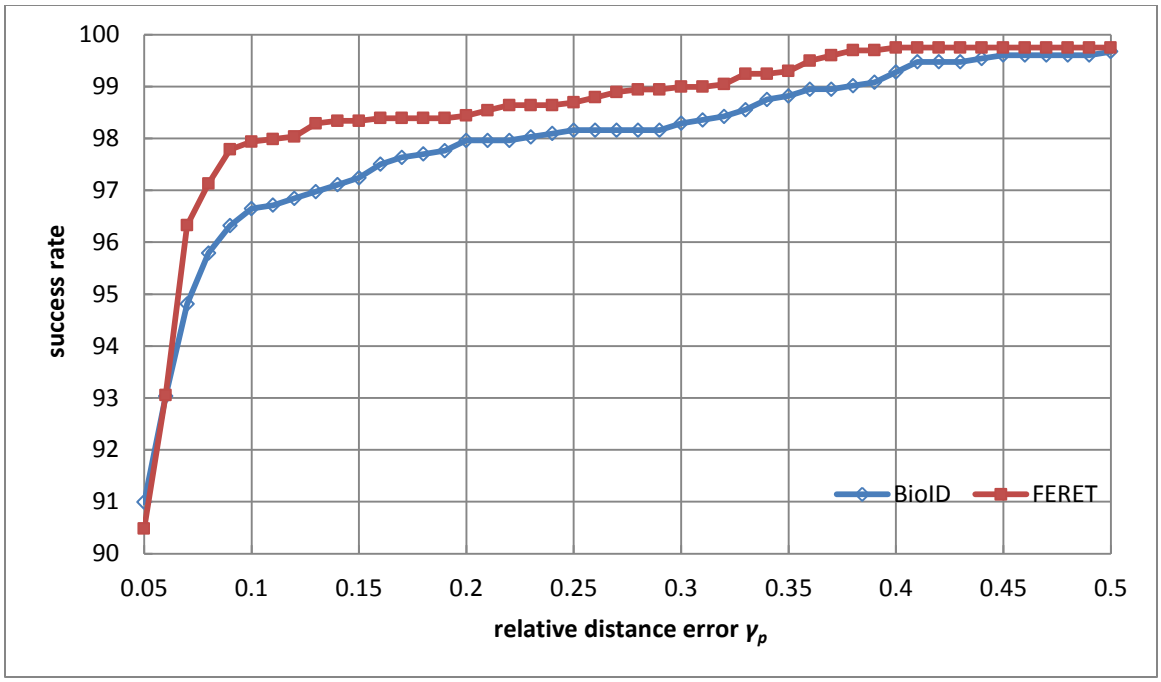

Figure 6.12 The eye detection success rates of the enhanced FLBP method for various γ_p on the BioID and FERET database.

6.8 The Stability of FLBP to Change of Eye Template

The eye template in the previous sections is constructed by well controlled samples. In the controlled samples, all eyes are open, about the same size, and do not wear eye glasses. Eye detection performance depends on the eye template. This section compares the eye detection performance of the LBP, FLBP methods using different eye templates. The new templates are constructed by the eye samples from the face images of the BioID and FERET databases. The samples from the BioID and FERET databases are uncontrolled due to closed eyes, eye glasses and variation in eye size. The BioID and FERET databases are equally divided to ten groups. Each group is used to construct an eye template. For each method two sets of experiments are conducted on the BioID database. Each set includes ten experiments. One set uses the ten eye templates from the

samples of the BioID database, and the other one uses the ten eye templates from the samples of the FERET database. When an experiment using the eye templates from the samples of the BioID database, the face images used to construct the eye template are excluded from eye the experiments. The results of each experimental set are reported as the means and standard deviations of the results of the ten experiments in each set.

Table 6.32 shows eye detection success rates for $\gamma \leq 0.25, 0.1, 0.05$ and the average γ of the LBP, FLBP and the enhanced FLBP methods on the BioID databases using different eye templates. The FLBP and enhanced FLBP methods are the same as the GS method in table 6.26 and the enhanced method in Table 6.30, respectively. The results of the methods using the eye templates from the samples of the BioID and FERET databases are shown as mean ± standard deviation. As expected the results show that a method achieves better performance using the template from the controlled samples than using the templates from the samples of the BioID and FERET databases. Table 6.32 shows when using the templates from the uncontrolled samples of the BioID and FERET databases, the performance of the FLBP and enhanced FLBP methods drops less than the performance of the LBP method, and the FLBP and enhanced FLBP methods have the smaller standard deviations than the LBP method. These results indicate that the FLBP and enhanced FLBP methods are less sensitive and more stable to the change of eye template than the LBP method.

Table 6.32 The Eye Detection Success Rates and the Average γ of the LBP, FLBP and the Enhanced FLBP Methods using Different Eye Templates

Method	Sample	$\gamma \leq 0.25$	$\gamma \leq 0.1$	$\gamma \leq 0.05$	Average γ
LBP	Controlled	92.34	90.34	83.14	0.0812
	BioID	86.06 ± 5.19	79.15 ± 6.24	63.48 ± 7.42	0.1256 ± 0.0307
	FERET	75.11 ± 6.66	68.49 ± 7.28	54.48 ± 6.81	0.1994 ± 0.0409
FLBP	Controlled	98.65	95.23	87.84	0.0385
	BioID	94.77 ± 2.64	87.93 ± 3.74	72.13 ± 7.48	0.0684 ± 0.0142
	FERET	92.71 ± 1.73	84.80 ± 2.76	68.61 ± 3.19	0.0842 ± 0.0104
Enhanced FLBP	Controlled	98.82	97.96	94.48	0.0280
	BioID	96.39 ± 1.88	92.85 ± 2.64	81.33 ± 3.89	0.0482 ± 0.0119
	FERET	95.16 ± 1.30	90.77 ± 2.07	77.60 ± 3.45	0.0585 ± 0.0086

6.9 Comparison with the Other Eye Detection Methods

The FLBP method is compared with other state of the art eye detection methods on the BioID and FERET databases. The FLBP method which is selected to compare with other methods is the enhanced GD+GM+GS method shown in Table 6.31.

Table 6.33 shows the eye detection success rates of the FLBP method and other methods on the BioID database. The results show the FLBP method achieves the highest success rates for $\gamma_p \leq 0.1$ and 0.05. The success rate for $\gamma_p \leq 0.05$ measures the accuracy of eye center localization. In comparison with the other methods, the FLBP method significantly improves the accuracy of eye center localization on the BioID database.

Table 6.34 shows the eye detection success rates of the FLBP method and Campadelli's [51] method on the FERET database. The face images used in two methods are different. Our method uses the entire fa and fb set which include 1986 face images.

Campadelli's method selected 1175 images of which 400 from fa set, 575 from fb set and 200 from ba set. Table 10 shows the FLBP method achieves the higher success rates for $\gamma_p \leq 0.1$ and 0.05. The results indicate the FLBP method also significantly improves the accuracy of eye center localization on the FERET database.

Table 6.33 The Eye Detection Success Rates of the FLBP and other Methods on the BioID Database

Method	$\gamma_p \leq 0.25$	$\gamma_p \leq 0.1$	$\gamma_p \leq 0.05$
Asterialdis (2009)	96.00	89.41	-
Valenti (2008)	98.49	90.85	84.10
Campadelli (2009)	99.30	93.20	80.70
FLBP	98.16	96.65	90.99

Table 6.34 The Eye Detection Success Rates of the FLBP and other Methods on the FERET Database

Method	$\gamma_p \leq 0.25$	$\gamma_p \leq 0.1$	$\gamma_p \leq 0.05$
Campadelli (2009)	99.70	97.30	67.70
FLBP	98.69	97.94	90.48

CHAPTER 7

EXPERIMENTAL RESULTS OF LQP-BASED AND FLQP-BASED METHODS

7.1 Comparative Assessment of FLQP and LQP

The experiments of the FLBP-based method show that 5 × 5 neighborhood size is better than 3 × 3 neighborhood size, and 3 × 4 grid of an eye window yields the best overall results among 3 × 3, 3 × 4, and 4 × 4 grid size. Therefore, the 5 × 5 neighborhood size and the 3 × 4 grid are applied to the LQP-based and FLQP-based eye detection methods. The features for FLQP-based eye detection are derived using the LRBT method with β = 0.2. The parameters α_v and α_t are set to 0.25 and 0, respectively. The parameter r of the threshold function in the experiments is set to either a constant value ($r = c$) or a relative value ($r = \tau g_c$). The LQP-based and FLQP-based methods are assessed using the BioID databases. The facial images are cropped and normalized to the size of 132 × 178. The success rate for $\gamma \leq 0.25, 0.1, 0.05$, $\gamma_p \leq 0.25, 0.1, 0.05$ and the average γ and γ_p are used to assess the performance of the eye detection methods.

Tables 7.1 and 7.2 show the results of the eye detection success rate for γ and $\gamma_p \leq$ 0.25, 0.1, 0.05, the average γ and γ_p of the LQP-based and FLQP-based eye detection methods, respectively. The ranks in the tables are derived by sorting the average γ or γ_p in ascending order. The results show that all the FLQP-based methods have lower average γ than any LQP-based method, and all the FLQP-based methods except when r = 8 have lower average γ_p than any LQP-based method. For the FLQP-based eye detection methods, a relative r achieves better eye detection performance than a constant r. For the LQP-based eye detection methods, a relative r and constant r have the similar result

Table 7.1 The Eye Detection Success Rates for $\gamma \leq 0.25$, 0.1, 0.05 and the Average γ of the FLQP-based and LQP-based Eye Detection Methods

Method		**$\gamma \leq 0.25$**	**$\gamma \leq 0.1$**	**$\gamma \leq 0.05$**	**Average γ**	**Rank Average γ**
FLQP $r = \tau g_c$	$\tau = 0.17$	98.59	96.09	**89.74**	0.0363	2
	$\tau = 0.18$	**98.75**	**96.19**	89.71	**0.0360**	1
	$\tau = 0.19$	**98.75**	96.12	89.38	0.0363	2
FLQP $r = c$	$c = 7$	98.59	94.81	88.59	0.0376	4
	$c = 8$	98.59	94.71	88.61	0.0377	5
	$c = 9$	98.62	94.94	88.42	0.0379	6
LQP $r = \tau g_c$	$\tau = 0.06$	98.13	95.36	88.95	0.0394	12
	$\tau = 0.07$	98.39	95.63	89.38	0.0382	8
	$\tau = 0.08$	98.19	94.43	89.48	0.0392	10
LQP $r = c$	$c = 6$	98.39	95.36	88.72	0.0385	9
	$c = 7$	98.55	95.40	88.10	0.0381	7
	$c = 8$	98.32	95.46	88.56	0.0391	10

Table 7.2 The Eye Detection Success Rates for $\gamma_p \leq 0.25, 0.1, 0.05$ and the Average γ_p of the FLQP-based and LQP-based Eye Detection Methods

Method		**$\gamma_p \leq 0.25$**	**$\gamma_p \leq 0.1$**	**$\gamma_p \leq 0.05$**	**Average γ_p**	**Rank Average γ_p**
FLQP $r = \tau g_c$	$\tau = 0.17$	97.63	93.56	**83.63**	0.0480	2
	$\tau = 0.18$	**97.90**	**93.75**	83.43	**0.0476**	1
	$\tau = 0.19$	**97.90**	93.56	82.77	0.0482	3
FLQP $r = c$	$c = 7$	97.63	91.12	81.72	0.0508	4
	$c = 8$	97.57	90.80	81.66	0.0512	7
	$c = 9$	97.70	91.58	81.79	0.0508	4
LQP $r = \tau g_c$	$\tau = 0.06$	96.91	92.50	82.38	0.0531	11
	$\tau = 0.07$	97.37	92.97	82.97	0.0513	8
	$\tau = 0.08$	97.17	92.83	83.04	0.0528	10
LQP $r = c$	$c = 6$	97.37	92.44	81.85	0.0515	9
	$c = 7$	97.70	92.37	81.07	0.0510	6
	$c = 8$	97.30	92.44	81.33	0.0531	11

7.2 Comparative Assessment of FLTP and LTP

The LTP and FLTP are implemented in the eye detection as well for comparison. The 5 × 5 neighborhood size and the 3 × 4 grid are applied to the LTP-based and FLTP-based eye detection methods. The features of FLTP-based eye detection are derived using the LRBT method with $\beta = 0.2$. The parameters α_v and α_t are set to 0.25 and 0, respectively. The parameter r of the threshold function is set to either a constant value ($r = c$) or a relative value ($r = \tau g_c$). The LTP-based and FLTP-based methods are access on the BioID databases. The success rate for $\gamma \leq 0.25, 0.1, 0.05$, $\gamma_p \leq 0.25, 0.1, 0.05$ and the average γ and γ_p are used to assess the performance of the eye detection method.

Tables 7.3 and 7.4 show the results of the eye detection success rate for γ and $\gamma_p \leq$ 0.25, 0.1, 0.05 and the average γ and γ_p of the LTP-based and FLTP-based eye detection methods, respectively. The ranks in the tables are derived by sorting the average γ or γ_p in ascending order. The results show that all the FLTP-based methods except when $r = 0.04g_c$ have lower or equal average γ than any LQP-based method, and all the FLTP-based methods have lower average γ_p than any LQP-based method except when $r = 4$. For both the FLTP-based and LTP-based eye detection methods a constant r achieves lower average γ and γ_p than a relative r.

Table 7.3 The Eye Detection Success Rates for $\gamma \leq 0.25$, 0.1, 0.05 and the Average γ of the FLTP-based and LTP-based Eye Detection Methods

Method		**$\gamma \leq 0.25$**	**$\gamma \leq 0.1$**	**$\gamma \leq 0.05$**	**Average γ**	**Rank Average γ**
FLTP $r = \tau g_c$	$\tau = 0.02$	98.46	94.81	88.63	0.0395	5
	$\tau = 0.03$	98.32	95.00	89.02	0.0388	2
	$\tau = 0.04$	98.06	95.00	89.02	0.0396	7
FLTP $r = c$	$c = 2$	**98.52**	95.04	88.46	0.0389	3
	$c = 3$	98.29	95.17	**89.12**	**0.0387**	1
	$c = 4$	98.16	95.17	88.89	0.0390	4
LTP $r = \tau g_c$	$\tau = 0.02$	97.53	94.87	87.34	0.0438	11
	$\tau = 0.03$	97.44	94.74	87.87	0.0438	11
	$\tau = 0.04$	97.30	94.48	87.84	0.0436	10
LTP $r = c$	$c = 3$	97.63	95.07	87.67	0.0429	9
	$c = 4$	98.03	**95.50**	88.95	0.0395	5
	$c = 5$	97.80	95.07	88.46	0.0401	8

Table 7.4 The Eye Detection Success Rates for $\gamma_p \leq 0.25$, 0.1, 0.05 and the Average γ_p of the FLTP-based and LTP-based Eye Detection Methods

Method		**$\gamma_p \leq 0.25$**	**$\gamma_p \leq 0.1$**	**$\gamma_p \leq 0.05$**	**Average γ_p**	**Rank Average γ_p**
FLTP $r = \tau g_c$	$\tau = 0.02$	97.44	91.45	81.72	0.0533	7
	$\tau = 0.03$	97.17	91.72	82.38	0.0525	3
	$\tau = 0.04$	96.91	91.91	**82.64**	0.0531	6
FLTP $r = c$	$c = 2$	**97.50**	91.64	81.07	0.0525	3
	$c = 3$	97.24	91.85	82.58	**0.0522**	1
	$c = 4$	96.91	**92.76**	82.12	0.0529	5
LTP $r = \tau g_c$	$\tau = 0.02$	96.25	92.04	80.08	0.0581	10
	$\tau = 0.03$	95.99	91.58	80.60	0.0585	12
	$\tau = 0.04$	95.79	91.45	80.47	0.0584	11
LTP $r = c$	$c = 3$	96.19	92.04	80.34	0.0579	9
	$c = 4$	96.78	92.70	**82.64**	0.0524	2
	$c = 5$	96.38	91.91	81.59	0.0537	8

7.3 Comparison of FLQP, LQP, FLTP, LTP, FLBP and LBP

Tables 7.5 and 7.6 compare the performance of the FLQP-based, the LQP-based, the FLTP-based, the LTP-based, the FLBP-based, and the LBP-based eye detection methods. The experiments with smallest average γ and γ_p are selected from each method for the comparison. Tables 7.5 and 7.6 rank the average γ and γ_p of eye detection and show the percentages increased from the average γ and γ_p of the FLQP method, respectively.

Table 7.5 The Average γ and Rank of the FLQP-based, the LQP-based, the FLTP-based, the LTP-based, the FLBP-based and the LBP-based Eye Detection Methods

Method	Average γ	% Higher than the FLQP Method	Rank
FLQP, $r = 0.18g_c$	**0.0360**	0	1
LQP, $r = 7$	0.0381	5.83	2
FLTP, $r = 3$	0.0387	7.50	4
LTP, $r = 4$	0.0395	9.72	5
FLBP	0.0385	6.94	3
LBP	0.0812	125.56	6

Table 7.6 The Average γ_p and Rank of the FLQP-based, the LQP-based, the FLTP-based, the LTP-based, the FLBP-based and the LBP-based Eye Detection Methods

Method	Average γ_p	% Increased from the FLQP Method	Rank
FLQP, $r = 0.18g_c$	**0.0476**	0	1
LQP, $r = 7$	0.0510	7.14	2
FLTP, $r = 3$	0.0522	9.66	4
LTP, $r = 4$	0.0524	10.08	5
FLBP	0.0513	7.77	3
LBP	0.1207	153.57	6

The results in these tables lead to the following findings.

- FLQP achieves the best eye detection performance. Specifically. The FLQP-based method has the smallest average γ and γ_p. The average γ of the LQP, FLTP, LTP, FLBP, and LBP-based eye detection methods are 5.83%, 7.50%, 9.72%, 6.94%, and 125.56% higher than the average γ of the FLQP-based method, respectively. The average γ_p of the LQP, FLTP, LTP, FLBP, and LBP-based eye detection methods are 7.14%, 9.66%, 10.08%, 7.77%, and 153.57% higher than the average γ_p of the FLQP-based method, respectively.

- LQP performs better than LTP and LBP, and FLQP performs better than FLTP and FLBP for eye detection in terms of average γ and γ_p. These results demonstrate that the proposed LQP and FLQP, which encode four relationships of local texture, are more effective than the LTP, FLTP, LBP, and FLBP for texture description and pattern recognition, such as eye detection.
- FLQP performs better than LQP, FLTP performs better than LQP, and FLBP performs better than LBP in terms of average γ and γ_p. The results illustrate that the feature local methods (FLQP, FLTP, and FLBP), which encode both local and feature information, perform better than the local methods (LQP, LTP, and LBP) that do not encode feature information.
- The LTP method improves upon the LBP method. However, the average γ and γ_p of the FLBP method is smaller than the FLTP method. The FLTP method does not outperform the FLBP method. This results are consistent with the experimental results reported by Tan and Triggs (2007, 2010) and Gritti et al. (2008) which showed that LTP and LBP achieved similar results for face and facial expression recognition, although LTP has a higher computational cost than LBP.

CHAPTER 8

FUTURE WORK AND CONCLUSION

8.1 Future Work

This dissertation introduces FLBP, LQP and FLQP and applies these new local texture descriptors to eye detection. The future work will be the application of FLBP, LQP and FLQP to face detection and contented-based image classification. Some preliminary experiments have been conducted and show promising results. To further improve the performance will be the focus of the future work.

8.1.1 FLBP Application to Face Detection

The FLBP and LBP face detection methods are tested on the BioID database. The system architecture of face detection is similar to the one shown on Figure 5.3 for eye detection. The face template is constructed from 85 face samples that are not from the BioID database. All face samples are aligned by their eye centers and normalized to the size of 40 × 36. The face samples are divided to a grid of 4 × 4. To find the faces in different scales, the test images are scaled to different size. In each searching route the scale of a test image is selected by the bisection method. The success rate for $\gamma_p \leq 0.25$, 0.1, 0.05, and the average γ_p is used to assess the performance of face detection. For face detection, a candidate face is considered to be successfully detected if $\gamma_p \leq 0.25$. Table 8.1 shows face detection success rates and average γ_p of the FLBP and LBP methods, where the feature pixels for FLBP are derived by the LRBT method. The results show that both methods have a high success rate for $\gamma_p \leq 0.25$, and the FLBP method achieves better

performance than the LBP method. To increase the success rates for $\gamma_p \leq 0.1$, 0.05, and decrease the average γ_p will be our future tasks.

Table 8.1 The Face Detection Success Rates and Average γ_p of the FLBP and LBP Methods

Method	$\gamma_p \leq 0.25$	$\gamma_p \leq 0.1$	$\gamma_p \leq 0.05$	**Average γ_p**
FLBP LRBT, $\beta = 0.4$, $\alpha_t = 0$, $\alpha_v = 0.25$	96.19	37.48	5.06	0.1369
LBP	94.15	32.35	3.94	0.1557

8.1.2 FLBP Application to Content-Based Image Classification

The content-based image classification using FLBP and LBP is tested on the MIT Scene database. The MIT Scene database has 2,688 color images in eight categories. All color images are converted to grayscale images in the experiments. The features used in FLBP and LBP methods are 256 bins FLBP and LBP histograms of an image, respectively. Principal Component Analysis (PCA) is first applied to reduce the dimensions of the FLBP and LBP histograms, and then Fisher Linear Discriminant (FLD) is further applied to extract the most discriminatory features. The performance of FLBP and LBP method is assessed using four-fold cross-validations. The database is equally divided to four groups. In each round of cross-validation three groups are used for training and one group is used for testing. For classification, a testing image compares to the sample means of each category and is assigned to the category which has the shortest distance to the image. The performance of classification is measured by the mean of the classification rates of all rounds of cross-validation. Table 8.2 is the classification rate of the FLBP and LBP method on MIT Scene database. The results show the FLBP method has the higher

classification rate than the LBP method. The future work will be focused on improving the performance.

Table 8.2 The Content-Based Image Classification Rates the FLBP and LBP Methods

Method	Classification Rate
FLBP LRBT, $\beta = 0.1$, $\alpha_t = 0$, $\alpha_v = 0.5$	81.23
LBP	77.91

8.2 Conclusion

LBP only compares a pixel with the pixels in its own neighborhood and encodes a little information about the relationship of local texture with the features. To solve the problems of FLBP, this dissertation introduces Feature Local Binary Patterns (FLBP) that compares a pixel with the pixels in its own neighborhood as well as in other neighborhoods, and encodes the information of both local texture and features. The features encoded in FLBP are broadly defined by any features which meet the requirements of specific applications. FLBP generalizes LBP which can be considered as a special case of FLBP. The FLBP method displays superior representational power and flexibility to the LBP method due to the introduction of feature pixels as well as its parameters. The FLBP method is assessed on eye detection using the BioID and FERET databases. The experimental results show that the FLBP method significantly improves upon the LBP method in terms of both eye detection rate and eye center localization accuracy. The FLBP method is less sensitive to the appearance change caused by the illumination and pose variations than the LBP method. A new feature pixel extraction method, the LBP with Relative Biased Threshold (LRBT) method is presented in the

dissertation. The experimental results show that the new LRBT feature pixel extraction method helps improve the FLBP eye detection performance when compared with the other feature extraction methods. This dissertation further introduces an enhanced FLBP eye detection method to improve the performance. In comparison with the state of the art eye detection methods, the enhanced FLBP method significantly improves the accuracy of eye center localization.

Local Ternary Patterns (LTP) was introduced to solve the problem that the LBP is sensitive to noise. However, LTP achieved similar results as LBP in some experiments, although LTP has a higher computational cost than LBP. To improve the performance of LTP, this dissertation introduces Local Quaternary Patterns (LQP). LQP which encodes four relationships of the local texture includes more information of the local texture than LBP and LTP. The LQP is further extended to FLQP which encodes both local and feature information. To reduce the feature dimension of LQP and FLQP, a new coding scheme is proposed to split an LQP code into two binary codes: the Upper LQP (ULQP) and the Lower LQP (LLQP), and an FLQP code into two binary codes: the Upper FLQP (UFLQP) and the Lower FLQP (LFLQP). The experiments of eye detection using the BioID database show the following results:

- FLQP achieves the best eye detection performance.
- LQP performs better than LTP and LBP, and FLQP perform better than FLTP and FLBP. These results demonstrate that the proposed LQP and FLQP, which encode four relationships of local texture, are more effective than the LTP, FLTP, LBP, and FLBP for texture description and pattern recognition, such as eye detection.
- FLQP performs better than LQP, FLTP performs better than LQP, and FLBP performs better than LBP in terms of average γ and γ_p. The results illustrate that the feature local methods (FLQP, FLTP, and FLBP), which encode both local and feature information, perform better than the local methods (LQP, LTP, and LBP) that do not encode feature information.

REFERENCES

Ahonen, T., Hadid, A., & Pietikäinen, M. (2004). Face Recognition with Local Binary Patterns. in *Proceedings of Eighth European Conf. on Computer Vision*, pp. 469-481.

Ahonen, T., Hadid, A., & Pietikäinen, M. (2006). Face Description with Local Binary Patterns: Application to Face Recognition. *IEEE Transactions on Pattern Analysis and Machine Intelligence*, 28(12), pp. 2037-2041.

Akhloufi, M., & Bendada, A. (2010). A new fusion framework for multispectral face recognition in the texture space. in *Proceedings of 10th International Conference on Quantitative Infrared Thermograph.*

Asteriadis, S., Nikolaidis, N., & Pitas, I. (2009). Facial feature detection using distance vector fields. *Pattern Recognition*, 42(7), pp. 1388-1398.

Banerji, S., Verma, A., & Liu, C. (2011). Novel Color LBP Descriptors for Scene and Image Texture Classification. in *Proceedings of 15th International Conference on Image Processing, Computer Vision, and Pattern Recognition*, pp. 537-543.

Banerji, S., Sinha, A., & Liu, C. (2013). New Image Descriptors Based on Color, Texture, Shape, and Wavelets for Object and Scene Image Classification. *Neurocomputing*, 117, pp. 173-185.

Campadelli, P., Lanzarotti, R., & Lipori, G. (2009). Precise eye and mouth localization, *International Journal of Pattern Recognition and Artificial Intelligencece*. 23(3), pp. 359-377.

Cao, J., & Tong, C. (2008). Facial expression recognition based on LBP-EHMM. in *Proceedings of Congr. Image Signal Process.*

Chen, S., & Liu, C. (2010). Eye detection using color information and a new efficient SVM. in *Proceedings of Fourth IEEE International Conference on Biometrics Theory, Applications and Systems*.

Chan, C., Kittler, J., & Messer, K. (2007). Multi-scale local binary pattern histograms for face recognition. in *Proceedings of the 2nd International Conference of Biometrics (ICB)*, pp. 809-818.

Costa, L. (2008). 2D Euclidean distance transforms - a comparative survey. *ACM Computing Surveys*, 40(1), pp. 2:1-2:44.

Dalal, N. & Triggs, B. (2005). Histograms of oriented gradients for human detection. in *Proceedings of IEEE Conference on Computer Vision and Pattern Recognition (CVPR) 2005*, 1, pp. 886-893.

Danielson, P. (1980). Euclidean distance mapping. *Computer Graphics and Image Processing*, 14(3), pp. 227-248.

Feng G., & Yuen, P. (1998). Variance projection function and its application to eye detection for human face recognition. *Pattern Recognition Letters*. 19(9), pp. 899-906.

Feng G., & Yuen, P. (2001). Multi-cues eye detection on gray intensity image. *Pattern Recognition*. 34(5), pp. 1033-1046.

Feng, X., Hadid, A., Pietikäinen, M. (2004a). A coarse-to-fine classification scheme for facial expression recognition. in *Proceedings of Int. Conf. Image Analysis and Recognition (ICIAR)* pp. 668-675

Feng, X. (2004b). Facial expression recognition based on local binary patterns and coarse-to-fine classification. in *Proceedings of Int. Conf. Computer Inform. Technol.*, pp. 178-183.

Feng, X., Pietikäinen, M., Hadid, A. (2005). Facial expression recognition with local binary patterns and linear programming. *Pattern Recognition and Image Analysis*, 15(2), pp. 546-548.

Fu, X., & Wei, W. (2008) Centralized binary patterns embedded with image Euclidean distance for facial expression recognition. in *Proceedings of Int, Conf Neural Computation (ICNC)*, pp. 115-119.

Gong, P., Marceau, D., & Howarth, P. (1992). A comparison of spatial feature extraction algorithms for land-use classification with SPOT HRV data, remote sensing of environment. *Remote Sensing of Environment*, 40(2), pp. 137-151.

Guo, Z., Zhang, L., & Zhang, D. (2010). A completed modeling of local binary pattern operator for texture classification. *IEEE Trans. Image Process*., 19(6), pp. 1657-1663.

Gritti, T., Shan, C., Jeanne, V., & Braspenning, R. (2008). Local features based facial expression recognition with face registration errors. in *Proceedings of IEEE Int. Conf. Automatic Face and Gesture Recognition (FG)*.

Hadid, A., Pietikäinen, M., & Ahonen, T. (2004) A discriminative feature space for detecting and recognizing faces. in *Proceedings of Int. Conf. Computer Vision and Pattern Recognition (CVPR)* pp. 797-804

Hadid, A., Pietikäinen, M., & Li, S.Z. (2006a). Boosting spatio-temporal LBP patterns for face recognition from video. in *Proceedings of Asia-Pacific Workshop on Visual Information Processing*, pp. 75-80.

Hadid, A., Pietikäinen, M. (2006b). A hybrid approach to face detection under unconstrained environments. in *Proceedings of Int. Conf. Pattern Recog.*, pp. I: 227-230.

Hadid, A., Pietikäinen, M., & Li, S.Z. (2007) Learning personal specific facial dynamics for face recognition from videos. in *Proceedings of Anal.Model. Faces Gestures*, pp. 1-15.

Hadid, A. (2008). The local binary pattern approach and its applications to face analysis. *Image Processing Theory, Tools and Applications, 2008. IPTA 2008. First Workshops on*, pp. 1-9.

Han, C., Liao, H., Yu, G., & Chen, L. (2002). Fast face detection via morphology-based pre-processing. *Pattern Recognition*, 33(10), pp. 1701-1712.

He, L., Zou, C., Zhao, L., & Hu, D. (2005). An enhanced LBP feature based on facial expression recognition. in *Proceedings of Ann. Int. Conf. Eng. Med. Biol. Soc.*, pp. 3300-3303.

Heikkilä, M., & Pietikäinen, M. (2006). A texture-based method for modeling the background and detecting moving objects. *IEEE Trans. Pattern Anal. Mach. Intell.*, 28(4), pp. 657-662.

Hillman, P., Hannah, J., & Grant, P. (2003). Global fitting of a facial model to facial features for model-based video coding. in *Proceedings of the 3rd International Symposium on Image and Signal Processing and Analysis 2003*, pp. 359-364.

Huang, D., Wang, Y., & Wang, Y. (2007). A robust method for near infrared face recognition based on extended local binary pattern. in *Proceedings of Int. Symp. Vis. Comput.*, pp. 437-446.

Huang, W., & Mariani, R. (2000). Face detection and precise eyes location. *Proceedings of the International Conference on Pattern Recognition ICPR '00*, pp. 4722.

Huang, X., Li, S., & Wang, Y. (2006) Shape localization based on statistical method using extended local binary pattern. in *Proceedings of Third Int Conf on Image and Graphics*, pp.184-187.

Huang, Y., Wang, Y., & Tan, T. (2006). Combining statistics of geometrical and correlative features for 3D face recognition. in *Proceedings of Brit. Mach. Vis. Conf.*, pp. III: 879-888.

Hussain, S. & Triggs, B. (2012). Visual Recognition using Local Quantized Patterns. in *Proceedings of 12th European Conference on Computer Vision (ECCV)*, pp. 716-729.

Jin, H., Liu, Q., Lu, H., & Tong, X. (2006) Face detection using improved LBP under Bayesian framework. in *Proceedings of Third Int Conf on Image and Graphics*, pp. 306-309.

Kampmann, M., & Zhang, L. (1998). Estimation of eye, eyebrow and nose features in videophone sequences. in *Proceedings of International Workshop on Very Low Bitrate Video Coding (VLBV 98)*.

Kawaguchi, T., & Rizon, M. (2003). Iris detection using intensity and edge information. *Pattern Recognition*, 36(2), pp. 549-562.

Kawato, S., & Ohya, J. (2000). Real-time detection of nodding and headshaking by directly detecting and tracking the between-eyes. in *Proceedings of the Fourth IEEE International Conference on Automatic Face and Gesture Recognition*, pp. 40-45.

Kawato, S., & Tetsutani, N. (2002). Real-time detection of between-the-eyes with a circle frequency filter. in *Proceedings of Fifth Asian Conference on Computer Vision*, pp. 442-447.

Khosravi, M., & Safabakhsh, R. (2008). Human eye sclera detection and tracking using a modified time-adaptive self-organizing map. *Pattern Recognition*, 41(8), pp. 2571-2593.

Kumar, V., Rao, N., & Rao, A. (2009). Reduced texture spectrum with lag value based image retrieval for medical images. *International Journal of Future Generation Communication and Networking*, 2(4), pp. 39-48.

Lam, K. & Yan, H. (1996). Locating and extracting the eye in human face images. *Pattern Recognition*, 29(5), pp. 771-779.

Lei, Z., Liao, S., He, R., Pietikäinen, M., & Li, S. Z. (2008). Gabor volume based local binary pattern for face representation and recognition. in *Proceedings of IEEE Int. Conf. Autom. Face Gesture Recog.*, pp. 1-6.

Li, S. Z., Zhao, C., Ao, M., & Lei, Z. (2005). Learning to fuse 3D+2D based face recognition at both feature and decision levels. in *Proceedings of International Workshop Anal. Model. Faces Gestures*, pp. 44-54.

Li, S. Z., Chu, R., Ao, M., Zhang, L., & He, R. (2006) Highly accurate and fast face recognition using near infrared images. in *Proceedings of Int. Conf. Adv. Biometrics.*, pp. 151-158.

Li, S. Z., Chu, R., Liao, S., & Zhang, L. (2007). Illumination invariant face recognition using near-infrared images. *IEEE Trans. Pattern Anal. Mach. Intell.*, 29(4), pp. 627-639.

Liao, S., Fan, W., Chung, A.C.S., & Yeung, D.Y. (2006). Facial expression recognition using advanced local binary patterns, tsallis entropies and global appearance features. in *Proceedings of IEEE Int Conf Image Processing (ICIP)*, pp. 665-668.

Liao, S., & Chung, A.C.S. (2007). Face recognition by using elongated local binary patterns with average maximum distance gradient magnitude. in *Proceedings of Asian Conf Computer Vision (ACCV)*, pp. 672-679.

Liao, S., & Li, S.Z. (2007). Learning multi-scale block local binary patterns for face recognition. in *Proceedings of Int Conf Biometrics (ICB)*, pp. 828-837.

Liao, S., Law, M., & Chung, A. (2009). Dominant Local Binary Patterns for Texture Classification. *IEEE Transactions on Image Processing*, 18(5) pp. 107-118.

Liao, S., Zhao, G., Kellokumpu, V. Pietikäinen, M., & Li, S. Z. (2010). Modeling pixel process with scale invariant local patterns for background subtraction in complex scenes. in *Proceedings of IEEE Conf on Computer Vision and Pattern Recognition* (CVPR), pp. 1301-1306.

Liu, C., & Wechsler, H. (2002). Gabor feature based classification using the enhanced Fisher linear discriminant model for face recognition. *IEEE Transactions on Image Processing*, 11(4), pp. 467-476.

Liu, C. (2003). A Bayesian discriminating features method for face detection. *IEEE Transactions on Pattern Analysis and Machine Intelligence*, 25(6), pp. 725-740.

Liu, C. (2004). Gabor-based kernel PCA with fractional power polynomial models for face recognition. *IEEE Transactions on Pattern Analysis and Machine Intelligence,* 26(5), pp. 572-581.

Liu, C. (2006). Capitalize on dimensionality increasing techniques for improving face recognition grand challenge performance. *IEEE Transactions on Pattern Analysis and Machine Intelligence*, 28(5), pp. 725-737.

Liu, C. (2007).The Bayes decision rule induced similarity measures. *IEEE Transactions on Pattern Analysis and Machine Intelligence*, 29(6), pp. 1086-1090.

Liu, C. (2008). Learning the uncorrelated, independent, and discriminating color spaces for face recognition. *IEEE Transactions on Information Forensics and Security,* 3(2) , pp. 213-222.

Liu, C., & Yang, J. (2009). ICA color space for pattern recognition. *IEEE Transactions on Neural Networks*, 20(2), pp. 248-257.

Liu, Z., & Liu, C. (2008a).Fusion of the complementary discrete cosine features in the YIQ color space for face recognition. *Computer Vision and Image Understanding*, 111(3), pp. 249-262.

Liu, Z., & Liu, C. (2008b). A hybrid color and frequency features method for face recognition. *IEEE Transactions on Image Processing*, 17(10), pp. 1975-1980.

Liu, Z., & Liu, C. (2010). Fusion of color, local spatial and global frequency information for face recognition. *Pattern Recognition*, 43(8), pp. 2882-2890.

Maurer, C., Qi, R., & Raghavan, V. (2003). A linear time algorithm for computing exact Euclidean distance transforms of binary images in arbitrary dimensions. *IEEE Transactions on Pattern Analysis and Machine Intelligence*, 25(2), pp. 265-270.

Moore, S. &, Bowden, R. (2011). Local binary patterns for multi-view facial expression recognition. *Computer Vision and Image Understanding*, 115, pp. 541-558.

Murala, S., & Maheshwari, R. P. (2012). Local Tetra Patterns: A New Feature Descriptor for Content-Based Image Retrieval. *IEEE Transactions On Image Processing,* 21(5), pp. 2874-2886.

Nanni, L., & Lumini, A. (2007). RegionBoost learning for 2D+3D based face recognition. *Pattern Recog. Lett.*, 28(15), pp. 2063-2070.

Nanni, L., & Lumini, A. (2008). Ensemble of multiple pedestrian representations. *IEEE Trans. Intell. Transp. Syst.*, 9(2), pp. 365-369.

Ojala, T., Pietikainen, M., & Harwood, D. (1994). Performance evaluation of texture measures with classification based on kullback discrimination of distributions. in *Proceedings of the 12th IAPR International Conference on Pattern Recognition*, pp. 582-585.

Ojala, T., Pietikainen, M., & Harwood, D. (1996). A comparative study of texture measures with classification based on feature distributions. *Pattern Recognition*, 29(1), pp. 51-59.

Ojala, T., Pietikainen, M., & Maenpaa, T. (2002). Multiresolution gray-scale and rotation invariant texture classification with local binary patterns. *IEEE Transactions on Pattern Analysis and Machine Intelligence*, 24(7), pp. 971-987.

Oliver, A., Llado, X., Freixenet, J., & Marti, J. (2007). False positive reduction in mammographic mass detection using local binary patterns. in *Proceedings of Med. Image Comput. Comput.-Assisted Intervention Conf.*, pp. 286-293.

Pan, H., Zhu, Y., & Xia, L. (2013). Efficient and accurate face detection using heterogeneous feature descriptors and feature selection. *Computer Vision and Image Understanding*, 117(1), pp. 12-28.

Pentland, A., Moghaddam, B. & Starner, T. (1994).View-based and modular eigenspaces for face recognition. in *Proceedings of* 1*994 IEEE Conf. on Computer Vision and Pattern Recognition*, pp. 84-91.

Pham-Ngo, P.T., & Jo, K.H. (2006). Multi-face detection system in video sequence. *Proceedings of Int Forum on Strategic Technology (IFOST)*, pp. 146-150.

Ryu, Y. & Oh, S. (2001). Automatic extraction of eye and mouth fields from a face image using eigenfeatures and multilayer perceptrons. *Pattern Recognition*, 34(12), pp. 2459-2466.

Shan, C., Gong, S., & McOwan, P. W. (2005a). Robust facial expression recognition using local binary patterns. in *Proceedings of IEEE Int. Conf. Image Process*, pp. II: 370-373.

Shan, C., Gong, S., & McOwan, P. W. (2005b). Recognizing facial expressions at low resolution. in *Proceedings of IEEE Conf. Adv. Video Signal Based Surveillance*, pp. 330-335.

Shan, C., Gong, S., & McOwan, P. W. (2005c). Appearance manifold of facial expression. in *Proceedings of ICCV Workshop Human Comput. Interac.*, pp. 221-230.

Shan, C., & Gritti, T. (2008). Learning discriminative LBP-histogram bins for facial expression recognition. in *Proceedings of Brit. Mach. Vis. Conf.*

Shan, C., Gong, S., & McOwan, P. W. (2009). Facial expression recognition based on local binary patterns: a comprehensive study. *Image and Vision Computing*, 27, pp. 803-816.

Sinha, A., Banerji, S., & Liu, C. (2012). Novel Color Gabor-LBP-PHOG (GLP) Descriptors for Object and Scene Image Classification. in *Proceedings of the Eighth Indian Conference on Vision, Graphics and Image Processing*.

Sirohey, S., & Rosenfeld, A. (2001). Eye detection in a face image using linear and nonlinear filters. *Pattern Recognition*, 34(7), pp. 1367-1391.

Sirohey, S., Rosenfeld, A., & Duric, Z. (2002). A method of detecting and tracking irises and eyelids in video. *Pattern Recognition*, 35(6), pp. 1389-1401.

Tan, X., & Trigg, B. (2007). Enhanced local texture feature sets for face recognition under difficult lighting conditions. in *Proceedings of IEEE International Workshop on Analysis and Modeling of Faces and Gestures (AMFG).* pp. 68-182.

Tan, X., & Trigg, B. (2010). Enhanced local texture feature sets for face recognition under difficult lighting conditions. *IEEE Transactions on Image Processing*, 19(6), pp. 1635-1650.

Turtinen, M., Pietikainen, M., & Silven, O. (2006). Visual characterization of paper using Isomap and local binary patterns. *IEICE Trans. Inform. Syst.*, vol. E89-D(7), pp. 2076-2083.

Valenti, R., & Gevers, T. (2008). Accurate eye center location and tracking using isophote curvature. in *Proceedings of IEEE Conference on Computer Vision and Pattern Recognition (CVPR).*

Viola, P., & Jones, M. (2004). Robust real-time face detection. *International Journal of Computer Vision*, 57(2), pp. 137-154.

Wang, L., & He, D. (1990). Texture classification using texture spectrum. *Pattern Recognition,* 23(8), pp. 905-910.

Wang, X., Han, T. X., & Yan, S. (2009). An HOG-LBP Human Detector with Partial Occlusion Handling. in *Proceedings of IEEE 12th International Conference on Computer Vision,* pp. 32-39.

Wu, J., & Zhou, Z. (2003). Efficient face candidates selector for face detection. *Pattern Recognition,* 36(5), pp. 1175-1186.

Xie, X., Sudhakar, R., & Zhuang, H. (1994). On improving eye feature extraction using deformable templates. *Pattern Recognition*, 27(6), pp. 791-799.

Yang, H. & Wang, Y. (2007). A LBP-based face recognition method with Hamming distance constraint. in *Proceedings of Int. Conf. Image Graph.*, pp. 645-649.

Yang, J., & Liu, C. (2007). Horizontal and vertical 2DPCA-based discriminant analysis for face verification on a large-scale database. *IEEE Transactions on Information Forensics and Security,* 2(4), pp. 781-792.

Yang, J., & Liu, C. (2008). Color image discriminant models and algorithms for face recognition. *IEEE Transactions on Neural Networks,* 19(12), pp. 2088-2098.

Yao, B., Al, H., Ijiri, Y., & Lao, S. (2007) Domain-partitioning rankboost for face recognition. in *Proceedings of IEEE International Conference of Image Processing,* pp. 129-132.

Yuan, X., Yu, J., Qin, Z., & Wan, T, (2011), A SIFT-LBP image retrieval model based on bag of features. in *Proceedings of 18th IEEE International Conference on Image Processing (ICIP 2011*), pp. 1061-1064.

Yuille, A., Hallinan, P., & Cohen, D. (1992). Feature extraction from faces using deformable templates. *Int. J. Computer Vision,* 8(2), pp. 99-111.

Zhang, B. & Gao, Y. (2010). Local Derivative Pattern Versus Local Binary Pattern: Face Recognition With High-Order Local Pattern Descriptor. *IEEE Transactions on Image Processing*, 19(2) pp. 533-544.

Zhang, G., Huang, X., Li, S. Z., Wang, Y., & Wu, X. (2004). Boosting local binary pattern (LBP)-based face recognition. *Advances in Biometric Person Authentication Lecture Notes in Computer Science*, 3338, pp. 179-186.

Zhang, H., & Zhao, D. (2004). Spatial histogram features for face detection in color images. in *Proceedings of Advances in Multimedia Information Processing: 5th Pacific Rim Conference on Mul-timedia*, pp. I:377-384.

Zhang, L. (1996). Estimation of eye and mouth corner point positions in a knowledge-based coding system. in *Proceedings of SPIE*, 2952, pp. 21-18.

Zhang, L., Chu, R., Xiang, S., & Li, S. Z. (2007). Face detection based on Multi-Block LBP representation. in *Proceedings of Int. Conf. Biometrics (ICB)*, pp. 11-18.

Zhang, W., Shan, S., Gao, W., Chen, X., & Zhang, H. (2005a). Local Gabor binary pattern histogram sequence (LGBPHS): A novel non-statistical model for face representation and recognition. in *Proceedings of the Tenth IEEE International Conference on Computer Vision (ICCV05)*, 1, pp. 786-791.

Zhang, W., Shan, S., Zhang, H., Gao, W., & Chen, X. (2005b). Multi-resolution Histograms of Local Variation Patterns (MHLVP) for robust face recognition. in *Proceedings of Audio- and Video-based Biometric Person Authentication (AVBPA)*, pp. 937-944.

Zhang, W., Shan, S., Qing, L., Chen, X., & Gao, W. (2008). Are Gabor phases really useless for face recognition? *Pattern Anal. Appl.*, 12(3), pp. 301-307.

Zhao, G., & Pietikainen, M. (2007a). Dynamic texture recognition using local binary patterns with an application to facial expressions. *IEEE Transactions on Pattern Analysis and Machine Intelligence*, 29(6), pp. 915-928.

Zhao, G., & Pietikainen, M. (2007b) Experiments with facial expression recognition using spatiotemporal local binary patterns. in *Proceedings of Int. Conf. Multimedia and Expo (ICME)*, pp. 1091-1094.

Zhao, J., Wang, H., Ren, H., & Kee, S. C. (2005). LBP discriminant analysis for face verification. in *Proceedings of IEEE conference on Computer Vision and Pattern Recognition – Workshops*, pp. 167.

Zhou, Z. & Geng, X. (2004). Projection functions for eye detection. *Pattern Recognition*, 37(5), pp. 1049-1056.